PERFORMANCE-BASED RELIABILITY ANALYSIS AND CODE CALIBRATION FOR RC COLUMN SUBJECT TO VEHICLE COLLISION

A Dissertation

by

HRISHIKESH SHARMA

Submitted to the Office of Graduate Studies of
Texas A&M University
in partial fulfillment of the requirements for the degree of

DOCTOR OF PHILOSOPHY

May 2012

Major Subject: Civil Engineering

Performance-Based Reliability Analysis and Code Calibration for RC Column Subject to Vehicle Collision

PERFORMANCE-BASED RELIABILITY ANALYSIS AND CODE CALIBRATION FOR RC COLUMN SUBJECT TO VEHICLE COLLISION

A Dissertation

by

HRISHIKESH SHARMA

Submitted to the Office of Graduate Studies of
Texas A&M University
in partial fulfillment of the requirements for the degree of

DOCTOR OF PHILOSOPHY

Approved by:

Chair of Committee,	Stefan Hurlebaus
Committee Members,	Paolo Gardoni
	John B. Mander
	Monique Head
	Anastasia Muliana
Head of Department,	John Niedzwecki

May 2012

Major Subject: Civil Engineering

ABSTRACT

Performance-Based Reliability Analysis and Code Calibration for RC Column Subject to Vehicle Collision. (May 2012)

Hrishikesh Sharma, B.E., Visvesvaraya National Institute of Technology, Nagpur, India;

M.S., Texas A&M University

Chair of Advisory Committee: Dr. Stefan Hurlebaus

Infrastructure and transportation facilities have increased rapidly over the years. The progress has been accompanied by an increasing number of vehicle collisions with structures. This type of collision might lead to the damage, and often, collapse of the structure. In reinforced concrete (RC) structures, columns are usually the most vulnerable members exposed to collisions. However, the existing design guidelines and provisions for protection of these members against collision of vehicles are not adequate. In particular, the desired behavior and the associated performance levels of a structure during a vehicle collision are not defined. Therefore, there is need to assess the vulnerability of structures against such collisions.

This research aims to develop a framework for the performance-based analysis and design of RC columns subject to vehicle impact. It helps mitigate maximum damage and achieve an economical design. The current research takes into account performance-based analysis and design as opposed to only collapse prevention design. The performance level is tied to the impact levels to estimate the reliability of the RC

column for the desired performance objectives. The performance-based probabilistic models for estimating shear resistance of RC column and shear demand on RC column are developed. The reliability of the RC column subject for selected performance levels is evaluated. The performance levels are tied to impact demand and load and resistance factors are proposed to achieve desired performance objectives of the RC column subject to vehicle collision.

ACKNOWLEDGEMENTS

The author takes this opportunity to acknowledge the technical guidance and financial assistance offered by Dr. Stefan Hurlebaus during the research period. I thank him for entrusting me with this prestigious research work, and helping me at all stages and through all my difficult times. I also thank him for his valuable time and promptness to clear my doubts anytime I approached him. Without him, this project would not be in its present shape.

I acknowledge all the technical assistance received from Dr. Paolo Gardoni and Dr. John B. Mander. I thank them for sharing their technical expertise and helping me improve my model from time to time during the research period. I thank Dr. Monique Head and Dr. Anastasia Muliana for their support and help during my research.

I also thank my father and mother for their blessings which have made this day possible.

TABLE OF CONTENTS

LIST OF FIGURES

Page

LIST OF TABLES

Page

1 INTRODUCTION

With the rapid increase in the number of infrastructure projects, the collision of vehicles with structures has increased. The collision can be accidental in the case of a vehicle going astray or intentional, as in a terrorist attack. This has made vehicle collisions one of the leading causes of the structural failure. Bridge columns, lower story columns of buildings, traffic signal structures and electric poles are the structural members most vulnerable to vehicle impact (El-Tawil et al., 2005, Tsang and Lam, 2008). The rise in structural collision cases has been reported in the USA as well as in other parts of the world. Hartik et al. (1990) analyzed 114 bridge failures in the United States over a 38-year period (1951-1988). Out of the 114 failures, 17 (15%) were due to truck collisions. In a similar study, Wardhana and Hadipriono (2003) analyzed 503 bridge failures over an 11-year period (1989-2000) and reported that 14 (3%) bridge failures were caused by collisions of trucks or other vehicles. A review of the causes of bridge failures in USA was done from 1966 to 2005 (Briaud, 2007). Fig. 1.1 shows the frequency of the various causes of the bridge failure in USA.

This dissertation follows the style of *Journal of Structural Engineering (ASCE).*

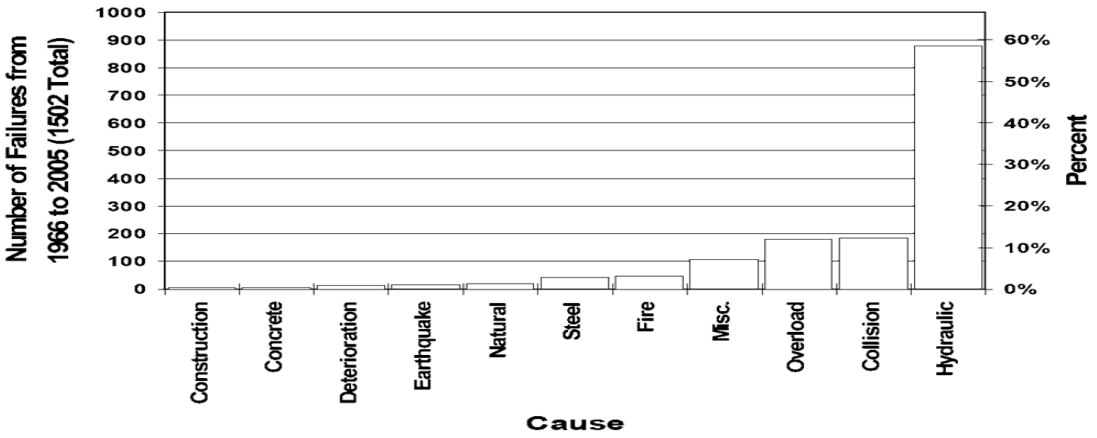

Fig. 1.1. Causes of bridge failure in USA from 1966 to 2005 (Briaud, 2007).

This study shows that after hydraulic causes, the most likely cause of bridge failure is collision (14%). Interestingly, while often more feared, failure due to earthquakes is only about 1%. Overall, 200 bridges failed due to collision from 1502 studied cases of bridge failure. Sharma et al. (2008) discusses various scenarios vehicle collision with a bridge. Suter (2005) mentions significant increases in the number of vehicle collisions with bridge columns in European countries.

Fig. 1.2 shows two examples of such incidents. The economic cost due to the closure of bridges, rerouting, maintenance, and repair becomes large combined with the invaluable loss of human life. The risk of damage to property and loss of human life increases for buildings subject to impact.

Fig. 1.2. (Left) Collision of truck with bridge column (Staples, 2007); (Right) Collapse of bridge on I-80 in Nebraska after being struck by a tractor trailer (El-Tawil et al., 2005).

Bridge columns, building columns, and electric poles are often made of reinforced concrete (RC). Therefore, the design and protection of RC columns subject to vehicle impact are important considerations. The RC column sustains damage during impact due to the transfer of a large shear force over a short interval of time. Due to the short interval, the resisting mechanism is based on shear, inertia, and local deformation rather than overall displacement. So, the dynamic shear force capacity of and demand on the RC column becomes important quantities rather than static shear quantities. Also, the damage state varies depending upon the type and severity of the impact. The current code provisions (AASHTO -LRFD 2007) do not account for various damage states and only design for collapse prevention. For minimizing the damage to the RC column and ensuring an economical design, a performance-based analysis and design is required.

The damage state has to be identified with the performance levels of the structure whose RC column might be subject to vehicle impact. These performance levels have to be associated with the different impact levels of vehicle for achieving the desired design criteria. The dynamic shear resistance of and demand on the RC column corresponding to these performance criteria needs to be estimated. The need for accurate procedures based on performance levels to estimate the dynamic shear resistance of the RC column and predicting the dynamic shear force demand imposed on it during vehicle collision becomes vital.

The current analysis methods and experimental procedures to estimate the shear resistance and demand of RC columns do not capture the complex mechanism of impact events. Current procedures of estimating the shear capacity of RC columns are based on static calculations and are verified and calibrated by quasi–static experiments (PEER, 2010, Gardoni et al., 2002, Moehle et al. 1999 and 2000, Kowalsky and Priestley 2000). These procedures are based on a cantilever RC column with the first mode approximation. However, experiments and simulations have shown that the shear resistance during an impact event can be higher than the values estimated by the static procedures (Louw et al., 1992, Sharma et al., 2009). The procedure in practice to calculate the energy absorbed by the structure is based on the static force-deformation, or moment-curvature methods (EUR 23738 EN, 2009). This in turn again leads to the inaccurate quantities. Tsang and Lam (2008) have shown the energy absorbed by the RC column based on elastic-plastic curvature. But the research does not provide

corresponding forces which could be used in design purposes. The energy calculations require dynamic simulations which could be impractical for use in design codes.

The increase in the shear resistance of the RC column during an impact can be attributed to various factors, such as increase in strength due to strain rate effects, crack propagation, inertia effect, viscous damping, relative stiffness between the impacting bodies, and composite action. The behavior of the RC column also changes from the first mode approximation of the cantilever column. The current code AASHTO -LRFD (2007) provision assumes a constant value for the shear force demand on a bridge column. The shear force demand imposed on the RC column is often underestimated in a real collision event (El-Tawil et al., 2005). Furthermore, uncertainties, such as relative stiffness between the bridge and vehicle, probability of occurrence, material properties, and dynamic effects, are not addressed in the present design codes.

The need to accurately estimate the dynamic shear resistance and demand on the RC column associated with the performance levels is important. The current code provisions do not take into account the dynamic shear resistance of the RC columns. The code provision does not take into consideration the varying demand imposed on the RC column. The code also does not account for the force levels based on different performance levels. Instead the RC column is designed for the collapse prevention limit state.

This research aims to develop a framework for the performance-based analysis and design of RC columns subject to vehicle impact. In the spirit of a performance-based analysis and design, three performance levels are defined based on four possible

damage levels of the structure subject to vehicle collision. This ensures that the desired performance of RC column is achieved when subject to a vehicle impact. It helps mitigate maximum damage and achieve an economical design. This research proposes a procedure to accurately estimate the different dynamic shear resistance of and demand on the RC columns subject to vehicle impact corresponding to different performance levels. The proposed procedure accounts for the interdependency of the capacity and demand on the configuration of RC columns and the nature of loading. The procedure is based on the analysis of the actual configuration of the RC columns. The dynamic shear resistance of and demand on the RC column is estimated by using representative vehicles and realistic values of velocity. The proposed method can be used to perform experiments as well as simulations. The finite element (FE) simulation is used to show an application of the described procedure. The proposed methodology is an improvement over the existing static or quasi-static analysis to the dynamic analysis, which is a more realistic representation of vehicle impacts with structures. The current research takes into account performance-based analysis and design as opposed to only collapse prevention design. The research aims to develop performance-based dynamic shear resistance and demand models for RC column subject to vehicle collision. The performance-based models will be used for code calibration to estimate the load and resistance factor. The hazard curves will be developed together with the performance-based dynamic shear resistance and demand models to develop framework to evaluate the total probability or the reliability of the RC column subject to the vehicle collision. The performance level will be tied to the impact levels to estimate the reliability of the

RC column for the desired performance objectives. The research done in the dissertation will lead to development of framework to achieve desired performance objectives of the RC column subject to vehicle collision based on the reliability analysis of the RC column.

This dissertation is organized in 10 sections. Following this introduction, the dynamic shear resistance of and demand on the RC column subject to vehicle impact based on performance levels are described. Then the procedure to estimate the different levels of dynamic shear resistance and demand are discussed. The next section presents the application of this procedure using the FE method. After that, case studies for estimating resistance of and demand on RC column by FE simulations are presented. Next, description of experimental design is presented. The section after that describes the development of performance-based dynamic shear resistance model. This section is followed by section describing development of dynamic shear demand model. The next section presents the result for reliability-based code calibration for RC column subject to vehicle collision. Finally, the dissertation concludes by assessing the applicability of the proposed procedure in conclusion section and the recommendations for future work are presented.

2 PERFORMANCE-BASED DYNAMIC SHEAR RESISTANCE OF AND DEMAND ON RC COLUMNS DURING VEHICLE COLLISION

The dynamic shear resistance of a RC column and the demand imposed on it during an impact depends both on the structural properties as well as on the loading conditions. Therefore, it is necessary to understand the behavior of the RC column during impact in order to accurately estimate the shear force capacity of the RC column. An accurate estimate of the dynamic shear resistance and the dynamic shear force demand is necessary so that the structural capacity can be kept more than the demand. This ensures the safety and smooth operation of the structure during a vehicle impact. The damage states observed during vehicle impact are identified and related with the performance levels of dynamic shear resistance of and demand on RC column. The performance levels are identified with the different impact scenarios of the vehicle to insure the desired design and behavior of the RC column.

2.1 Behavior of RC Column during Vehicle Impact

A number of experiments have been conducted to understand the failure mechanism and dynamic effects during vehicle impact. The salient features can be summarized as follows:

- Cracks propagate through the aggregate thickness, thus increasing the strength and toughness of the concrete member (Mendis et al., 2000) (system).

- In concrete, the brittle behavior increases with the increase in loading rate (material).
- The strength of the reinforcing steel bar increases with loading rate (Malvar, 1998) (material).
- Shear failure mode becomes predominant with increasing loading (system).
- A plastic hinge is formed at the point of contact (system).

The damage in RC columns is due to the large instantaneous force applied. The behavior of a RC column during vehicle impact is explained as follows. The impact process can be divided into two phases. In the first phase, the vehicle comes in contact with the RC column with an initial velocity. The first phase is the duration from the time of initial contact of the RC column with the vehicle to the time when part of the RC column and vehicle acquire a common velocity and move together. Due to the inertia of the RC column, a large contact force develops in a very short time period (a few milliseconds), as evident from the results presented in the research (Sharma et al., 2009). The vehicle extends large force in order to move the column from rest. Since column is at rest and has a large mass, a large contact force develops in order that both the RC column and the impacting vehicle acquire a common velocity. The area of the RC column in contact with the vehicle experiences large force and acceleration. This phase is governed by the inertia of the RC column. The force is localized to the area in contact. In the second phase, the vehicle and part of RC column acquires a common velocity and move together. The second phase is thus the duration from the time when a part of the RC column and vehicle acquire a common velocity to the time when either

the failure of column occurs or vehicle comes to rest. The kinetic energy is transferred from the vehicle to the RC column. The amount of kinetic energy transferred to the column is proportional to the stiffness of the column and the inertia of the column. Local displacement in the RC column occurs due to the crushing of the concrete and shear deformation of the column. Part of the initial kinetic energy is absorbed by the vehicle as result of deformation of the vehicle. The amount of energy absorbed by the vehicle is proportional to the stiffness of the vehicle. Typically vehicles are made to deform and dissipate energy so that passengers have a better protection in the event of an accident. Because of this, the force developed in the first phase is low. While the forces developed in the second phase are larger and might lead to failure of the RC column. A shear failure is usually observed with the crushing of concrete and in plane crack across the thickness of the member. A hinge formation occurs at the point of contact, near the bottom of the column.

The force imparted to the RC column during the impact is the demand on the RC column. The demand changes with the stiffness of the vehicle, mass and the velocity of vehicle as well as the structural configuration and properties of the RC column. The demand on the RC column is not a constant quantity. To emphasize its interdependency on the impacting vehicle as well as the body being impacted the demand will be called the dynamic force demand on the RC column. The initial kinetic energy of vehicle is shared between the vehicle and RC column during the collision. The vehicle absorbs part of the total kinetic energy due to its deformation. The RC column also absorbs part of the energy due to deformation and the energy required to set the RC column in

motion. The energy transfer and in turn the force transferred are proportional to the stiffness of the RC column, stiffness of the vehicle, inertia of the RC column and vehicle. These properties are in turn dependent on the structural configuration and properties of the RC column and the vehicle. So the applied force is dependent on the above properties. This dynamic demand should used for analysis and design purposes as opposed to the equivalent shear force defined in El-Tawil et al. (2005) because it reflects the actual demand on the RC column. The RC column gets time to develop the full response and it is not governed by inertia alone. Similarly, the force required to cause the failure of the RC column is greater than its static capacity. The vehicle along with the RC column comes to rest after the kinetic energy is dissipated in the form of deformation, heat and sound. For analysis purposes, the heat and sound energy are ignored.

2.2 Dynamic Shear Capacity

The resistance mechanism of column consists of strength of the column called capacity, inertial resistance and damping resistance. The capacity of the column increases during impact event due to the strain rate dependency of the materials. The member contribution is therefore called dynamic shear capacity and the total contribution of member, inertia and damping is called dynamic shear resistance. The dynamic shear capacity of the column is evaluated by performing push over analysis and accounting for the strain rate effect in the concrete and steel.

2.3 Performance Levels for Vehicle Impact

During an impact with a vehicle, the RC column sustains different levels of damage depending on the geometry, material properties and boundary condition of the column and velocity and type of vehicle. The radial velocity defined as radial component of the velocity v_R controls the damage to the RC column due to the vehicle impact. The tangential velocity defined as tangential component v_T does not have significant contribution to the damage of the RC column. The velocity components are shown in Fig. 2.1.

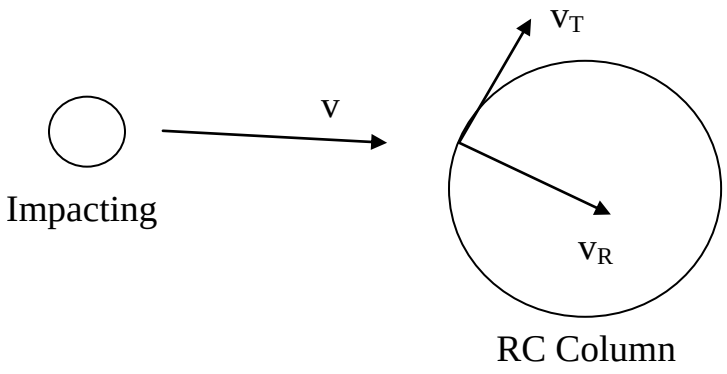

Fig. 2.1. Velocity components affecting the damage to the RC column.

The proposed damage levels can be categorized into four levels with increasing intensity. In the spirit of a performance-based analysis and design, three performance

levels are defined based on four possible damage levels of the structure subject to vehicle collision.

Table 2.1 lists the damage levels, the associated damage description, and the corresponding performance level and the description of the performance levels.

Table 2.1. Performance Level of RC Column Subject to Vehicle Impact.

Damage Level	Damage Description	Performance Level	Performance level Description
D1	Insignificant damage		
		← P1	Fully operational with no damage
D2	Minor spalling of concrete, yielding of longitudinal steel		
		← P2	Operational structure with damage
D3	Significant cracking of concrete, Spiral and longitudinal bar exposed, buckling of bars		
		← P3	Collapse prevention
D4	Loss of axial load capacity, longitudinal bar fracture		

The damage levels increase in intensity from insignificant damage to total collapse of column. The corresponding defined performance levels are fully operational with no damage (P1), operational structure with damage (P2), and collapse prevention of structure (P3). The defined performance levels ensure the desired behavior of the RC column during an impact scenario. The severity of the impact scenario also varies depending upon the type of vehicle and its velocity. Table 2.2 groups the intensity of the

impact scenario in three categories: low (L), moderate (M), and severe (S) based on the mass of the vehicle m_v and the velocity of the vehicle v_0. Table 2.3 shows the desired performance levels of the structure whose RC column is subject to vehicle impact.

Table 2.2. Categorization of Impact levels.

		Velocity of Vehicle (v_0)		
Mass of Vehicle (m_v)		$v_0 \leq 15$ m/s (54 km/hr)(Low)	15 m/s (54 km/hr)< v_0<27 m/s (97 km/hr)(Intermediate)	$v_0 \geq 27$ m/s (97 km/hr) (High)
	$m_v \leq 2722$ kg (Passenger cars)	L	L	M
	2722 kg < m_v< 11793 kg(Commercial Vehicles)	L	M	S
	$m_v \geq 11793$ kg Heavy (Trucks, Buses)	M	S	S

Table 2.3. Design Performance Objectives for RC Column Subject to Vehicle Impact.

		Performance Level		
		Fully operational with no damage (P1)	Operational structure with damage (P2)	Collapse prevention (P3)
Loading	Impact level (L)			
	Impact level (M)			
	Impact level (S)			

The inclined line stands for the desired performance levels for the RC column during different impact scenarios. This design requirement ensures that the structure remains fully operational (P1) during low (L) impact intensity and operational with damage (P2) during moderate (M) intensity event. It also helps to design the structure so that total collapse (P3) is prevented during severe (S) intensity events. The performance-based design helps in ensuring that the structure has minimum damage during low intensity impact scenarios and collapse prevention is ensured during high intensity events with sufficiently high probability.

A frequent case of vehicle collision involves bridge columns with heavy vehicles. In such an event, the dynamic shear action affects the shear capacity of the column. These cases are critical, as shown in Fig. 1.2, because they can lead to failure of the column and it turn of the bridge. In an earlier study, Tsang and Lam (2008) have addressed the issue of building columns subject to impact. The dynamic shear action is not considered in the analysis. It was based on the assumption that the time required to develop the full contact force is much larger than the duration required by the shear wave velocity to travel. Full scale Finite Element (FE) simulations of the impact of vehicles (NCAC, 2010) with bridges were carried out. It was noted that the time required for the full contact to develop is comparable to the duration of shear wave velocity in the case of a large mass and velocity. It can be attributed to the localized contact, the inertia of the vehicle, and the relative stiffness of the contact region compared to the global stiffness. Modified Compression Field theory gives an estimate

of the increase in the shear capacity based on the influence of strain rate on material properties (Mendis et al., 2000).

Currently, no method is available to estimate the dynamic shear resistance and demand on the RC column subject to vehicle collision. The analysis and design methods do not account for varying damage states and the required performance levels. In light of the conclusions drawn, it is necessary to lay a standard procedure to estimate the dynamic shear resistance of the RC column and to estimate the dynamic shear force demand imposed on it corresponding to different performance levels and impact scenarios. The following section explains the proposed method.

3 PROCEDURE FOR ESTIMATING DIFFERENT LEVELS OF PERFORMANCE-BASED DYNAMIC SHEAR RESISTANCE AND DEMAND

The estimation of dynamic shear resistance of and demand on RC column corresponding to different performance levels and impact scenario are done from the crash test on the RC column. According to the definition provided earlier, the dynamic shear resistance at a particular performance level is computed in this analysis as the lateral force resisted by the RC column showing the defined damage state. The dynamic shear force demand is the maximum lateral force imposed on the RC column. Different levels of the dynamic shear force demand can be obtained corresponding to the weight and velocity of the impacting vehicle as categorized in Table 2.2. The actual structural configuration and boundary conditions are used.

3.1 Performance-Based Dynamic Shear Resistance of RC Column

The RC column whose dynamic shear resistance needs to be evaluated is subject to a dynamic loading. The dynamic shear resistance is interdependent on the structural configuration and properties as well as the rate of applied loading, mass, and contact area. Thus, the dynamic shear resistance is characterized as a function of the applied loading. With many available variables to characterize the loading, the analysis procedure becomes more difficult. It is dependent on all the variables: the change in velocity, relative stiffness of the bodies, and inertia. In an impact event the loads are

applied suddenly, and there is no reversal of the loading. The studies for the estimation of acceleration for a column subject to vehicle impact give a range of about $10g - 50g$ where g is the acceleration due to gravity 9.81 m/s^2 (Ydenius and Kullgren, 2001, Steffan et al., 1998, Kloeden et al., 1999). There is large variability in the type of vehicles. This variation leads to different contact areas and point of application when a RC column is subject to impact by a vehicle. The appropriate vehicle with corresponding velocity is used as loading for estimation of the dynamic shear resistance.

The dynamic shear resistance obtained gives an estimate of the resistance offered by the RC column during a vehicle impact scenario. The dynamic shear resistance for the performance level of fully operational (P1) is the maximum horizontal force resisted by the RC column before the limiting damage state (D2), mentioned in Table 2.1 begins to occur. Similarly, the dynamic shear resistance for the performance level of operational with damage (P2) is the maximum horizontal force resisted by the RC column before the limiting damage state (D3), mentioned in Table 2.1 begins to occur. In the same lines, the dynamic shear resistance for the performance level of total collapse (P3) is the maximum horizontal force resisted by the RC column before the limiting damage state (D4), mentioned in Table 2.1 begins to occur.

3.2 Performance-Based Dynamic Shear Force Demand on RC Column

The dynamic shear force demand is the maximum lateral force applied to the RC column by impacting vehicle. The appropriate vehicle with corresponding velocity is used as loading for estimation of the dynamic demand. The dynamic shear demand can be used

in design and analysis purposes. Due to the deformable nature of the vehicle, the contact response during the initial phase is not large. Therefore, the entire response is not governed by the inertia effect. The RC column gets the time to develop the resistance against the collision. Hence the applied force gives a true estimate of the demand imposed on the RC column. The dynamic shear force demand can be categorized into various demand levels depending on the three vehicle impact levels low (L), moderate (M), and severe (S), as defined in Table 2.2.

These procedures can be applied experimentally to estimate the dynamic shear resistance and demand of a RC column. The proposed procedure can also be simulated numerically to estimate the quantities of interest. The following section provides a demonstration of the proposed procedure using FE simulation.

4 FINITE ELEMENT MODEL

This section uses the proposed procedure to assess the performance-based dynamic shear resistance of RC columns and the dynamic shear force demand due to vehicle impacts using data from detailed FE analysis. A parametric study is performed using the FE method. In this study, the commercial FE program LS-DYNA is used for the FE analysis (Livermore Software Technology Corporation, 2003). The FE models considered in this study are generated using HyperMesh (Altair Computing, 2003). The quantities of interest monitored are the force applied to the column, strain rate, shear force at the bottom, and the acceleration. The explicit integration scheme based on the central difference method is used for the analysis.

4.1 Structural Configuration, Imposed Load, and Boundary Conditions

A three dimensional solid model is used for modeling the impact of vehicle with the RC column. The RC column is modeled by a fully integrated quadratic eight node element with nodal rotations. The reinforcement bars are modeled explicitly using a one dimensional element. The contact between the concrete and reinforcements is modeled using the Langragian coupling method. This method saves the effort of matching the nodes of the reinforcement and the concrete which might be very difficult in some cases. The RC column supports the load imposed by the structure. This is called the imposed load. In order to model this imposed load a solid body is placed over the RC column to uniformly distribute the imposed load on the top surface of the RC column. The total

mass of the solid body placed over the body imposes the same load as imparted by the structure. This is done in order to study the behavior of the RC column with realistic imposed load. The imposed load and the gravitational load are supported by the RC column during normal operation of the structure. To model this effect a static analysis is first performed in which the forces due to imposed load and gravity are transferred to the RC column. The state of the RC column after transfer of these forces and their subsequent effects is used as an initial condition for the dynamic analysis in which the RC column is subject to collision with a vehicle. The foundation is modeled by restricting the nodes at the base or by equivalent springs. Mesh refinement achieves convergence and hourglass energy is minimized.

4.2 Material Models

A rate dependent material model is used for all the materials due to the sensitivity of material properties with loading rate. In this research, a continuous surface cap model available in the software is used to model the concrete. This model also takes into account the strain rate dependency of the concrete strength. A strain rate dependent elasto-plastic model is used as the material model for the reinforcement bars. The RC column supports the structure which in turn exerts load on the RC column. This is called imposed load. In order to model the imposed load, a solid body is placed over the RC column as described in Section 4.1. The total imposed load on the RC column is then divided by the volume of the solid body placed over the RC column to calculate the

density of material used for the imposed load. The material models for the vehicles are used as provided in the input files (NCAC, 2010).

4.3 Dynamic Shear Resistance of and Demand on RC Columns

The estimation of the dynamic shear resistance and demand involves monitoring the lateral force applied on the RC column. The vehicles for the analysis purpose are chosen from the available pool of vehicles developed for the crash analysis purpose (NCAC, 2010). The RC column is impacted with the vehicle with the expected velocity with no eccentricity. The impact is thus symmetric to the RC column. The impact velocity becomes the radial velocity. The applied force reaches a maximum value and then decreases with a steep slope indicating a shear failure. The applied force then becomes constant at a lower value called residual force. The erosion and cracking of the elements of RC column and vehicle are monitored. A detailed description of the FE model is provided in Appendix-I. The total lateral force resisted by the RC column is monitored to determine the different dynamic shear force capacities of the column corresponding to the three performance levels. The total force imparted by the vehicle to the RC column is monitored. The maximum force is the dynamic shear force demand imposed on the RC column by the vehicle during the collision.

The FE method shows that the proposed procedure can be used to estimate the dynamic shear resistance of and demand on the RC column subject to a vehicle impact. Different case studies are presented to study the variation of the dynamic shear resistance of and demand on the RC column with structural properties, configuration and

loading conditions. The FE modeling requires validation so that the results obtained can be accepted. The following section presents validation of the material model, contact algorithm, and modeling assumptions.

4.4 Validation of the Finite Element Model

One of the critical aspects of FE modeling is the validation of the obtained results with experimental results or agreement with the physical phenomenon. Validating the FE model has different aspects like confirming that the material model used exhibits the physical properties of the actual material, the realistic boundary conditions are achieved in the modeling, the contact between different parts and materials is achieved, and the loading is accurately modeled. This paper presents three cases for validation. Similar modeling techniques are used for the validation cases as well as presented earlier in Section 4.1 and 4.2.

The first validation is using the results for a bogie impact experiment conducted by the Texas Transportation Institute (TTI). The details of the experiment can be obtained from the report (Murray et al., 2007). Fig. 4.1 shows the validation of the impact experiment. Fig. 4.1 (top) shows the high speed photograph of the impact experiment. Fig. 4.1 (bottom) shows the simulated FE model of the impact experiment. Fig. 4.1 (top) and (bottom) are extracted at the same time of the impact. The figure shows an agreement between the shapes of the impacted beam. The cracks on the actual beam are similar to the simulated beam.

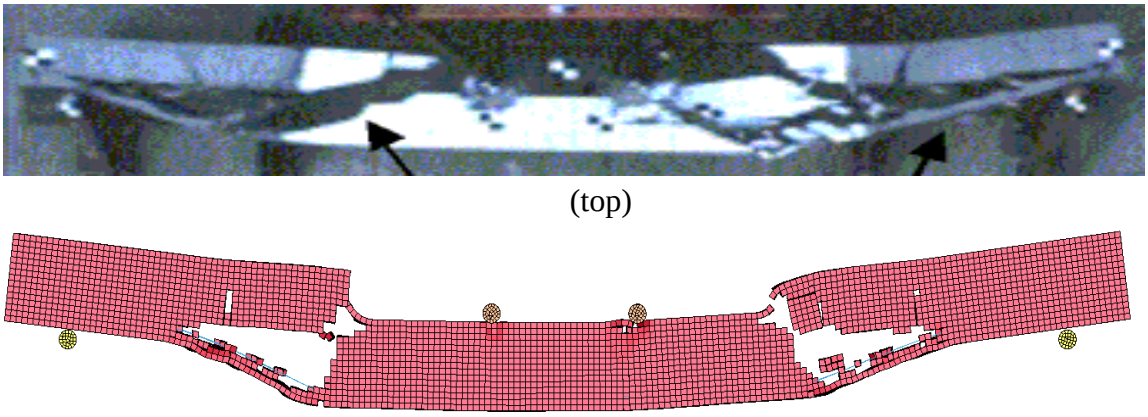

(top)

(bottom)

Fig. 4.1. Validation of TTI bogie impact experiment at 48 ms. (top) High speed photograph of the impact experiment; (bottom) FE simulated model of the experiment.

The second validation is done for the composite column and wall systems for impact and blast resistance (COSIMB) project conducted in Europe for different types of columns subject to impact, blast, and fire loading (EUR 23738 EN, 2009). A detailed description of the FE model is provided in Appendix-I. The experimental displacement time history at the mid span of the beam subject to impact is compared with the FE simulation in Fig. 4.2.

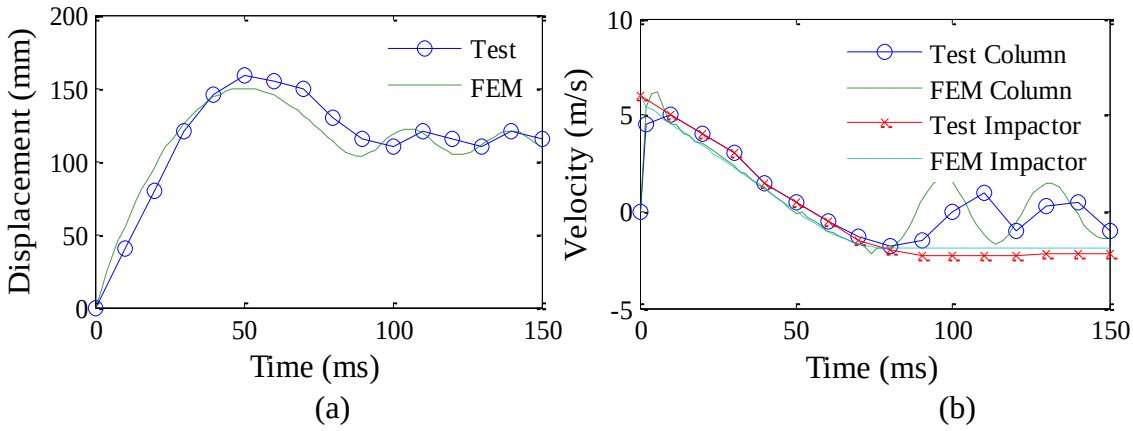

Fig. 4.2. Validation of the COSIMB experiment. (left) Displacement time history of the column at mid span; (right) Velocity time history of the column at mid span and impacting body.

Fig. 4.2 also shows the comparison between the velocity profiles of the experiment and simulated values. The experimental values were obtained from the graph provided in the COSIMB report by the authors by interpolation, so the values are less in number. This might explain the slight discrepancy in the comparison, however, overall the values agree well with each other.

The third validation is presented next. Several cases of vehicle collision are listed in Buth (2009) including an actual vehicle collision with an exterior RC column of a three column bent of a bridge over I-20 in Tyler, Texas. A detailed description of the FE model is provided in Appendix-I. Fig. 4.3 shows the comparison of the FE simulation and the crash photograph of the column.

(a) (b)

Fig. 4.3. Validation for a tractor-truck collision with bridge column of IH-20, Longview, Texas.(left) RC Column after collision with the vehicle; (right) FE simulation of the collision event.

The details of the column are mentioned in the report (Buth, 2009). The impacted column is a 0.6 m diameter exterior column of an interior 3-pier bent. The column had eight 22.2 mm diameter rebars in the longitudinal direction. The transverse reinforcement consisted of 6.35 mm spiral stirrups with 150 mm pitch. In the report, only the type, mass and velocity of the vehicle are mentioned. The impacting vehicle had a mass of 36 Mg. This case was simulated using an IVECO truck (Atahan et al., 2007) as it has a comparable mass as mentioned in the report. A general agreement on the observed failure mechanism of the RC column and crack pattern is shown in Fig. 4.3.

These verifications provide sufficient confidence that the modeling technique used in the FE models is able to capture the complex process of a vehicle crash with a RC column. The verification shows that the material, contact, boundary and other

conditions are appropriately modeled. The total energy, the energy balance, ratio of hourglass energy to the total energy is monitored to check the stability and validity of the numerical simulation. The initial energy is compared with the hand calculation to check the accuracy of the numerical simulation. The final velocities are compared with hand calculations to provide sanity check for the numerical simulations. The results obtained are reliable and agree to the physical phenomenon observed during the impact. Thus, the results obtained by the FE model can be used for making inferences and drawing conclusions. Several case studies are simulated in the next section to understand the behavior of a RC column during impact and estimate dynamic shear force capacity of and demand on the RC column.

5 CASE STUDIES FOR ESTIMATING RESISTANCE OF AND DEMAND ON RC COLUMN BY FE SIMULATION

The FE model is used to simulate the behavior of representative RC columns and estimate the dynamic shear resistance of and demand. A parametric study is performed to understand the variation of the dynamic shear resistance and demand with the loading conditions.

5.1 Structural Configuration, Material Property and Loading

Two different types of RC columns are simulated. The first one is similar to the exterior column of the three column bent presented previously. It represents the bridge RC column (C1). The second RC column has a similar configuration to the exterior building column presented in Tsang and Lam (2008) (C2). The material properties used for these two RC columns are presented in Table 5.1. The configuration of the columns is presented in Table 5.2.

Table 5.1. Material Properties of RC Columns.

Material	Density ρ [kg/m^3]	Modulus of Elasticity E [GPa]	Poisson's ratio υ	Unconfined Compressive Strength [MPa]	Unconfined Tensile Strength [MPa]	Yield Stress [MPa]
Concrete	2500	25.7	0.2	30.0	3.0	-
Steel	7850	210.0	0.3	-	-	415

Table 5.2. Static Shear Response of RC Columns.

No.	Diameter [m]	Length [m]	Longitudinal Reinforcement	Transverse Reinforcement	Static Shear Capacity [kN]
C1	0.61	5.18	8- ϕ 22mm bars	ϕ6.35mm-0.15m pitch	342.0
C2	0.40	3.00	8- ϕ 22mm bars	ϕ 9.6mm-0.30m pitch	178.5

An imposed loading of 250 kN is applied at the top of both columns to simulate the effect of the structure supported by the columns. For the RC columns, the imposed loads are usually 7% of the axial load capacity based on gross sectional area with 25% COV (Gardoni et al., 2002). To account for the variation, the bridge column C1 has an imposed ratio of 3% and the building column C2 has an imposed load ratio of 7%. The bases of both of the columns have fixed condition. The horizontal and transverse direction refers to the directions in the plane of the cross section of the RC column. For the bridge column C1, the horizontal direction is along the flow of the traffic and

transverse direction is perpendicular to the horizontal direction. For the bridge column C1, rotation along the transverse direction at the top of the RC column is constrained. For the building column C2, rotations along both the horizontal and transverse directions at the top of RC column are constrained. The static shear capacity is also reported in Table 5.1 (ACI-318, 2005).

Four vehicles are used for the impact loading. The vehicles used for loading are a 8,000 kg (8 Mg) Ford truck (NCAC, 2010), a 30,000 kg (30 Mg) IVECO truck (Atahan et al., 2007), a 38,000 kg (38 Mg) tractor trailer (NCAC, 2010), and a 50,000 kg (50 Mg) IVECO truck (Atahan et al., 2007). Each vehicle collides with the RC columns C1 and C2 six times by varying the velocity. The values of velocities for each vehicle are 18 m/s, 22 m/s, 27 m/s, 32 m/s, 36 m/s and 45 m/s (65 km/h, 80 km/h, 96 km/h, 113 km/h, 128 km/h, and 161 km/h respectively). The RC columns C1 and C2 are simulated for 24 cases with variation of four vehicles and six velocity cases for each type of vehicle. The impacts are central impact with no eccentricity between the centroid of the vehicle and the RC column. The impact velocity thus comprises of the radial velocity only.

5.2 Dynamic Shear Force Resistance for Performance Levels

The dynamic shear resistance is estimated for both bridge and building columns (C1 and C2). Fig. 5.1 shows the contour plot of the variation of dynamic shear resistance (MN) with radial velocity (m/s) on the vertical axis and mass (Mg) on the horizontal axis for the performance levels. The Fig. 5.1 (a), Fig. 5.1 (c), and Fig. 5.1 (e) is for the RC

column C1. Fig. 5.1 (b), Fig. 5.1 (d), and Fig. 5.1 (f) is for the RC column C2. In Fig. 5.1 (a) and Fig. 5.1 (b), the performance level P1 for the two columns C1 and C2 is compared. Similarly in Fig. 5.1 (c) and Fig. 5.1 (d), the performance level P2 for the two columns C1 and C2 is compared. Following the same trend, Fig. 5.1 (e) and Fig. 5.1 (f), compares the performance level P3 for the columns C1 and C2. Fig. 5.1 shows that each of the three performance levels increases with increase in radial velocity as well as the mass of the vehicle. This is because the strength increases with the strain rate and more inertia is utilized for the resistance. The performance levels have higher value for C1 as compared to C2 as C1 has more strength than C2 which is evident from its configuration presented in Table 5.1 and Table 5.2. The performance level P1 is less than P2 which is in turn less than P3 in all the cases. This is due to the fact that P1 corresponds to less severe damage state and hence the force required for maintaining the damage state is also lower than the next higher performance level P2. The same conclusion applies for P2 being lower than P3.

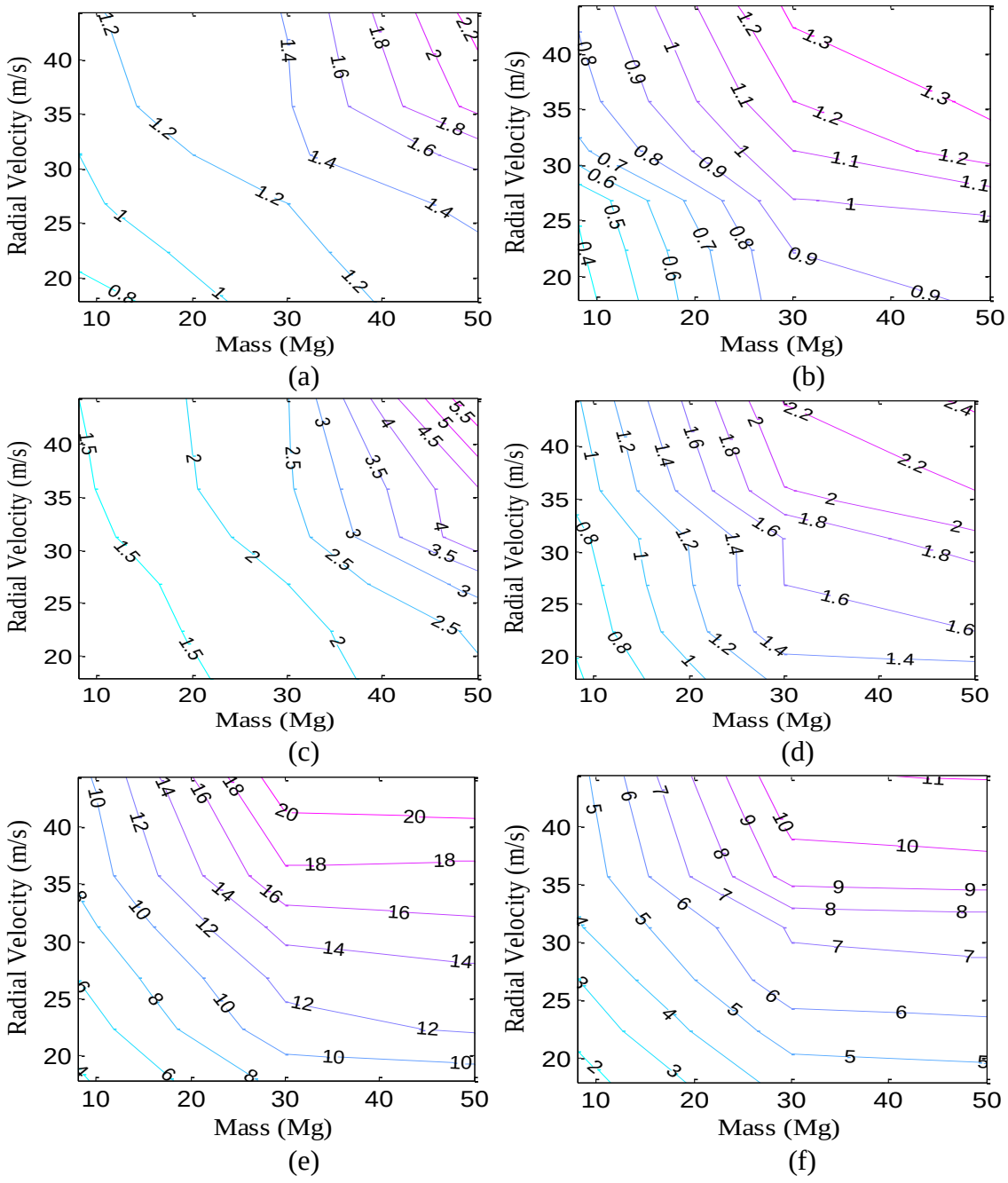

Fig. 5.1. Variation of dynamic shear resistance of RC column with velocity and mass. Dynamic shear resistance (MN) of column (a) C1 for performance level P1; (b) C2 for performance level P1; (c) C1 for performance level P2; (d) C2 for performance level P2; (e) C1 for performance level P3; (f) C2 for performance level P3.

These simulations confirm the notion that the capacity of a RC column is not a static value. It is dependent on the structural configuration as well as the applied loading. The failure of the column occurs by shear failure mode. The dynamic shear resistance corresponding to different performance levels can be evaluated by the proposed procedure.

5.3 Dynamic Shear Force Demand on RC Column

The dynamic shear force demand is estimated for both bridge and building columns (C1 and C2). Fig. 5.2 shows the collision for one case each of C1 and C2 with a vehicle velocity of 18 m/s (65 km/h).

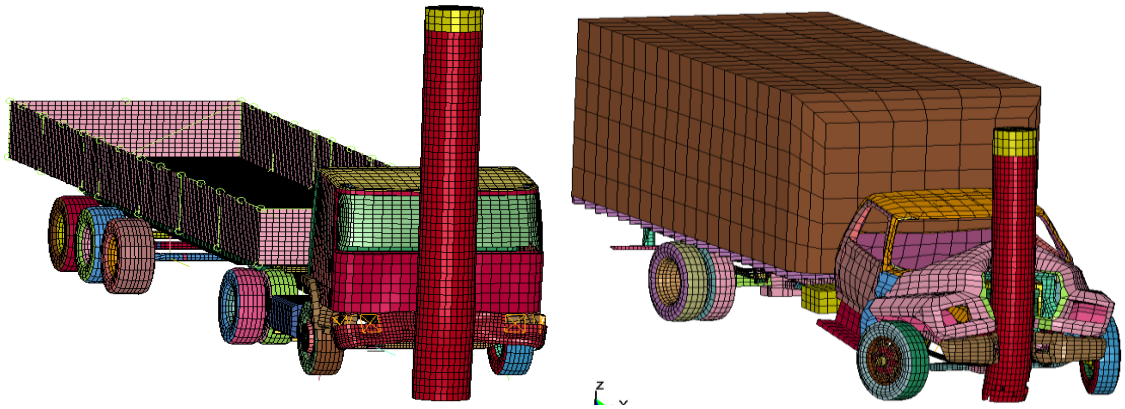

(a) (b)

Fig. 5.2. FE simulation of collision of RC column with vehicles with no failure. (a) column C1 impacted by a vehicle of mass 38 Mg and velocity 18 m/s; (b) column C2 impacted by a vehicle of mass 8 Mg and velocity 18 m/s.

No significant damage is observed in either of the collisions. The velocity of the vehicle is only 18 m/s which is the allowable velocity inside city limits. Due to this, a low demand is applied to the columns, hence no failure is observed with only some spalling. Four cases of vehicle collision are shown in Fig. 5.3, two for column C1 and two for column C2.

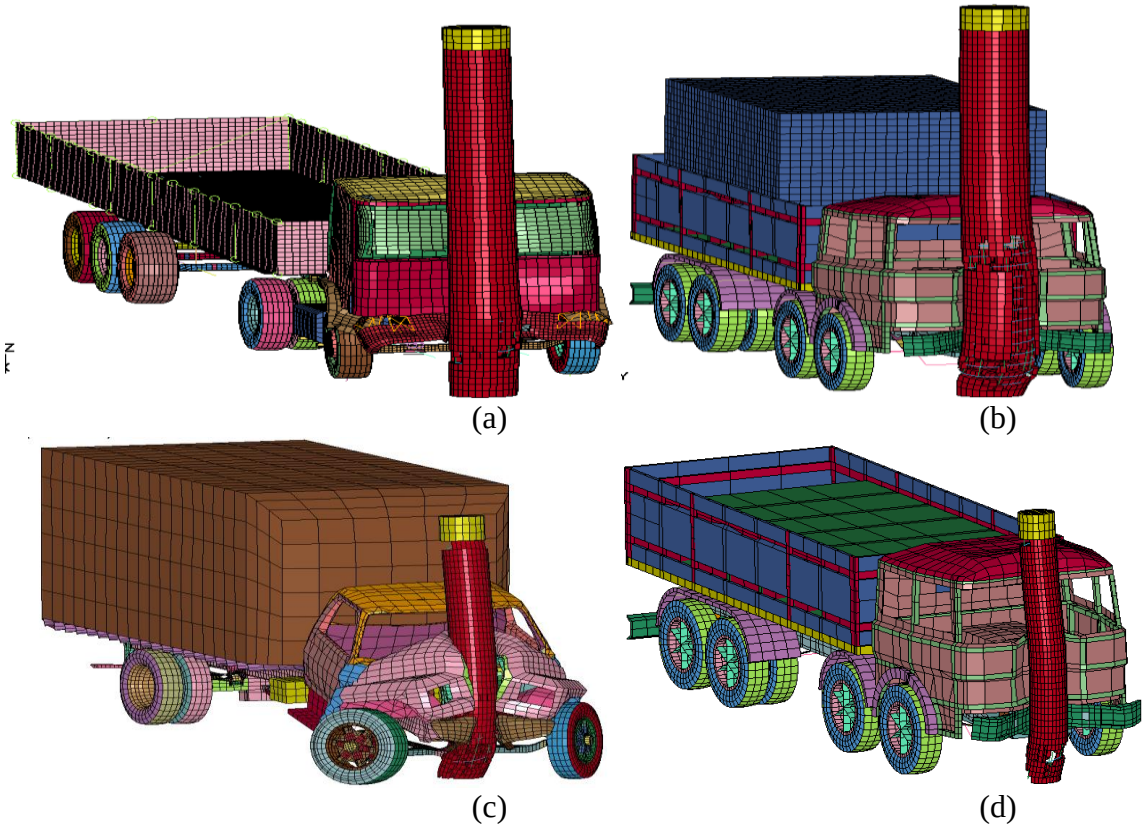

Fig. 5.3. FE simulation of collision of RC column with vehicles with shear failure (a) C1 impacted by a vehicle of mass 38 Mg and velocity 32 m/s; (b) C1 impacted by a vehicle of mass 50 Mg and velocity 32 m/s; (c) C2 impacted by a vehicle of mass 8 Mg and velocity 32 m/s; (d) C2 impacted by a vehicle of mass 30 Mg and velocity 32 m/s.

The impact velocity is 32 m/s (113 km/h) which is the common velocity on most highways. Shear failure is observed in all the cases. The hinge formation at the base is more dominant at the base than at the top. It is because the main thrust of the impact is concentrated at the lower part of the column. For column C1 (Fig. 5.3 (a) and (b)) the hinge is formed near the base of the column. The cracking is observed in the lower part only for vehicle with mass 38 Mg whereas the cracking occurs in the entire contact length for vehicle with mass 50 Mg. For column C2 (Fig. 5.3 (c) and (d)) the hinge is formed near the base with cracking occurring at the base as well as at the top of the column. It is because for column C2, the percentage of the contact area is more than C1. Hence a large portion of the column is utilized in resisting the force, so some cracks are formed in the top portion of the column along with the base. The vehicle bends itself around the column in all the cases. The shape of bending is influenced by the net area in contact (after subtracting the area for openings like windows, etc.).

Fig. 5.4 (a) shows the contour plot of the variation of dynamic shear force demand (MN) with radial velocity (m/s) on the vertical axis and mass (Mg) on the horizontal axis for the various simulated cases. The dynamic shear demand for column C1 increases with mass and velocity (Fig. 5.4 (a)).

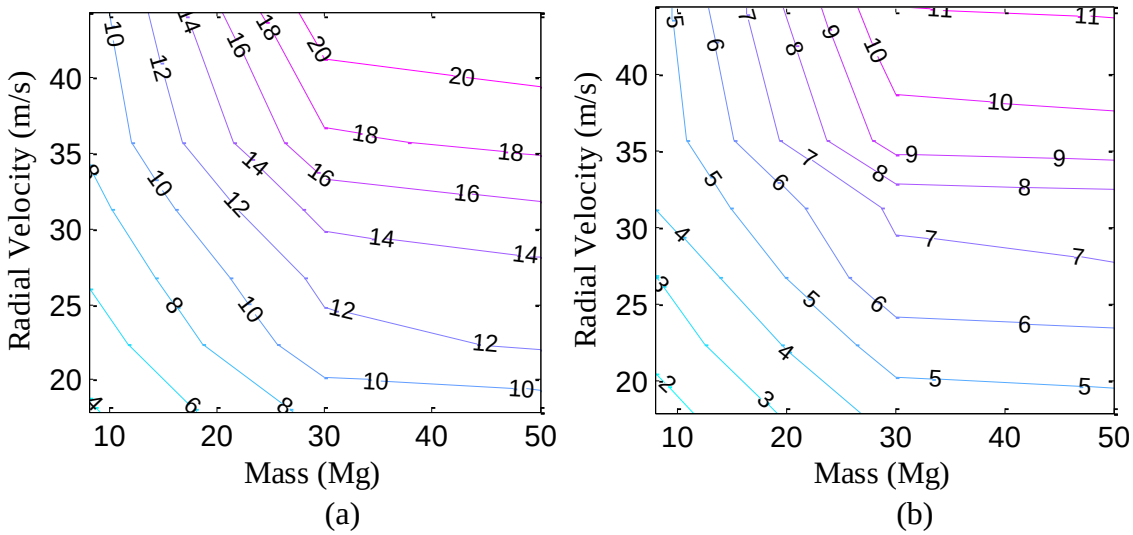

Fig. 5.4. Response of RC column during impact with vehicle. Dynamic shear demand (MN) of column (a) C1; (b) C2.

The increase of the dynamic shear force demand with mass and velocity confirms the earlier notion and is in accordance with the physical phenomenon of an increase in shear demand due to inertia, rate, and other effects. Fig. 5.4 (b) presents the results for column C2. The figure is a contour plot of the dynamic shear force demand (MN) on column C2 with the variation of radial velocity (m/s) on the vertical axis and mass (Mg) on the horizontal axis. A similar trend is observed in the increase in dynamic shear force demand with increase in mass and velocity.

The dynamic shear force demand imposed on a RC column is interdependent on the structural properties of the RC column and the loading. It increases with an increase in mass and velocity of the impacting vehicle. The demand imposed can be greater than the maximum design value adopted by the current code. The shear cracking and hinge

formation occurs near the base of the RC column as the main thrust of impact is concentrated in that zone. The dynamic shear force demand on the RC column can be categorized into different demand levels depending on the categorization of the vehicle mass and velocity as mentioned in Table 2.2. This will give different dynamic demands corresponding to different impact scenarios for which a RC column can be designed for desired performance level.

The dynamic shear resistance is less than the dynamic force demand for the cases in which damage is observed. This serves as an additional validation for the proposed methodology. The proposed procedure is able to estimate the dynamic shear resistance of and demand on the RC column corresponding to different performance levels. The change in dynamic shear resistance and demand with the variation of structural configuration and loading is also observed. A corresponding dynamic shear resistance and demand can be evaluated to estimate the safety of the RC column during an impact event.

5.4 Conclusion

The work in this section focuses on shifting the existing paradigm in the analysis and design of RC columns subject to vehicle impact in a number of ways. It lays out a framework to quantify the different observed damages into applicable damage levels. The damage levels are then related to the appropriate performance levels. The performance levels are tied to the different impact scenarios of vehicle impacts to ensure that the desired performance of the structure is met when the RC column is impacted.

Then a procedure to estimate the different dynamic shear resistance corresponding to performance levels is established.

The proposed procedure shifts the existing methodology based on static or quasi-static analysis to the dynamic analysis which is a more realistic representation of the vehicle impact with structures. A method to estimate the dynamic shear force demand on the RC column during vehicle impact is also laid out. The dynamic shear force demand can be categorized into different demand levels depending on the intensity of the impact. A FE model is used to implement the framework. The FE model is validated with experimental and realistic crash scenarios. The case studies show that the dynamic shear resistance of and demand on RC column are interdependent on the structural configuration as well as the loading. The dynamic shear resistance of and demand on RC column varies with the mass and velocity of the vehicle. This agrees with the proposed methodology which uses the quantities to estimate the dynamic shear force capacity and demand. The estimated dynamic shear resistance is more than the static shear capacity evaluated by ACI 318 (2005). The estimated dynamic shear force demand quantities are greater than the static quantity and vary with the loading. The proposed procedure gives a better estimate for design and analysis of RC columns subject to impact. The performance-based dynamic shear resistance and demand can be used to determine the performance of a structure in a given scenario and evaluate the survival of the structure. Actual structural configurations and loading scenarios are used to evaluate the response which is more accurate in representing the complex impact scenario.

The proposed procedure has its merits for application in the design of RC columns to minimize damage and meet a set of performance objectives during different vehicle impact scenarios. The performance-based proposed procedure can be used for other hazards such as high velocity impacts due to blasts or missiles impact. The current work can be extended to estimate the resistance of and demand on for other members such as prestressed columns, steel columns, and beams.

6 EXPERIMENTAL DESIGN

The validity of a probabilistic model is only within the range of the data used for the model. Therefore, an accurate probabilistic model requires representative data that cover the entire range of the input variables. Also there should be a sufficiently large amount of data to minimize the statistical uncertainty (Gardoni et al., 2002). Therefore, a large number of full-scale experiments would be needed to generate the required data. However, the availability of number of full-scale experiments on RC column subject to different loading rates is currently limited. Furthermore, creating an adequate database would require a large amount of resources and time. So, in this dissertation, virtual experiments are conducted using refined FE analyses. The range of variables used for the experimental design is optimally selected so that they are representative of the range of actual RC column and applied loading. The FE analyses have the additional advantage of providing any response of interest and allow for parametric variations.

The design of virtual experiments for FE simulations requires the creation of a number of models of the RC column and loading. A detailed review of national bridge inventory (NBI) was made by Nielson and DesRoches (2006) to assess representative ranges of the variables $\mathbf{x}$ for RC columns and is followed in this dissertation. However, if all the variables that characterized the material and geometric properties of RC columns are randomly combined an unrealistic case may result. To prevent having an unrealistic bridge, the material and geometric variables are divided into basic and derived variables. The variables that capture the basic design requirements are

categorized as basic variables. Table 6.1 gives the ranges for these variables. The expression or ranges of the derived variables are obtained by satisfying the design requirements and they are given in Table 6.2. Defining basic and derived variables ensures that the bridge models from this pool are realistic. AASHTO -LRFD (2007) requirements are used as design specifications.

Table 6.1. Range of Basic Variables for the Experimental Design.

Variable	Symbol	Range
Column Height (m)	H	3−10
Column Diameter (m)	D_g	0.40−2.00
Longitudinal reinforcement ratio (%)	ρ_l	1−4
Volumetric transverse reinforcement ratio (%)	ρ_s	0.70−3.00
Compressive strength of concrete (MPa)	f_c'	20−55
Yield strength of longitudinal and transverse reinforcement (MPa)	f_y, f_{yh}	250−550
Boundary condition at the top of the column	B_T	Propped (Simply Supported)
Boundary condition at the bottom of the column	B_B	Fixed
Initial velocity of the vehicle (m/s)	v_0	15.70−53.60
Mass of the vehicle (Mg)	m_v	8.00, 30.00, 50.00
Stiffness of vehicle (kN/m)	k_v	1200 (Light), 1500 (Medium), 2500 (Heavy)

Table 6.2. Expression and Range of Derived Variables for the Experimental Design.

Variable	Symbol	Expression/Range
Diameter of longitudinal bar (mm)	d_l	25.4, 28.575, 31.75, 34.925, 44.45, 57.15
Diameter of longitudinal bar (mm)	d_s	9.525, 12.7, 15.875, 19.05, 22.225, 25.4
Number of longitudinal bar	n_l	$100\rho_l D_g^2 / d_l^2$
Pitch of spiral (mm)	s	$100\pi d_s^2 / \rho_s D_c$
Clear cover (mm)	c	$(0.05\text{-}0.10)D_g$
Axial load (kN)	N	$\mu f_c' \frac{\pi}{4} D_g^2, \mu = 0.07, COV = 0.25$

The range of column heights H spans from the height of an overpass on a rural road to the height of a multilane bridge. The column diameter D_g ranges between the diameter of columns in multi column bent to the diameter of single column bents. The range of values for longitudinal reinforcement ratio ρ_l and volumetric transverse reinforcement ratio ρ_s are as per AASHTO -LRFD (2007) and construction practices. The range for the yield strength of longitudinal reinforcement f_y and compressive strength of concrete f_c' is adopted from the values that are most widely used for construction steel. The yield strength of the spiral reinforcement f_{yh} is taken to be the same as that of longitudinal reinforcement. The diameter of longitudinal d_l and transverse spiral reinforcement d_s covers the size of the bars widely used in the engineering practice. The bar sizes were consistent with the values in representative drawings of the bridges available at the Texas Department of Transportation (TxDOT)

website (TxDOT 2010). The boundary condition at the bottom of the column is taken as fixed while variation of three boundary conditions, free, fixed and propped are used at the top of the RC column. The axial load N is the load due to the superstructure. It is taken as 7% of the axial capacity based on the cross sectional area with 25% Coefficient of Variation (COV) (Gardoni et al. 2002). In this dissertation, the axial load percentage of the total axial load N for each RC column is randomly generated from the above mentioned mean and COV. This randomly generated quantity is then multiplied with the gross cross sectional area to get the total axial load N. In this way the variation in the axial load N is accounted for the each simulated RC column.

The dynamic shear force capacity also depends on the velocity and type of the vehicle involved in the collision. Three models of vehicle are used for FE simulation. The vehicles used for loading are an 8,000 kg (8 Mg) Ford truck representative of a light medium vehicle (modeled by the National Crash Analysis Center, NCAC 2010), a 30,000 kg (30 Mg) IVECO truck representative of a medium weight vehicle (modeled by Atahan et al., 2007), and a 50,000 kg (50 Mg) IVECO truck representative of a heavy vehicle (modeled by Atahan et al., 2007). The velocity of the vehicles is varied between 15.7 m/s (56.5 km/hr) to 53.6 m/s (192.6 km/hr) to cover the entire range. The stiffness of vehicle is taken as 1200 kN/m for light vehicle, 1500 kN/m for medium vehicle, and 2500 kN/m for heavy vehicle.

The design is split into design of column and design of load cases. The load cases are separately designed to create cases of all combinations as shown in Table 2 (low, moderate and severe impact events). The experimental design considers 50 RC

columns and each RC column are run with 5 variations of the velocity and mass of the vehicle combination. By this strategy, each column experiences the three impact events. In case of designing the column and load cases together, there would have been cases when some columns do not experience all the impact events. This is avoided by splitting the design into column and load cases. The D-optimal point selection scheme (Myers and Montgomery 1995) is used for the selection of the best set of cases from a given range. The D-optimal scheme is chosen because it has the flexibility of allowing any number of designs to be placed appropriately in a design space with an irregular boundary. Overall, 250 cases are simulated to assess the probabilistic dynamic shear capacity models which is the sample size N_s.

7 PERFORMANCE-BASED DYNAMIC SHEAR RESISTANCE MODELS

The dynamic shear resistance is defined as the maximum resistance offered by an RC column during a vehicle impact scenario at each performance level. That is, the dynamic shear resistance for the performance level of fully operational (P1), V_{P1} is the maximum shear force resisted by the RC column before D2 begins to occur. Similarly, the dynamic shear resistance for the performance level of operational with some damage (P2), V_{P2} is the maximum shear force resisted by the RC column before D3 begins to occur. Finally, V_{P3} is defined as the maximum shear force resisted by the RC column before D4 begins to occur. This section develops probabilistic resistance models for performance levels P1, P2 and P3.

The section presents the result for the variation of the dynamic shear capacity with increasing velocity. Using the results of the FE simulations, this section develops probabilistic models for estimating the dynamic shear resistance of RC columns subject to vehicle collision for each of the three performance levels. The models take into account the relevant uncertainties including model error and statistical uncertainty as described in Gardoni et al. (2002). Because the data used for the model assessment come from FE simulations, it is assumed that there is no measurement error in the data. The probabilistic models are unbiased and incorporate current understanding on the mechanics of the problem. The natural logarithm is used to stabilize the model variance

in order to satisfy the homoskedasticity and the normality assumptions. Following the general formulation for probabilistic models proposed by Gardoni et al., 2002, the dynamic shear resistance model for performance level Pi, i=1, 2, 3 is formulated as

$$\ln[v_{Pi}(\mathbf{x},\boldsymbol{\Theta}_{Pi})] = \ln[\hat{v}_{Pi}(\mathbf{x})] + \gamma_{Pi}(\mathbf{x},\boldsymbol{\theta}_{Pi}) + \sigma_{Pi}e_{Pi} \qquad (7.1)$$

where $v_{Pi} = V_{Pi} / NF_{Pi}$ = normalized dynamic shear resistance for performance levels Pi, i=1, 2, 3; V_{Pi} = dynamic shear resistance; NF_{Pi} = normalizing factor for dynamic shear resistance; $\hat{v}_{Pi}(\mathbf{x})$ = normalized dynamic shear resistance obtained from mechanical model $\hat{V}_{Pi}$; $\gamma_{Pi}(\mathbf{x},\boldsymbol{\theta}_{Pi})$ = correction term for the bias inherit in the mechanical model is defined as

$$\gamma_{Pi}(\mathbf{x},\boldsymbol{\theta}_{Pi}) = \sum_{j=1}^{k_{Pi}} \theta_{Pi,j} h_{Pi,j}(\mathbf{x}) \qquad (7.2)$$

where $h_{Pi,j}(\mathbf{x}),\ j = 1,...,k$ = explanatory function and $\theta_{Pi,j}(\mathbf{x}),\ j = 1,...,k_{Pi}$ is the parameter associated with the explanatory function, $\sigma_{Pi}e_{Pi}$ model error; e_{Pi} = random variable with zero mean and unit variance and normal distribution (normality assumption); σ_{Pi} = standard deviation of the model error, which is assumed to be independent of $\mathbf{x}$ (homoskedasticity assumption), and $\boldsymbol{\Theta}_{Pi} = (\boldsymbol{\theta}_{Pi}, \sigma)$ = set of unknowns model parameters.

For each performance level Pi, the maximum shear force calculated in each FE simulation is classified as an equality datum if the simulated RC column reached a damage level larger than Di in shear, and as a lower-bound or censored datum if otherwise.

7.1 Dynamic Shear Capacity Estimation

A moment curvature analysis is performed on the simulated column to estimate the dynamic shear capacity of the column as described in Sub-section 2.1. The estimated capacity without considering the strain rate effect is called static shear capacity and the estimated capacity with strain rate effect is called dynamic shear capacity. The ratio between dynamic shear capacity and static shear capacity is called Dynamic shear ratio (DSR). Fig. 7.1 shows the variation of the DSR with the velocity of the column.

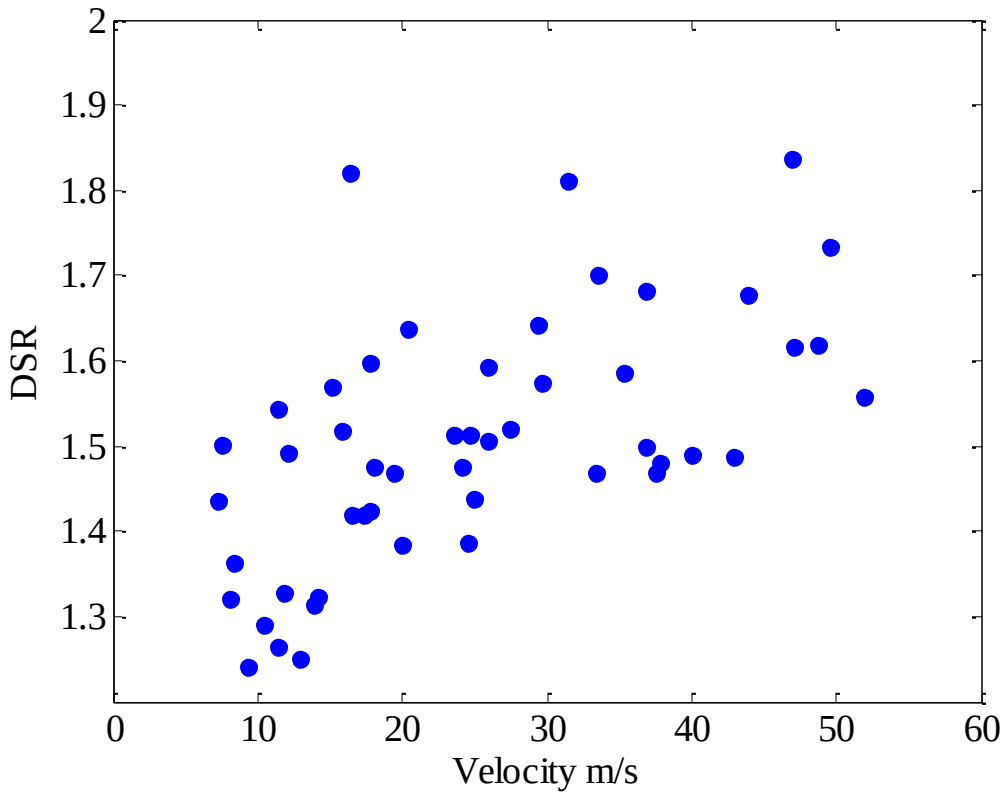

Fig. 7.1. Variation of DSR with velocity.

The figure shows that the dynamic shear capacity increases with the increase in velocity of the column. The increase is attributed to the increase in corresponding strain rate with the velocity. Therefore in a dynamic event such as impact, the contribution from the shear capacity can increase as high as 1.9 times the static value. So the consideration of the strain rate becomes an important factor. A detailed description of DSR is provided in Appendix-II.

7.2 Mechanical Model for Performance Level P1

The estimate of the dynamic shear resistance for P1 is proposed in this research by

$$\hat{V}_{P1} = \frac{2.8 f_t' I_c H^3}{D_g H_a (H - H_a)^2 (H_a + 2H)} \tag{7.3}$$

where f_t' = tensile strength of concrete, I_c = gross 2nd moment of area of cross section of column, H = height of the column, D_g = diameter of the column, and H_a = distance from the bottom of the column to the impact point of the vehicle as shown in Fig. 7.2.

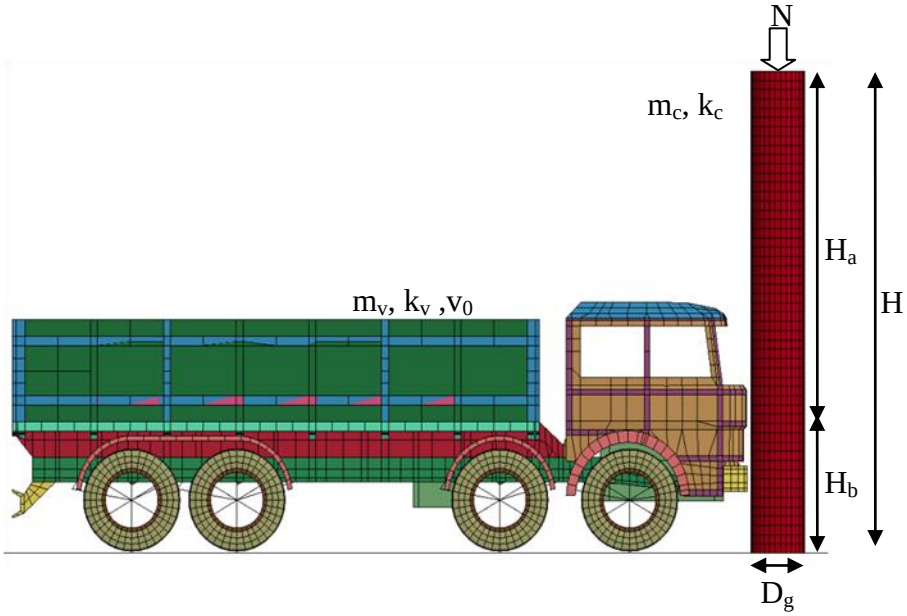

Fig. 7.2. Schematic of vehicle collision with RC column.

7.3 Mechanical Model for Performance Level P2

The estimate for the dynamic shear resistance for P2 is proposed in this dissertation by

$$\hat{V}_{P2} = 2.23 k_c d_{P2} \exp(-3.5 f) \tag{7.4}$$

where, $k_c = k_r E_c I_c / (0.77H)^3$, $d_{P2} = \dfrac{0.67\sigma_y I_{cc} H^3 H_a^{0.5}}{D_g E_c I_c (H_a + 2H)^{3/2}}$, $f = \dfrac{ND_g}{f'_{ty} A_g H}$, $\sigma_y = f'_c DIF$,

$$k_r = \left[\int_0^{H_a} [\phi_1''(x)]^2 + \int_{H_a}^{H} [\phi_2''(x)]^2 \right] H^3 / [\max(\phi_1, \phi_2)]^2 \quad ,$$

$$\phi_1 = H_b^2 x(3H_a H^2 - 2Hx^2 - H_a x^2)/H^3, \phi_2 = H_a (H-x)^2 (3H^2 x - H_a^2 x - 2H_a^2 H)/H^3,$$

where, E_c = modulus of concrete of RC column, I_{cc} = 2nd moment of area of cross section of column considering diameter = $D_g - 2c$, c = clear cover of the column, f'_{ty} =

tensile strength of concrete considering yield stress σ_y, A_g = gross are of column, *DIF* =dynamic increase factor accounting for increase in strength of concrete due to strain rate (Mander et al. 1988).

The probabilistic model to estimate the strain rate is proposed in this research by

$$\ln \dot{\varepsilon} = \begin{bmatrix} 1 & \ln k_r & \ln(v_s/15) & \ln(m_v/2000) \end{bmatrix} \begin{bmatrix} \theta_{\dot{\varepsilon}1} & \theta_{\dot{\varepsilon}2} & \theta_{\dot{\varepsilon}3} & \theta_{\dot{\varepsilon}4} \end{bmatrix}^T + \sigma_{\dot{\varepsilon}} e_{\dot{\varepsilon}} \quad (7.5)$$

where, $\dot{\varepsilon}$ = predicted strain rate (1/s), k_r = stiffness ratio as defined above, $v_s = \frac{m_v}{m_v + m_c} v_0$ is the system velocity (m/s), m_v = mass of vehicle (kg), $\sigma_{\dot{\varepsilon}} e_{\dot{\varepsilon}}$ model error for strain rate model; $e_{\dot{\varepsilon}}$ = random variable with zero mean and unit variance and normal distribution (normality assumption); $\sigma_{\dot{\varepsilon}}$ = standard deviation of the model error, which is assumed to be independent of **x** (homoskedasticity assumption). A noninformative prior is selected to estimate the parameters. The posterior estimate of the parameters is given in Table 7.1. The median estimate of the probabilistic model is given by

$$\dot{\varepsilon} = 0.4(k_r)^{1/5}(v_s/15)^{1.5}(m_v/2000)^{3/5} \quad (7.6)$$

Table 7.1. Posterior Statistics of Parameters in Strain Rate $\dot{\varepsilon}$ Model.

Parameter	Mean	Standard deviation	Correlation Coefficient				
			$\theta_{\dot{\varepsilon}1}$	$\theta_{\dot{\varepsilon}2}$	$\theta_{\dot{\varepsilon}3}$	$\theta_{\dot{\varepsilon}4}$	$\sigma_{\dot{\varepsilon}}$
$\theta_{\dot{\varepsilon}1}$	−0.871	0.791	1.00				
$\theta_{\dot{\varepsilon}2}$	0.213	0.139	−0.97	1.00			
$\theta_{\dot{\varepsilon}3}$	1.510	0.110	−0.26	0.27	1.00		
$\theta_{\dot{\varepsilon}4}$	0.594	0.076	−0.40	0.17	−0.14	1.00	
$\sigma_{\dot{\varepsilon}}$	0.602	0.038	0.01	−0.01	0.02	0.00	1.00

Fig. 7.3 shows a comparison between the measured and predicted values of the strain rate. The median predictions are shown for the probabilistic model.

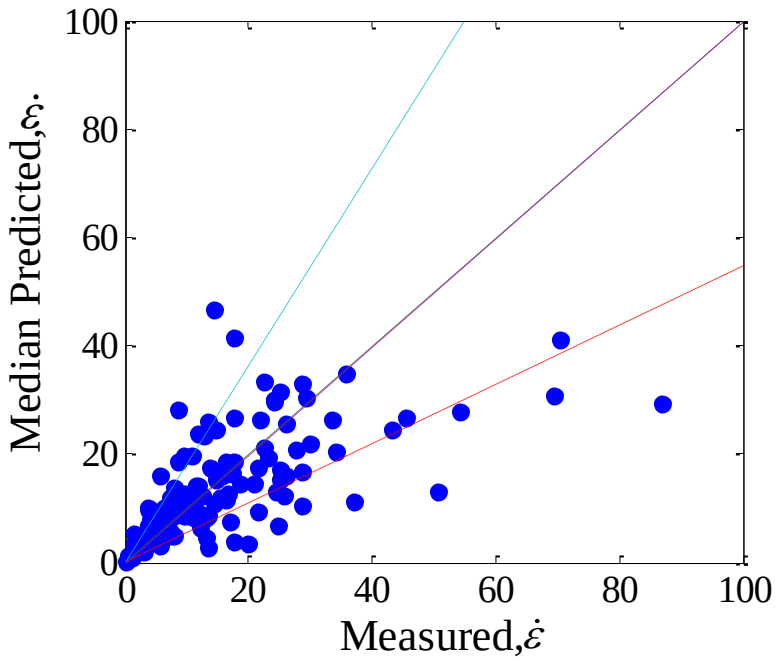

Fig. 7.3. Comparison between measured and predicted strain rate $\dot{\varepsilon}$.

For a perfect model, the failure data should line up along the 1:1 line. The dashed lines indicate the bounds obtained as the ±1 standard deviation (SD). The median of Equation 7.5 is assessed using the data generated from experimental design. The median of the model in the Equation 7.6 is used in Equations 7.4 and 7.7.

7.4 Mechanical Model for Performance Level P3

The estimate of the dynamic shear resistance for P3 is proposed in this dissertation by

$$\hat{V}_{P3} = \frac{2.4 f'_{cc} I_c H^3 DIF}{D_g H_a H_b^2 (H_a + 2H)} \tag{7.7}$$

where f'_{cc} = compressive strength of confined concrete.

7.5 Model Correction

The model correction terms are used to capture the physical phenomena that are not accounted for in the mechanical model. Table 7.2 lists the selected explanatory functions. The table also lists the physical quantity which influences the model and is captured by the explanatory functions. All functions are dimensionless.

Table 7.2. List of Explanatory Functions for Resistance Models.

Variable	Description	Expression
$h_1(\mathbf{x})$	constant bias	1
$h_2(\mathbf{x})$	longitudinal reinforcement	ρ_l
$h_3(\mathbf{x})$	axial load	$ND_g / (f'_{ty} A_g L)$
$h_4(\mathbf{x})$	transverse reinforcement	$A_v f_{yh} D_g / (f'_{ty} A_g s)$
$h_5(\mathbf{x})$	energy	$(m_v + m_c) v_s^2 / m_v v_0^2$
$h_6(\mathbf{x})$	inertia	$(m_v + m_c) / m_v$
$h_7(\mathbf{x})$	frequency	$t_c f_e$
$h_8(\mathbf{x})$	slenderness ratio	H / D_g
$h_9(\mathbf{x})$	Stress	$f'_{cc} DIF / \sigma_y$
$h_{10}(\mathbf{x})$	acceleration	$(m_v + m_c) v_s / (f'_{ty} t_c A_g)$
$h_{11}(\mathbf{x})$	displacement	d_f / H
$h_{12}(\mathbf{x})$	stiffness ratio	k_r
$h_{13}(\mathbf{x})$		$\ln h_4(\mathbf{x})$
$h_{14}(\mathbf{x})$		$\ln h_9(\mathbf{x})$
$h_{15}(\mathbf{x})$		$\ln h_{10}(\mathbf{x})$
$h_{16}(\mathbf{x})$		$\ln \hat{v}_{P1}$

The first explanatory function $h_1(\mathbf{x})$ is designed to capture a potential constant bias present in the mechanical model. The second explanatory function $h_2(\mathbf{x})$ accounts for the contribution of the longitudinal reinforcement to the dynamic shear resistance. The imposed load at the top of the RC column affects its behavior in bending and shear. The third explanatory function $h_3(\mathbf{x})$ accounts for this effect. The fourth explanatory function $h_4(\mathbf{x})$ accounts for the contribution of the transverse reinforcement to the dynamic shear resistance. The effect of energy transferred to the column from the vehicle is accounted by the fifth explanatory function $h_5(\mathbf{x})$. In a dynamic scenario, the

inertia contributes to resist the imposed load. The sixth explanatory function $h_6(\mathbf{x})$ takes into consideration this contribution. The contribution of the natural frequency and the time of applied loading are accounted by the seventh explanatory function $h_7(\mathbf{x})$.

In the definition of $h_7(\mathbf{x})$, f_e = the natural frequency of the column written as $f_e = \sqrt{k_c / m_e}$, where $m_e = m_v + m_r m_c =$ equivalent mass of the system, $m_r = \left[\int_0^{H_a} [\phi_1(x)]^2 + \int_{H_a}^{H} [\phi_2(x)]^2 \right] / H \left[\max(\phi_1, \phi_2) \right]^2$ = mass ratio of the column, t_c = the time period of the collision.

The time period t_c of the collision is given by the following expression (Goldsmith 1960)

$$t_c = \frac{\pi \alpha_m}{1.068 v_s} \tag{7.8}$$

where, $\alpha_m = \left[\frac{5 v_s^2}{4 k_1 k_2} \right]^{2/5}$, $k_1 = \frac{m_c + m_v}{m_c m_v}$, $k_2 = \frac{4 q_k}{3(\delta_1 + \delta_2)(A + B)}$, $q_k = 0.318$, $\delta_1 = \frac{1 - \mu_v^2}{E_v \pi}$, $\delta_2 = \frac{1 - \mu_c^2}{E_c \pi}$, $A = B = \frac{1}{D_g - 2c - d_s}$.

The slenderness ratio is the eighth explanatory function $h_8(\mathbf{x})$ that accounts for the potential effect of the slenderness on the dynamic shear resistance.

The effect of state of stress is modeled by $h_9(\mathbf{x})$. The effect of the acceleration of the bodies is accounted by $h_{10}(\mathbf{x})$. The effect of the deformation of the RC column is accounted by $h_{11}(\mathbf{x})$. The contribution of bending stiffness is accounted by the 12th

explanatory function $h_{12}(\mathbf{x})$. Finally, $h_{13}(\mathbf{x}), h_{14}(\mathbf{x}), h_{15}(\mathbf{x})$, and $h_{16}(\mathbf{x})$ take into account the nonlinear contributions of the transverse reinforcement, the state of stress, the acceleration and the normalized dynamic shear resistance for performance level P1 by taking the natural logarithm of $h_4(\mathbf{x})$, $h_9(\mathbf{x})$, $h_{10}(\mathbf{x})$ and $\hat{v}_{P1}$ respectively.

7.6 Model Assessment

Bayesian inference is chosen for the estimation of the model parameters $\boldsymbol{\Theta}$. A noninformative prior is selected (Box & Tiao 1992). A step wise deletion process is used for selecting the parsimonious model. In this method, diagnostic plots are created between the explanatory function and the residual of the dynamic shear resistance of the FE model and the mechanical model. Suitable explanatory functions are chosen one at a time which shows the strongest correlation. The mean of the standard deviation is monitored to check the adequacy of the model.

7.7 Parameter Estimation for Performance Level P1

The most important explanatory functions for the performance level P1 are $h_{13}(\mathbf{x})$, $h_{14}(\mathbf{x}), h_{15}(\mathbf{x})$,and $h_{16}(\mathbf{x})$. These terms takes into account the contributions from the transverse reinforcement, the state of stress, the acceleration and $\hat{v}_{P1}$. Table 7.3 lists the posterior statistics of the model.

Table 7.3. Posterior Statistics of Parameters in Selected Dynamic Resistance (P1) Model.

Parameter	Mean	Standard deviation	Correlation Coefficient				
			θ_{13}	θ_{14}	θ_{15}	θ_{16}	σ_{P1}
θ_{13}	1.244	0.224	1.00				
θ_{14}	−1.965	0.656	−0.85	1.00			
θ_{15}	−0.530	0.136	0.66	−0.76	1.00		
θ_{16}	−0.362	0.267	0.30	−0.34	0.86	1.00	
σ_{P1}	1.035	0.096	0.00	0.00	0.00	0.00	1.00

Fig. 7.4 shows the comparison between the estimates of normalized dynamic shear resistance based on the proposed mechanical model (left) and the median of the developed probabilistic model (right) where the median predication for the normalized dynamic shear resistance v_{P1} is given by

$$v_{P1} = \hat{v}_{P1}^{-0.362} \left[\frac{A_v f_{yh} D_g}{f'_{ty} A_g s} \right]^{1.244} \left[\frac{f'_{cc} DIF}{\sigma_y} \right]^{-1.965} \left[\frac{(m_v + m_c) v_s}{f'_{ty} t_c A_g} \right]^{-0.53} \tag{7.9}$$

$v_{P1} = V_{P1} / f'_t A_g$ normalized dynamic shear resistance, and $\hat{v}_{P1} = \hat{V}_{P1} / f'_t A_g$ normalized dynamic shear resistance given by the mechanical model.

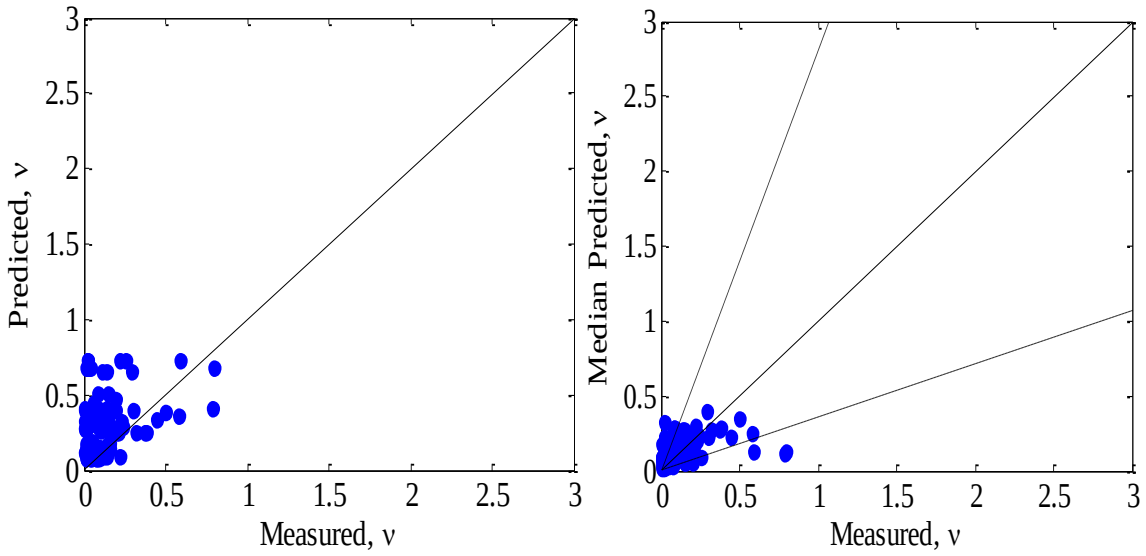

Fig. 7.4. Comparison between measured and predicted Dynamic Shear Resistance for P1 based on deterministic (left) and probabilistic (right) models.

The mechanical and probabilistic models are both plotted against the resistance values estimated from the simulations. All the data are equality data as the Performance Level P1 was reached in all simulated cases. The predictions of mechanical model are biased as majority of the data lies above the 1:1 line. The probabilistic model corrects this bias.

7.8 Parameter Estimation for Performance Level P2

The most important explanatory functions for the performance level P2 are $h_1(\mathbf{x})$, $h_2(\mathbf{x})$, $h_3(\mathbf{x})$, and $h_9(\mathbf{x})$. These terms correct for a constant bias, and account for the influence

of longitudinal reinforcement, the contribution of applied load at the top, and the stress in the column, respectively. Table 7.4 lists the posterior statistics of the model.

Table 7.4. Posterior Statistics of Parameters in Selected Dynamic Shear Resistance (P2) Model.

Parameter	Mean	Standard deviation	Correlation Coefficient				
			θ_1	θ_2	θ_3	θ_9	σ_{P2}
θ_1	−2.577	0.269	1.00				
θ_2	0.243	0.044	−0.54	1.00			
θ_3	0.904	0.247	−0.40	0.17	1.00		
θ_9	0.846	0.125	−0.83	0.09	0.14	1.00	
σ_{P2}	0.525	0.041	−0.08	0.08	0.14	0.05	1.00

Fig. 7.5 shows the comparison between the estimates of normalized dynamic shear resistance based on the proposed mechanical model (left) and the median of the developed probabilistic model (right) where, the median predication for the normalized dynamic shear resistance v_{P2} is given by

$$v_{P2} = \hat{v}_{P2} \exp\left[-2.577 + 0.243\rho_l + 0.904 \frac{PD_g}{f'_{ty} A_g L} + 0.846 \frac{f'_{cc} DIF}{\sigma_y} \right] \tag{7.10}$$

where, $v_{P2} = V_{P2} / f'_c A_g$ normalized dynamic shear resistance, $\hat{v}_{P2} = \hat{V}_{P2} / f'_c A_g$ normalized dynamic shear resistance given by the mechanical model.

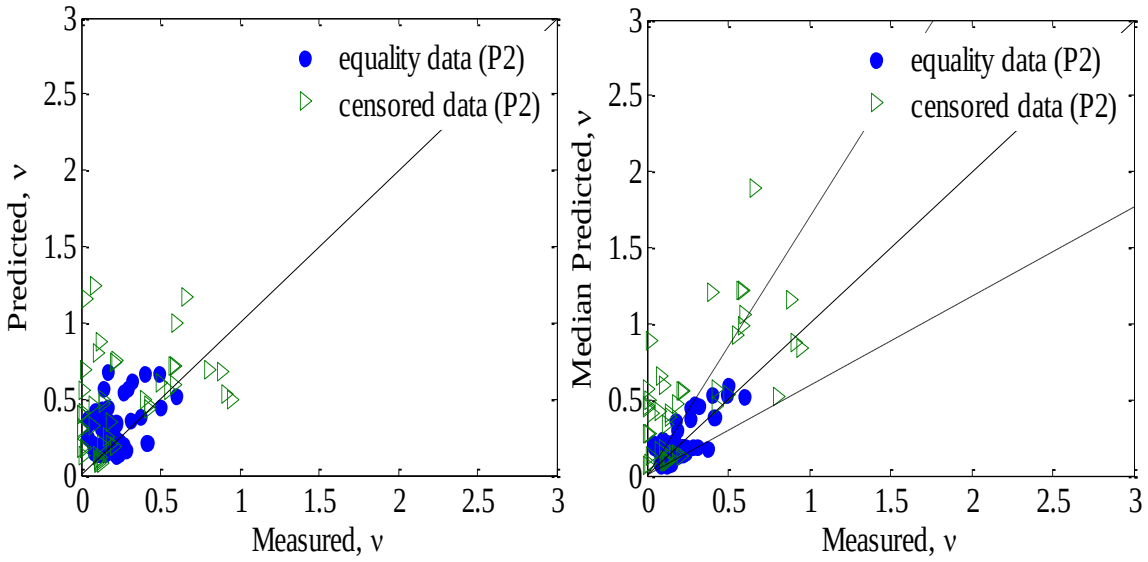

Fig. 7.5. Comparison between measured and predicted Dynamic Shear Resistance for P2 based on deterministic (left) and probabilistic (right) models.

The mechanical and probabilistic models are both plotted against the resistance values estimated from the simulations. The data contains equality data as well as the censored data for the Performance Level P2. The predictions of mechanical model shows that the equality data lays both above and below the 1:1 line and majority of censored data lies above the line. The probabilistic model corrects this inherent bias in the model.

7.9 Parameter Estimation for Performance Level P3

The most important explanatory functions for the performance level P3 are $h_1(\mathbf{x}), h_3(\mathbf{x}),$ $h_6(\mathbf{x})$,and $h_{12}(\mathbf{x})$. These terms takes into correct for a constant bias, the contribution of

applied load at the top, the inertia and the stiffness of the column, respectively. Table 7.5 lists the posterior statistics of the model.

Table 7.5. Posterior Statistics of Parameters in Selected Dynamic Shear Resistance (P3) Model.

Parameter	Mean	Standard deviation	Correlation Coefficient				
			θ_1	θ_3	θ_6	θ_{12}	σ_{P3}
θ_1	0.336	0.268	1.00				
θ_3	−2.434	0.329	−0.03	1.00			
θ_6	0.679	0.253	−0.68	−0.60	1.00		
θ_{12}	−0.005	0.001	−0.27	0.69	−0.49	1.00	
σ_{P3}	0.429	0.040	−0.22	0.02	0.22	0.00	1.00

Fig. 7.6 shows the comparison between the estimates of normalized dynamic shear resistance based on the proposed mechanical model (left) and the median of the developed probabilistic model (right) where the median predication for the normalized dynamic shear resistance v_{P3} is given by

$$v_{P3} = \hat{v}_{P3} \exp\left[0.336 - 2.434 \frac{PD_g}{f'_{ty} A_g L} + 0.679 \frac{m_v + m_c}{m_v} - 0.005 k_r \right] \tag{7.11}$$

where, $v_{P3} = V_{P3} / f'_c A_g$ normalized dynamic shear resistance, $\hat{v}_{P3} = \hat{V}_{P3} / f'_c A_g$ normalized dynamic shear resistance given by the mechanical model.

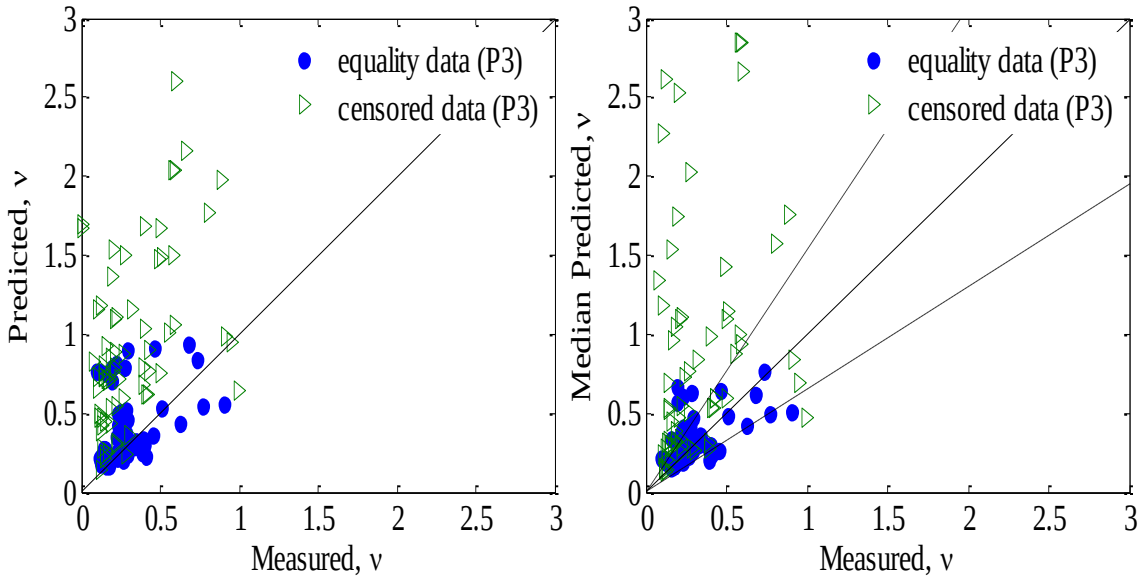

Fig. 7.6. Comparison between measured and predicted Dynamic Shear Resistance for performance level P3 based on deterministic (left) and probabilistic (right) models.

The mechanical and probabilistic models are both plotted against the resistance values estimated from the simulations. The data contains equality data as well as the censored data for the Performance Level P3. The predictions of mechanical model shows that the equality data lays both above and below the 1:1 line and majority of censored data lies above the line. The probabilistic model corrects this inherent bias in the model.

The proposed mechanical model is compared with the shear model proposed by Moehle et al. (1999, 2000), which is a refinement of the FEMA 273 (1997) model. Table 7.6 presents comparison of the model statistics for the two model forms. Four model statistics are used for the comparison and selection of the model form, the

standard deviation of the model form, the Akaike Information Criterion (Akaike, 1974), Bayesian Information Criterion (Schwarz, 1978), Mean Absolute Percentage Error (MAPE).

Table 7.6. Comparison of Model Statistics for the Different Developed Models for P3.

$\hat{v}_{P3}(\mathbf{x})$ based on	Number of terms in $\gamma(\mathbf{x},\boldsymbol{\theta})$	σ	*AIC*	*BIC*	*MAPE*(%)
Moehle et al. (1999, 2000), refinement of FEMA 273 (1997)	4	0.464	−231.8	−223.3	42.9
⟶Proposed Model	4	0.429	−231.0	−222.5	38.8

The proposed mechanical model form has smaller values of standard deviation, AIC, BIC, and MAPE among the models.

$$AIC = -2\ln(L) + 2N_p \tag{7.12}$$

$$BIC = -2\ln(L) + N_P \ln(N_S) \tag{7.13}$$

$$MAPE = \frac{1}{N_s}\sum_{i=1}^{n}\left|\frac{\text{Measured},\nu - \text{Predicted},\nu}{\text{Measured},\nu}\right| \times 100 \tag{7.14}$$

where, L= maximum of the likelihood function for the estimated model, N_k= number of explanatory function, N_s= sample size.

7.10 Fragility Estimates

The fragility estimates gives an estimate of the reliability of the bridge with the variation in the demand imposed to the RC column. It also shows the behavior of the different performance levels with the variation in the demand imposed on the RC column. The fragility of the RC column subjected to vehicle column is formulated as

$$F(\mathbf{x},\boldsymbol{\Theta}) = P[g(\mathbf{x},\boldsymbol{\Theta}) \le 0 \mid v_D] \tag{7.15}$$

where, $g_{Pi}(\mathbf{x},\boldsymbol{\Theta})$ is the limit state function defined as

$$g_{Pi}(\mathbf{x},\boldsymbol{\Theta}) = v_{Pi}(\mathbf{x},\boldsymbol{\Theta}) - v_D, \quad Pi = 1,2,3 \tag{7.16}$$

for the three performance levels P1, P2, and P3. The fragility of a representative RC column is estimated by directly conditioning on the dynamic shear demand. The configuration and properties of the RC column is taken same as the exterior bridge column which was subject to an impact by a tractor-trailer over IH-20 at Longview, Texas (Buth, 2009). Fig. 4.3 shows the comparison of the FE simulation and the crash photograph of the column. A general agreement on the observed failure mechanism of the RC column and crack pattern is shown in Fig. 4.3. Fig. 7.7 shows the fragility estimates of the RC column for the three performance levels.

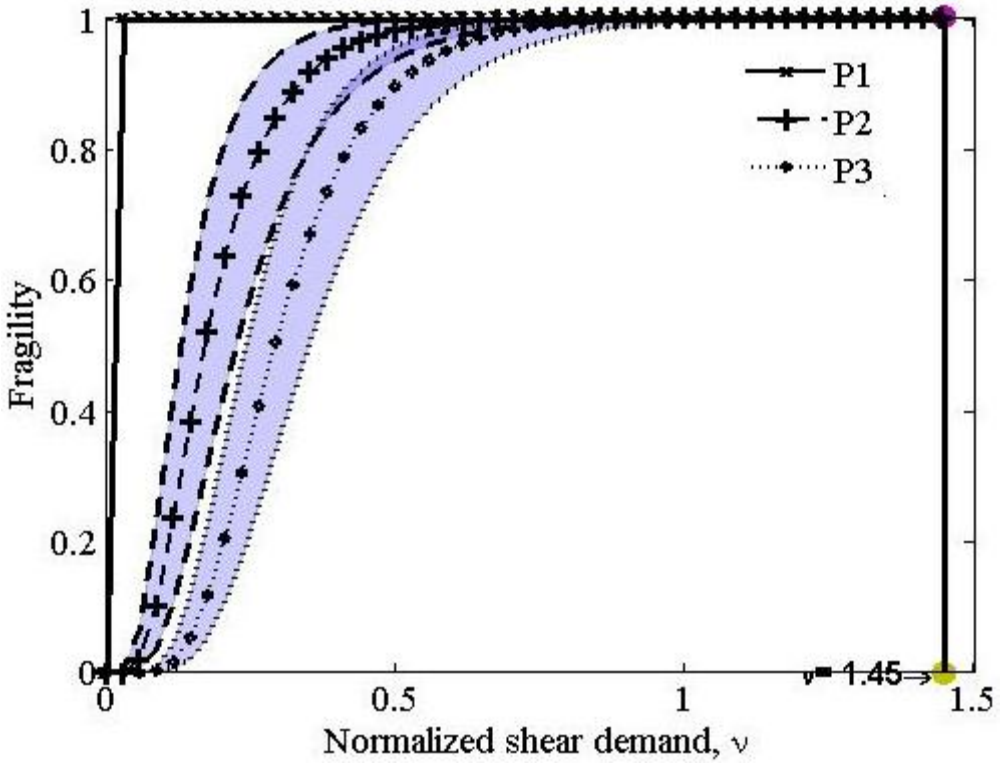

Fig. 7.7. Fragility curves for case study structure for P1, P2 and P3.

The fragility estimate is directly conditioned on the normalized dynamic shear demand. The performance level P1 depicted by solid line. The performance level P2 is shown by dashed lines and performance level P3 is shown by dotted lines. The 15% and 85% confidence bound for each performance level is also shown in the figure. The performance level P1 has the steepest curve as compared to other performance levels. The performance level P3 has the least steep curve as it is the collapse limit state and it takes more shear demand to achieve a state of collapse. The normalized dynamic shear demand imposed on the RC column is 1.45 as calculated from the simulation. For this

value the failure probability of performance levels P1, P2, and P3 is 1.0. The RC column lies in the damage state D4 as $P_{D4}=P_{P3}=1$ as shown in the figure. This is consistent with the observed occurrence in the field. The RC column failed during this vehicle collision. This is reflected by the state of RC column being in damage state 4 and probability of failure of all performance levels being 1. This establishes the validity of the developed models for P1, P2, and P3 and the framework to estimate the reliability of the RC column.

7.11 Conclusion

In the present section a performance-based resistance models are developed which can be used to achieve the desired behavior of the RC column under different impact scenarios. The probabilistic resistance model captures the dynamic behavior of the RC column and accounts for the associated uncertainties. A framework to assess the fragility of RC column subjected to vehicle impact is developed. The framework provides an accurate estimate of the fragility. The performance-based dynamic resistance can be used to determine the performance of structure in a given scenario and evaluate the survival of the structure. Actual structural configurations and loading scenarios are used to evaluate the response which is more accurate in representing the complex impact scenario.

The developed models advance the knowledge of behavior of RC columns subject to vehicle collision. The model is simple and easy to implement. This work can be extended to develop a demand model for the bridge system and enhance the goal of a

reliability based design. The developed models can be used to design safer columns and the work can be extended to other structures under similar loading conditions. The state of knowledge can be applied to study similar cases of collision such as ship collision to a barge, projectile collision into concrete walls and develop adequate models.

8 DYNAMIC SHEAR FORCE DEMAND MODEL

Using the results of the FE simulations, this section develops probabilistic models for estimating the dynamic shear force demand on RC columns subject to vehicle collision. The model take into account the relevant uncertainties including model error and statistical uncertainty as described in Gardoni et al. (2002). Because the data used for the model assessment come from FE simulations, it is assumed that there is no measurement error in the data. The probabilistic model is unbiased and incorporates current understanding on the mechanics of the problem. The natural logarithm is used to stabilize the model variance to satisfy the homoskedasticity and the normality assumptions. Following the general formulation for probabilistic models proposed by Gardoni et al. (2002), the dynamic shear force demand model is formulated as

$$\ln[v_D(\mathbf{x},\boldsymbol{\Theta})] = \ln[\hat{v}_D(\mathbf{x})] + \gamma_D(\mathbf{x},\boldsymbol{\theta}) + \sigma_D e_D \tag{8.1}$$

where $v_D = V_D / NF_D$ = normalized dynamic shear force demand, V_D = dynamic shear force demand, NF_D = normalizing factor for dynamic shear force demand; $\hat{v}_D(\mathbf{x})$ = normalized dynamic shear force demand obtained from mechanical model $\hat{V}_D$, $\gamma_D(\mathbf{x},\boldsymbol{\theta})$ = correction term for the bias inherit in the mechanical model for demand is defined as

$$\gamma_D(\mathbf{x},\boldsymbol{\theta}) = \sum_{j=1}^{k_D} \theta_{D,j} h_{D,j}(\mathbf{x}) \tag{8.2}$$

where $h_{D,j}(\mathbf{x}), j = 1,...,k$ = explanatory function and $\theta_{D,j}(\mathbf{x}), j = 1,...,k$ is the parameter associated with the explanatory function, $\sigma_D e_D$ model error for demand model; e_D =

random variable with zero mean and unit variance and normal distribution (normality assumption); σ_D = standard deviation of the model error, which is assumed to be independent of $\mathbf{x}$ (homoskedasticity assumption), and $\boldsymbol{\Theta}=(\boldsymbol{\theta},\boldsymbol{\sigma})$ = set of unknowns model parameters.

The maximum shear force calculated in each FE simulation is classified as an equality datum as the calculated value is the actual estimate of the force applied to the RC column.

8.1 Mechanical Model

The estimate of the dynamic shear force demand is proposed in this dissertation by the following equation which has contributions from Hertz's contact law (Goldsmith 1960) and force utilized for the deformation of the vehicle

$$\hat{V}_D = \frac{0.26v_s^2}{k_1\alpha_m} - k_v d_f \tag{8.3}$$

where, $d_f = \frac{0.4 f'_{cc} DIFH^3 H_a^{0.5}}{D_g E_c (H_a + 2H)^{3/2}}$ = deformation of the bodies at failure, $v_s = \frac{m_v}{m_v + m_c} v_0$ is the system velocity (m/s), m_v = mass of the vehicle, m_c = mass of the column,. E_c = modulus of concrete of RC column, E_v = modulus of steel of the vehicle, μ_c = poisson's ratio of concrete of the RC column, μ_v = poisson's ratio of steel of the vehicle.

8.2 Model Correction

The model correction terms are used to capture the physical phenomena that are not accounted for in the mechanical model. Table 8.1 lists the explanatory functions. The table also lists the physical quantity which influences the model and is captured by the explanatory functions. All functions are dimensionless.

Table 8.1. List of Explanatory Functions for Demand Model.

Variable	Description	Expression
$h_1(\mathbf{x})$	constant bias	1
$h_2(\mathbf{x})$	longitudinal reinforcement	ρ_l
$h_3(\mathbf{x})$	axial load	$ND_g / (f'_{ty} A_g L)$
$h_4(\mathbf{x})$	transverse reinforcement	$A_v f_{yh} D_g / (f'_{ty} A_g s)$
$h_5(\mathbf{x})$	energy	$(m_v + m_c) v_s^2 / m_v v_0^2$
$h_6(\mathbf{x})$	inertia	$(m_v + m_c) / m_v$
$h_7(\mathbf{x})$	frequency	$t_c f_e$
$h_8(\mathbf{x})$	slenderness ratio	H / D_g
$h_9(\mathbf{x})$	stress	$f'_{cc} DIF / \sigma_y$
$h_{10}(\mathbf{x})$	acceleration	$(m_v + m_c) v_s / (f'_{ty} t_c A_g)$
$h_{11}(\mathbf{x})$	displacement	d_f / H
$h_{12}(\mathbf{x})$	stiffness ratio	k_r

The first explanatory function $h_1(\mathbf{x})$ is designed to capture a potential constant bias present in the mechanical model. The second explanatory function $h_2(\mathbf{x})$ accounts for the contribution of the longitudinal reinforcement to the dynamic shear force demand. The imposed load at the top of the RC column affects the column behavior in bending and shear. The third explanatory function $h_3(\mathbf{x})$ accounts for this effect. The

fourth explanatory function $h_4(\mathbf{x})$ accounts for the contribution of the transverse reinforcement to the dynamic shear force demand. The effect of energy transferred to the column from the vehicle is accounted by the fifth explanatory function $h_5(\mathbf{x})$. In a dynamic scenario, the inertia contributes to resist the imposed load. The sixth explanatory function $h_6(\mathbf{x})$ takes into consideration this contribution. The contribution of the natural frequency and the time of applied loading are accounted by the seventh explanatory function $h_7(\mathbf{x})$. The slenderness ratio is the eighth explanatory function $h_8(\mathbf{x})$ that accounts for the potential effect of the slenderness on the dynamic shear force demand.

The effect of state of stress is modeled by $h_9(\mathbf{x})$. The effect of the acceleration of the bodies is accounted by $h_{10}(\mathbf{x})$. The effect of the deformation of the RC column is accounted by $h_{11}(\mathbf{x})$. The contribution of bending stiffness is accounted by $h_{12}(\mathbf{x})$.

8.3 Model Assessment

Bayesian inference is chosen for the estimation of the model parameters. A noninformative prior is selected (Box & Tiao 1992). A step wise deletion process is used to obtain a parsimonious model. In this method, diagnostic plots are created between the explanatory function and the residual of the dynamic shear demand on the FE model and the mechanical model. Suitable explanatory functions are chosen one at a time which shows the strongest correlation. The mean of the standard deviation is monitored to check the adequacy of the model.

8.4 Parameter Estimation

The most important explanatory functions for the dynamic shear force demand are $h_1(\mathbf{x})$, $h_5(\mathbf{x})$, $h_6(\mathbf{x})$,and $h_{10}(\mathbf{x})$. These terms takes correct for a constant bias, and account for the energy of the system, the inertia of the system, the contribution of acceleration, respectively. Table 8.2 lists the posterior statistics of the model.

Table 8.2. Posterior Statistics of Parameters in Selected Dynamic Shear Demand Model.

Parameter	Mean	Standard deviation	Correlation Coefficient				
			θ_1	θ_5	θ_6	θ_{10}	σ_D
θ_1	−1.630	0.294	1.00				
θ_5	0.884	0.351	−0.97	1.00			
θ_6	0.208	0.047	−0.87	0.76	1.00		
θ_{10}	0.002	0.000	0.52	−0.65	−0.35	1.00	
σ_D	0.427	0.026	−0.01	0.01	−0.00	−0.02	1.00

Fig. 8.1 shows the comparison between the estimates of normalized dynamic shear force demand based on the proposed mechanical model (left) and the median of the developed probabilistic model (right) where, the median predication for the normalized dynamic shear force demand v_D is given by

$$v_D = \hat{v}_D \exp\left[-1.63 + 0.884 \frac{(m_v + m_c)v_s^2}{m_v v_0^2} + 0.208 \frac{m_v + m_c}{m_v} + 0.002 \frac{(m_v + m_c)v_s}{f'_{ty} t_c A_g} \right] \tag{8.4}$$

where, $v_D = \dfrac{V_D}{2 f'_{cc} DIFA_g}$ normalized dynamic shear force demand, $\hat{v}_D = \dfrac{\hat{V}_D}{2 f'_{cc} DIFA_g}$ normalized dynamic shear force demand given by the mechanical model.. The

mechanical and probabilistic models are both plotted against the demand values estimated from the simulations.

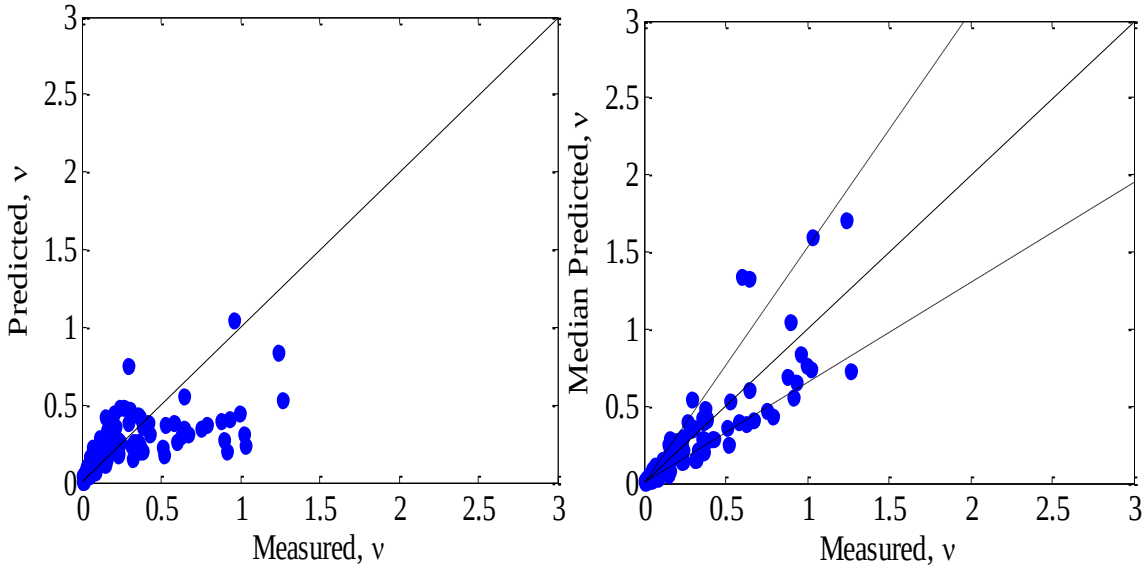

Fig. 8.1. Comparison between measured and predicted Dynamic Shear Demand based on deterministic (left) and probabilistic (right) models.

The prediction of mechanical model shows that the data lies both above and below the 1:1 line. The probabilistic model corrects the inherent bias in the model. In the probabilistic model the spread of the data is minimized as that they lie close to the 1:1 line as compared to the mechanical model.

8.5 Fragility Estimates

The fragility estimates gives an estimate of the reliability of the bridge with the variation in the demand imposed to the RC column. It also shows the behavior of the different performance levels with the variation in the demand imposed on the RC column. The fragility of the RC column subjected to vehicle column is formulated as

$$F(\mathbf{x},\boldsymbol{\Theta}) = P[g(\mathbf{x},\boldsymbol{\Theta}) \le 0 \,|\, (v_0, m_v)] \tag{8.5}$$

where, $g_{Pi}(\mathbf{x},\boldsymbol{\Theta})$ is the limit state function defined as

$$g_{Pi}(\mathbf{x},\boldsymbol{\Theta}) = v_{Pi}(\mathbf{x},\boldsymbol{\Theta}) - v_D, \quad Pi = 1,2,3 \tag{8.6}$$

for the three performance levels P1, P2, and P3. The performance-based probabilistic models for the three performance levels P1, P2, and P3 are constructed in previous section. The fragility of a representative RC column is estimated by conditioning on the initial velocity of the vehicle is v_0 and mass of the vehicle is m_v. The configuration and properties of the RC column is taken same as the exterior bridge column which was subject to an impact by a tractor-trailer over IH-20 at Longview, Texas (Buth, 2009). Fig. 8.2 shows the contour plot for the fragility estimates of the RC column for performance level 1.

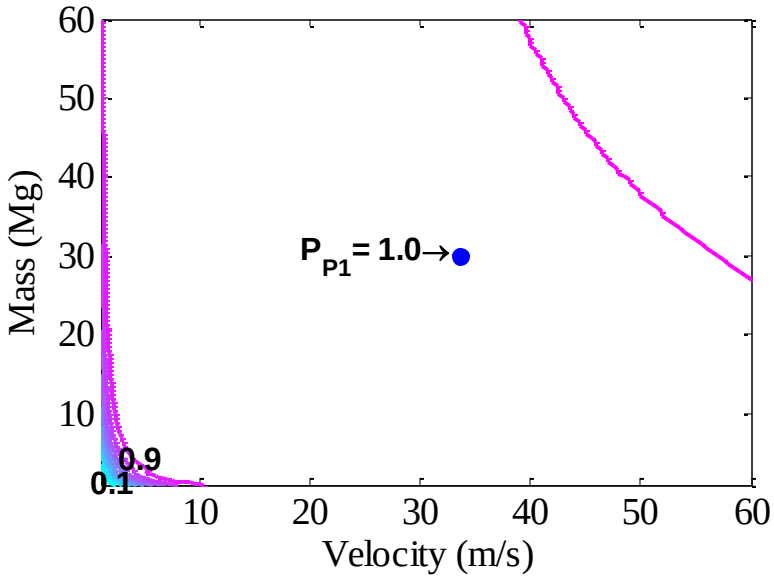

Fig. 8.2. Contour plot for the fragility estimate for the RC column for P1.

The plot is done with range of initial velocity of the vehicle (m/s) on x axis and range of mass of the vehicle (Mg) on y axis. The contours show the variation of the fragility over the domain of the velocity and mass. For the performance level P1, there is steep increase in the value of the fragility from 0.1 to 0.9 as shown in the Fig. 8.2. This is because the performance level P1 is exceeded with a low value of the dynamic shear demand. The figure also shows that the fragility estimate of the RC column located over IH-20 at Longview, Texas is 1. The result is in accordance of the observation in the field as the RC column failed after the collision with the vehicle. So, the probability of failure of performance level P1 is 1 which is shown in Fig. 8.2.

In accordance with the Fig. 8.2, Fig. 8.3 shows the contour plot for the fragility estimates of the RC column for performance level P2. The plot is done with range of

initial velocity of the vehicle (m/s) on x axis and range of mass of the vehicle (Mg) on y axis.

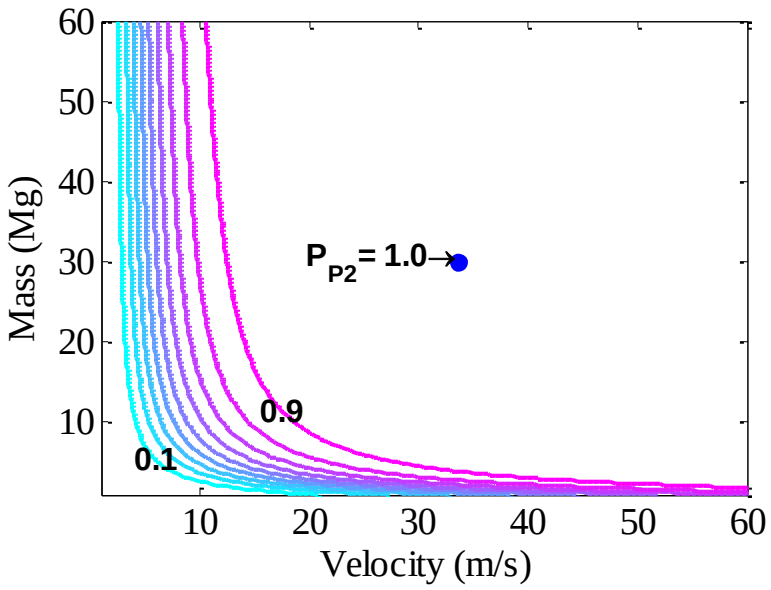

Fig. 8.3. Contour plot for the fragility estimate for the RC column for P2.

The contours show the variation of the fragility over the domain of the velocity and mass. The increase in the value of fragility is less steep than for performance level 1. This is because more shear demand is required to exceed the performance level P2 than performance level P1. There is a region velocity of the vehicle for which the fragility remains zero no matter how much the value of mass of vehicle is increased. Similarly a thin region also exists for the mass of the vehicle for which the increase in velocity of vehicle does not result in the increase in the value of the fragility. The figure also shows that the fragility estimate of the RC column located over IH-20 at Longview,

Texas is 1 for performance level P2. The result is in accordance of the observation in the field as the RC column failed after the collision with the vehicle. So, the probability of failure of performance level P2 is 1 which is shown in Fig. 8.3.

Continuing from Fig. 8.3, Fig. 8.4 shows the contour plot for the fragility estimates of the RC column for performance level P3. The plot is done with range of initial velocity of the vehicle (m/s) on x axis and range of mass of the vehicle (Mg) on y axis.

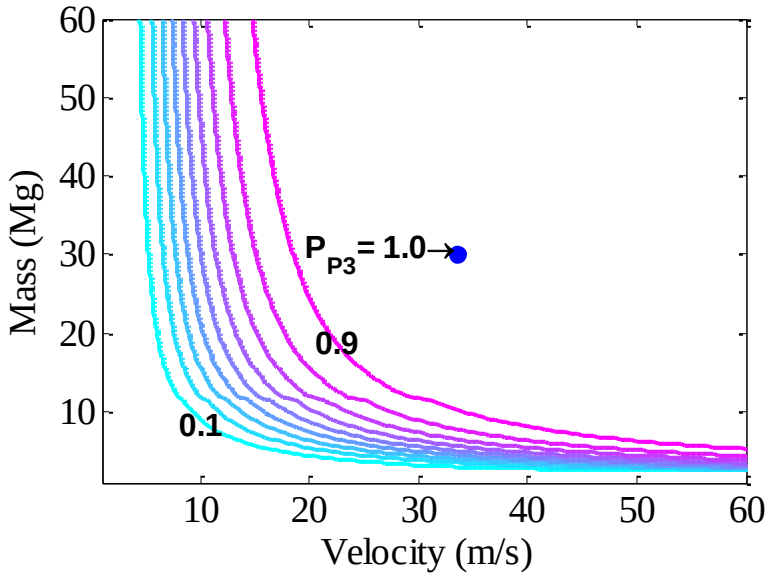

Fig. 8.4. Contour plot for the fragility estimate for the RC column for P3.

The contours show the variation of the fragility over the domain of the velocity and mass. The increase in the value of fragility is well spread and less steep than for performance level 2. This is because more shear demand is required to exceed the

performance level P3 than performance level P1 and P2. There is a region velocity of the vehicle for which the fragility remains zero no matter how much the value of mass of vehicle is increased and the region is greater than observed for performance level P2. Similarly a region for the mass of the vehicle for which the increase in velocity of vehicle does not result in the increase in the value of the fragility is also greater. The figure also shows that the fragility estimate of the RC column located over IH-20 at Longview, Texas is 1 for performance level P3. The result is in accordance of the observation in the field as the RC column failed after the collision with the vehicle. So, the probability of failure of performance level P3 is 1 which is shown in Fig. 8.4.

The results obtained from the contour plots of the fragility for three performance levels are consistent with the observed occurrence in the field. The RC column failed during this vehicle collision. This is reflected by probability of failure of all performance levels being 1. This establishes the validity of the developed models for performance levels P1, P2, and P3 and developed dynamic shear model and the framework to estimate the reliability of the RC column.

8.6 Conclusion

In the section, a performance-based demand model is developed which can be used to achieve the desired behavior of the RC column under different impact scenarios. The probabilistic demand model captures the dynamic interaction between the RC column the vehicle during collision and accounts for the associated uncertainties. A framework to assess the fragility of RC column subjected to vehicle impact based on performance-

based models is developed. The framework provides an accurate estimate of the fragility. The performance-based fragility estimates can be used to determine the performance of structure in a given scenario and evaluate the survival of the structure. Actual structural configurations and loading scenarios are used to evaluate the response which is more accurate in representing the complex impact scenario.

The section advances the knowledge of behavior of RC columns subject to vehicle collision. The developed demand model is simple and easy to implement. This work can be extended to develop load and resistance factors for the bridge system and enhance the goal of a reliability based design. The developed models can be used to design safer columns and the work can be extended to other structures under similar loading conditions. The state of knowledge can be applied to study similar cases of collision such as ship collision to a barge, projectile collision into concrete walls and develop adequate models.

9 RELIABILITY-BASED CODE CALIBRATION FOR RC COLUMNS

The performance-based dynamic shear force capacity and force models developed in previous sections are used to calibrate the load and resistance factors for RC columns subject to vehicle collision. Currently AASHTO -LRFD 2007 has a load factor of 1.0 for vehicle impact scenario. In the light of the present research, this load and resistance factors need to be revisited and reexamined. This section presents a code calibration for the RC column. The hazard curve for the mass of the vehicle and the velocity of the vehicle colliding with RC column are developed. This hazard curves are used for estimating the total probability of the failure/survival of the RC column subject to vehicle collision. The framework is developed to estimate the reliability of RC columns subject to vehicle impact under different hazard conditions as developed in Table 2.2. This approach ties the performance-based models to the relevant hazard scenarios and estimates the reliability of the RC column for desired response.

9.1 Hazard Curves

Buth et al. (2010) presents data for the collision of vehicles with RC column in Texas for the period of 1998-2001. This data is used to develop the hazard curve for the mass of the vehicle that collides with the RC column in this period. The inverse CDF approach is used to find the goodness-of-fit of the candidate distribution for the four year variation of the mass of the vehicle. Fig. 9.1 shows the comparison of the goodness-of-fit for the

candidate distributions. The data collected is plotted on the x-axis as mass of the vehicle in Mg. The mass of the vehicle predicted by the distributions is plotted on the y-axis in Mg. The distributions compared are 'Normal', 'Log-Normal', 'Extreme Type –I'. The prediction of Log-Normal and Extreme Type I distribution is closer than that of the 'Normal' distribution. Extreme Type I distribution is chosen as the best fit as it is closer than the Normal distribution and it has been used for the prediction of wind, snow and other extreme events.

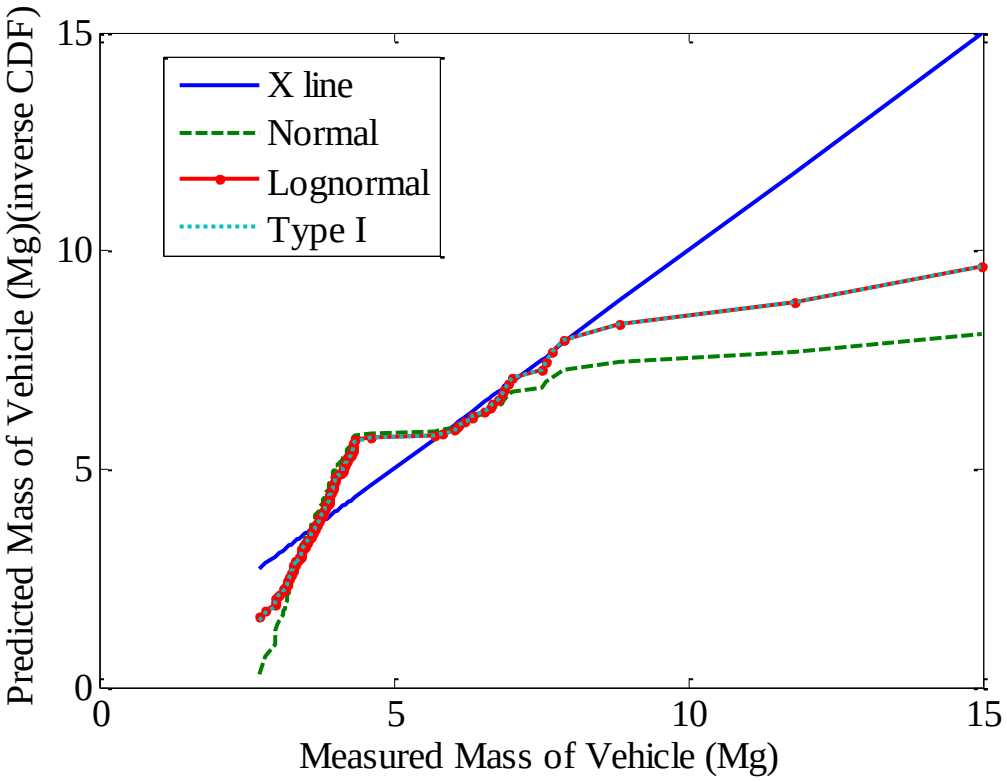

Fig. 9.1. Comparison of goodness-of-fit of the candidate distribution for four year variation of the mass of the vehicle.

The four year hazard curve based on the Extreme Type I distribution for the mass of the vehicle has parameters mean = 4.20 Mg and COV = 0.37. Fig. 9.2 shows the hazard curve developed for the four year exceeding probability of the mass of the vehicle and the corresponding PDF for the Extreme Type I distribution. The exceeding probability and $f(m_v)$ is plotted in the y-axis against mass of the vehicle plotted on the x-axis. The data collected had the lowest mass of the vehicle at 2.00 Mg. This is the reason for the sharp decline in the developed PDF for the mass of the vehicle.

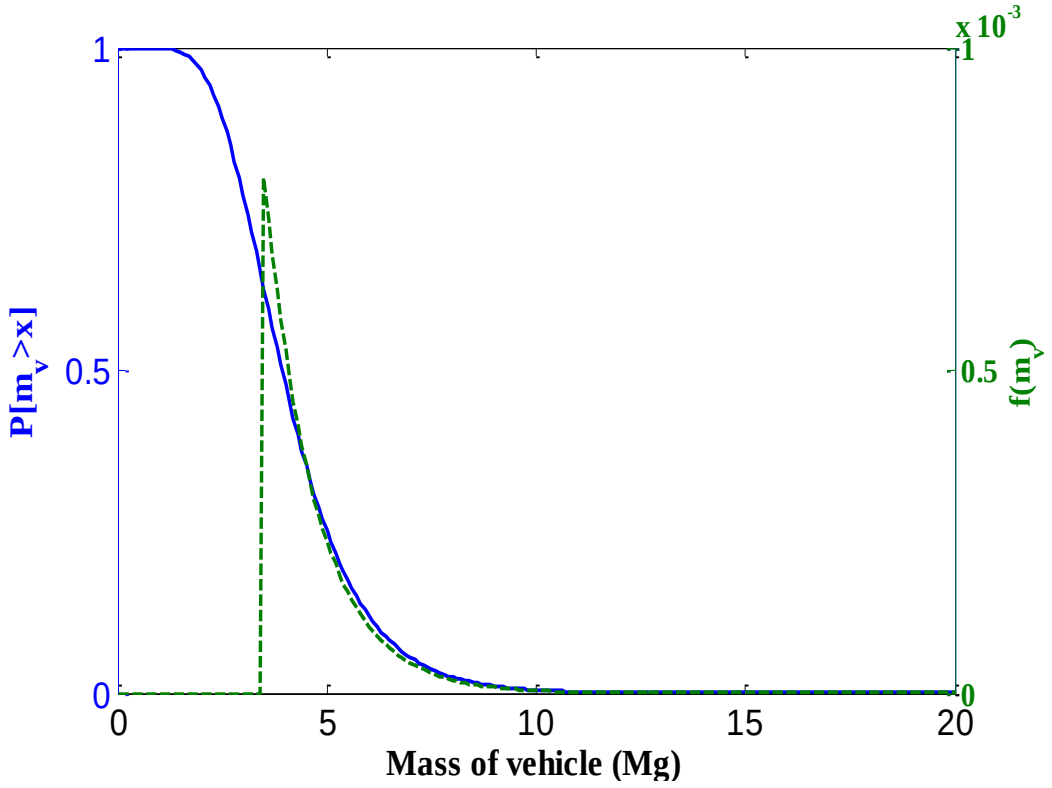

Fig. 9.2. Four year exceeding probability of the mass of the vehicle and PDF for Extreme Type I distribution.

Fig. 9.3 shows the hazard curves developed for the annual and 75 year exceeding probability of the mass of the vehicle and the corresponding PDF's for the Extreme Type I distribution. The exceeding probability and $f(m_v)$ is plotted in the y-axis against mass of the vehicle plotted on the x-axis. The annual hazard curve based on the Extreme Type I distribution for the mass of the vehicle has parameters mean = 2.46 Mg and COV = 0.64. The 75 year hazard curve based on the Extreme Type I distribution for the mass of the vehicle has parameters mean = 7.80 Mg and COV = 0.20.

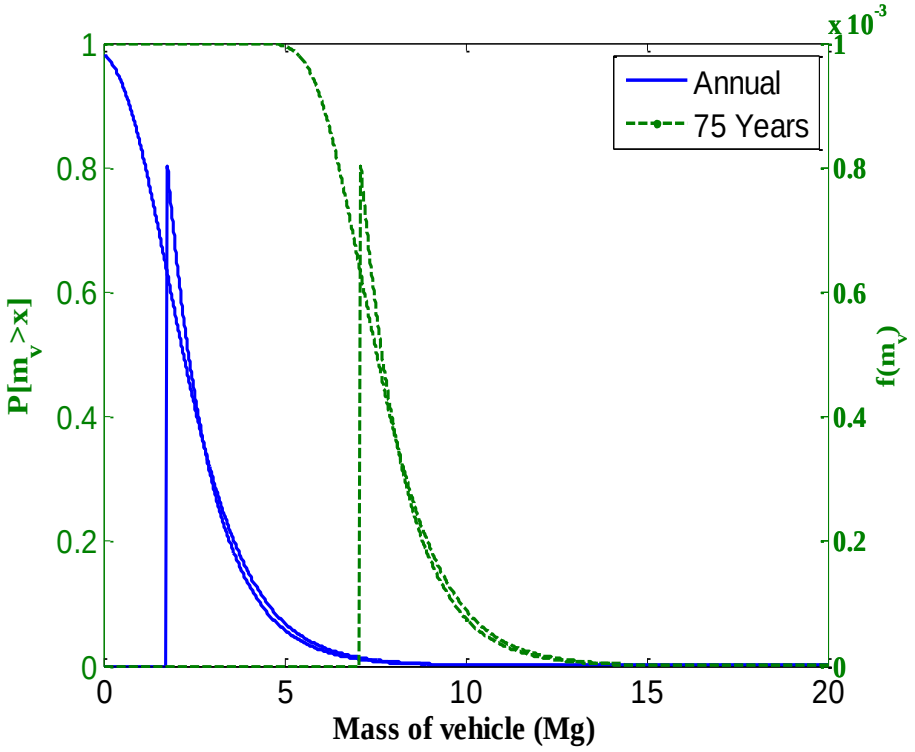

Fig. 9.3. Annual and 75 year exceeding probability of the mass of the vehicle and PDF for Extreme Type I distribution.

Hazards curves are developed for the velocity of the vehicle colliding with the RC column. In absence of significant data required to find an appropriate distribution, Extreme Type I distribution is chosen to model the distribution of the vehicle of the velocity. Three different distributions are developed as per the three increasing levels of velocity of the vehicle mentioned in Table 2.2. Fig. 9.4 shows the hazard curve developed for the 75 year exceeding probability of the velocity of the vehicle for low category velocity and the corresponding PDF for the Extreme Type I distribution.

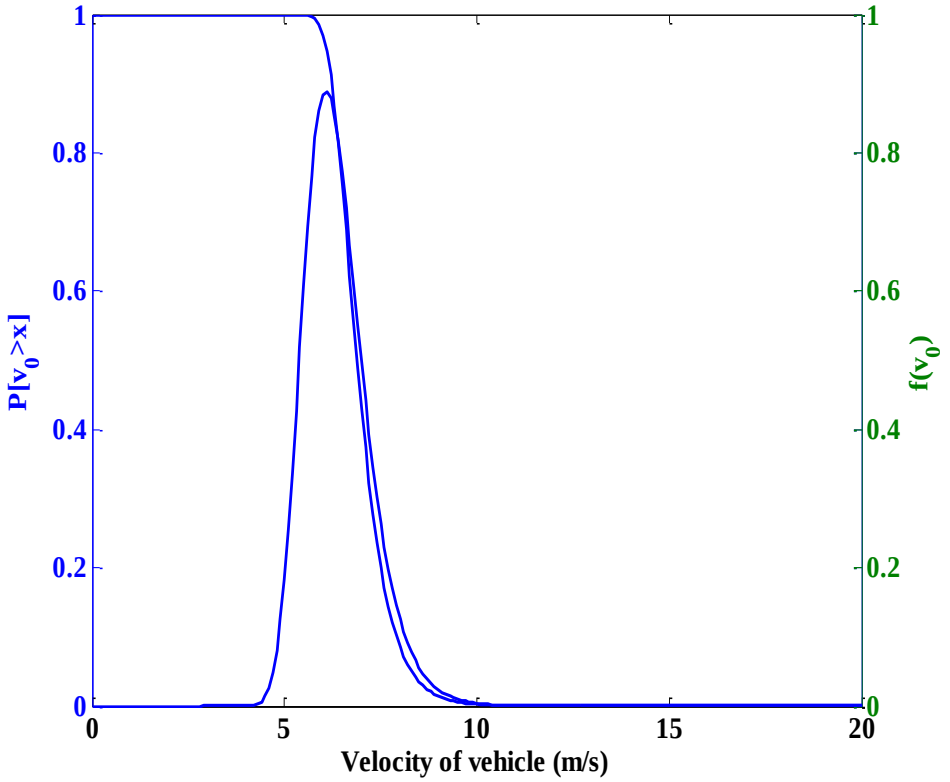

Fig. 9.4. 75 year exceeding probability of the velocity of the vehicle and PDF for Extreme Type I distribution for low category shown in Table 2.2.

The exceeding probability and $f_I(v_0)$ is plotted in the y-axis against mass of the vehicle plotted on the x-axis. The 75 year hazard curve based on the Extreme Type I distribution for the mass of the vehicle has parameters mean = 7 m/s (16 miles/h) and COV = 0.10.

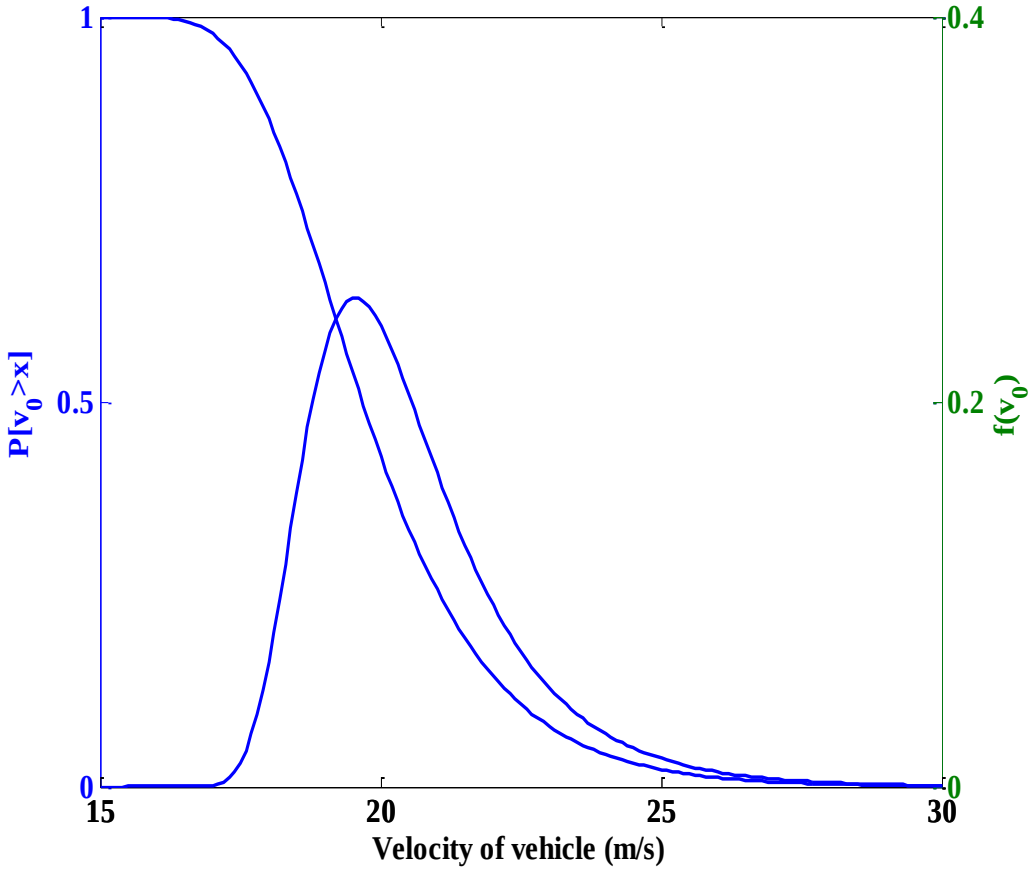

Fig. 9.5. 75 year exceeding probability of the velocity of the vehicle and PDF for Extreme Type I distribution for intermediate category shown in Table 2.2.

Fig. 9.5 shows the hazard curve developed for the 75 year exceeding probability of the velocity of the vehicle for intermediate category velocity and the corresponding PDF for the Extreme Type I distribution. The exceeding probability and $f_i(v_0)$ is plotted in the y-axis against mass of the vehicle plotted on the x-axis. The 75 year hazard curve based on the Extreme Type I distribution for the mass of the vehicle has parameters mean = 20 m/s (45 miles/h) and COV = 0.10.

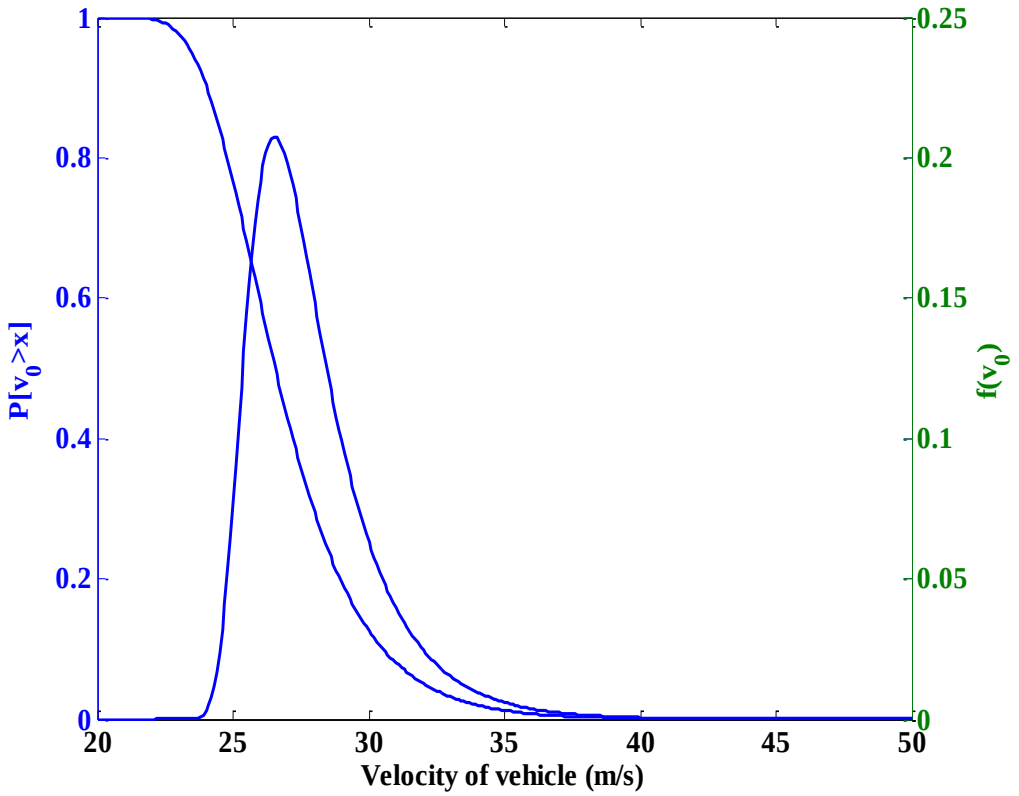

Fig. 9.6. 75 year exceeding probability of the velocity of the vehicle and PDF for Extreme Type I distribution for high category shown in Table 2.2.

Fig. 9.6 shows the hazard curve developed for the 75 year exceeding probability of the velocity of the vehicle for high category velocity and the corresponding PDF for the Extreme Type I distribution. The exceeding probability and $f_h(v_0)$ is plotted in the y-axis against mass of the vehicle plotted on the x-axis. The 75 year hazard curve based on the Extreme Type I distribution for the mass of the vehicle has parameters mean = 27 m/s (60 miles/h) and COV = 0.10.

9.2 Code Calibration

The performance-based shear resistance and demand models developed in previous sections are used for the code calibration to estimate the load and resistance factors for RC column subject to vehicle collision. The current AASHTO -LRFD 2007 code has load and resistance factor 1.0 for the vehicle impact scenario. The adequacy of these factors is examined. The load factor is only for the ultimate limit state. So, using the performance-based models developed in this research load and resistance factors for other limit states are proposed. The general equation for the load and resistance factor design is given by

$$\phi R_n \geq \gamma D_n \tag{9.1}$$

The equation for the load and resistance factor design corresponding to the three performance levels P1, P2, and P3 is given by

$$\phi V_{Pin} \geq \gamma V_{Dn} \qquad Pi = P1, P2, P3 \tag{9.2}$$

The limit state for the three performance levels is given by

$$g_{Pi} = \frac{V_{Pi}}{\phi V_{Pin}} - \frac{V_D}{\gamma V_{Dn}} \qquad Pi = P1, P2, P3 \tag{9.3}$$

where, V_{Pi} = mean value of the dynamic shear resistance for performance level Pi, V_{Pin} = nominal value of the dynamic shear resistance for performance level Pi, ϕ = resistance factor, V_D = mean value of the dynamic shear force demand, V_{Dn} = nominal value of the dynamic shear force demand, γ =demand factor.

The statistics for the models is given in Table 9.1. The mean-to-nominal value is kept constant at 1.000 for the three performance levels and demand model. The COV of the models are taken equal to the COV of the predicted model in the earlier sections.

Table 9.1. Statistical Information for the Models.

Performance Level	Mean-to-Nominal	COV
P1	1.000	1.386
P2	1.000	0.564
P3	1.000	0.449
D	1.000	0.447

A parametric study on the variation of the reliability index β with load γ and resistance ϕ factors is performed for the three limit states given by Equation 9.3. This parametric analysis is used to calculate the suitable value of load γ and resistance ϕ factors for a safe design of RC column subject to vehicle collision. The value of target reliability index β is kept at 2.0 for the performance level P1 and it is kept at 2.5 for the performance levels P2 and P3. A lower reliability index β is chosen for the performance level P1 because this level corresponds to minor damage, hence this state is

less severe. The performance levels P2 and P3 correspond to significant damage and collapse respectively. So, a higher reliability index β is used for these more severe performance levels. The value of 2.5 is chosen as this value has been widely accepted in the literature as a target reliability index for shear failure (Ellingwood et al., 1980). Fig. 9.7 shows the variation of reliability index β with load γ and resistance ϕ factors for performance level P1. The load factor γ is plotted on x axis and reliability index β is plotted on y axis. Three curves are shown which are for the varying values of the resistance factor ϕ.

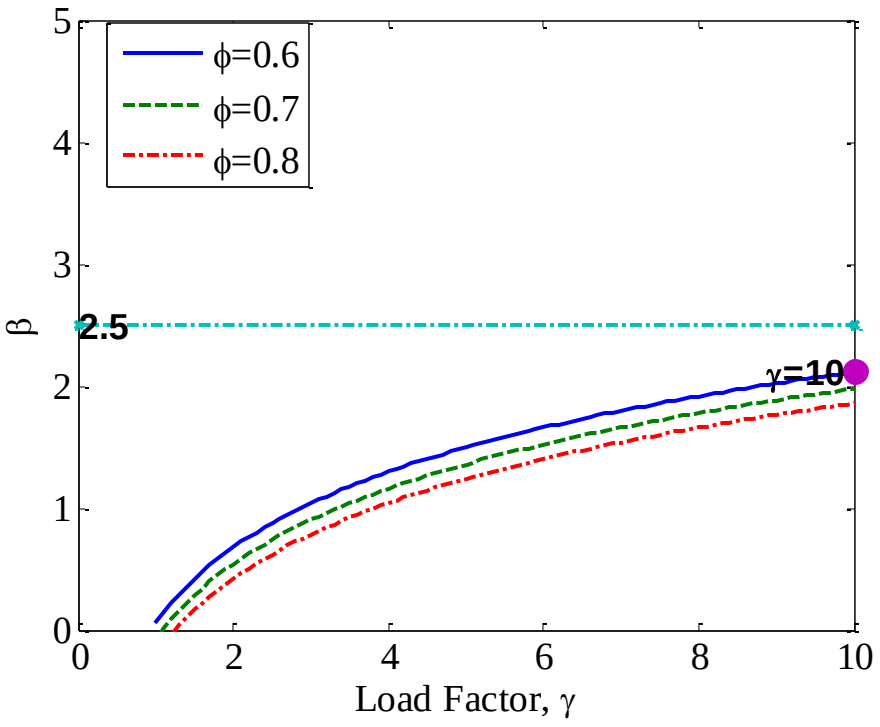

Fig. 9.7. Variation of reliability index β with load factor γ for P1.

The value of reliability index β decreases with the increase in the value of resistance factor ϕ. The value of reliability index β increases with the increase in the value of load factor γ. A value of 10 is chosen for load factor γ corresponding to 0.6 value of resistance factor ϕ for the reliability index β=2.0. The large value of load factor γ is attributed to the large variation in prediction of the dynamic shear resistance for performance level P1 evident from its COV value of 1.386.

Fig. 9.8 shows the variation of reliability index β with load γ and resistance ϕ factors for performance level P2. The load factor γ is plotted on x axis and reliability index β is plotted on y axis. Three curves are shown which are for the varying values of the resistance factor ϕ.

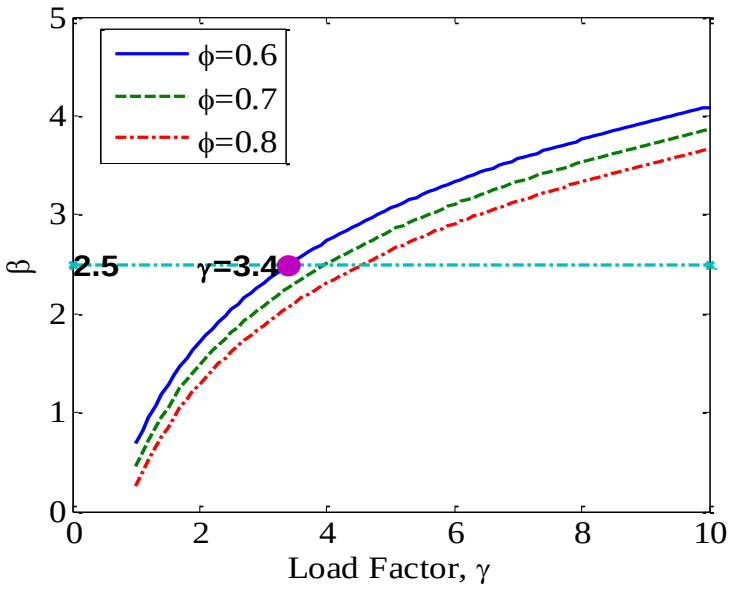

Fig. 9.8. Variation of reliability index β with load factor γ for P2.

The value of reliability index β decreases with the increase in the value of resistance factor ϕ. The value of reliability index β increases with the increase in the value of load factor γ. This consistent with the trend observed in Fig. 9.7. A value of 3.4 is chosen for load factor γ corresponding to 0.6 value of resistance factor ϕ for the reliability index β=2.5. The value of load factor γ is greater than the present code value for the other load factors. This is due to the greater value of the COV for the dynamic shear resistance and demand for the performance level P2 than the COV of the resistance factors such as in shear or dead, and live loads.

Fig. 9.9 shows the variation of reliability index β with load γ and resistance ϕ factors for performance level P3. The load factor γ is plotted on x axis and reliability index β is plotted on y axis. Three curves are shown which are for the varying values of the resistance factor ϕ.

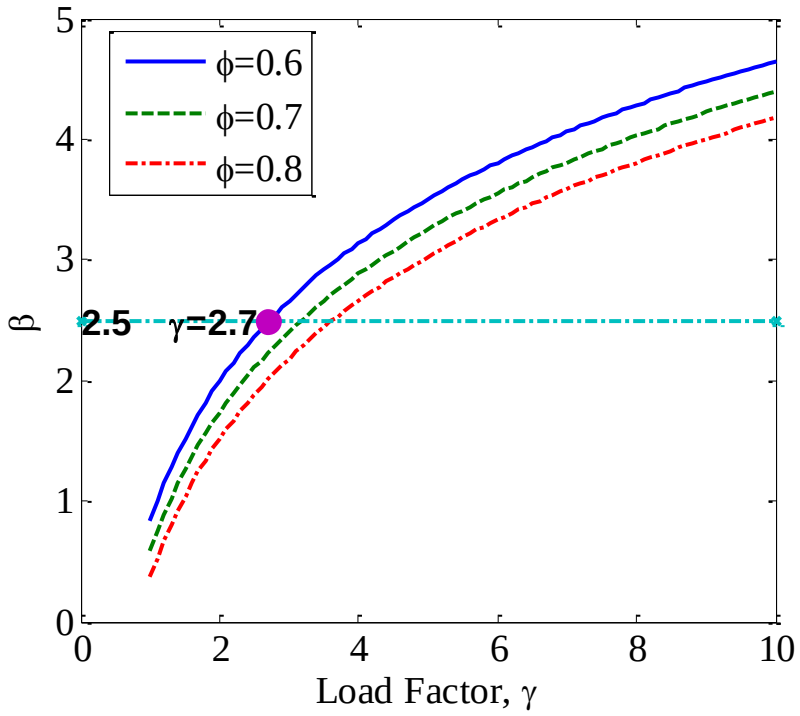

Fig. 9.9. Variation of reliability index β with load factor γ for P3.

The value of reliability index β decreases with the increase in the value of resistance factor ϕ. The value of reliability index β increases with the increase in the value of load factor γ. This consistent with the trend observed in Fig. 9.7 and Fig. 9.8. A value of 2.7 is chosen for load factor γ corresponding to 0.6 value of resistance factor ϕ for the reliability index β =2.5. The value of load factor γ is again greater in this case than the present code value for the other load factors. This is due to the greater value of the COV for the dynamic shear resistance and demand for the performance level P3 than the COV of the resistance factors such as in shear or dead, and live loads.

Table 9.2 lists the load and resistance factors obtained from the code calibration. A consistent value of 0.6 is adopted for the resistance factor ϕ for all the three limit states. The value of load factor γ is 10, 3.4, and 2.7 respectively for the limit states corresponding to performance levels P1, P2, and P3.

Table 9.2. Proposed Load and Resistance Factors.

Limit State	ϕ	γ
for P1	0.6	10.0
for P2	0.6	3.4
for P3	0.6	2.7

9.3 Total Probability and Coupled Reliability Index

The performance-based dynamic shear resistance and demand model are used to develop framework to estimate total probability of the failure and coupled reliability index β of RC column subject to vehicle collision. The performance levels is linked to the impact levels given in Table 2.2 to evaluate the reliability of the RC column subject to vehicle collision based on desired design performance objectives given in Table 2.3. The generalized form to evaluate total probability of failure of RC column subject to vehicle collision is given by

$$P_{fPi} = \iint P[g_{Pi}(\mathbf{x},\boldsymbol{\Theta}) \le 0 \,|(v_0, m_v)]\, f(v_0)\, f(m_v)\mathrm{d}v\mathrm{d}m \quad Pi = P1, P2, P3 \tag{9.4}$$

$$F_{pi}(\mathbf{x},\boldsymbol{\Theta}) = g_{Pi}(\mathbf{x},\boldsymbol{\Theta}) \le 0 \,|\, (v_0, m_v) \qquad Pi = P1, P2, P3 \tag{9.5}$$

$$g_{Pi}(\mathbf{x},\boldsymbol{\Theta}) = v_{Pi} - v_D \qquad Pi = P1, P2, P3 \tag{9.6}$$

where, P_{fPi}=Probability of failure for the performance levels P1,P2, and P3, $g_{Pi}(\mathbf{x},\boldsymbol{\Theta})$ =limit state for the performance levels P1,P2, and P3, $f(v_0)$=PDF of the distribution of the velocity of vehicle, $f(m_v)$=PDF of the distribution of the mass of the vehicle.

The generalized Equation 9.4 can be used to estimate the probability of failure or reliability of the RC column subject to vehicle collision based on desired design performance objectives given in Table 2.3. The limit state and fragility for the performance levels P1, P2, and P3 are developed in the previous sections. The PDF of the distribution of the velocity of vehicle and the mass of the vehicle has been developed earlier in this section.

Using the above information, the probability of the failure of RC column for performance level P1 in low impact level is estimated by

$$P_{fP1} = \int_0^{l_m}\int_0^{l_v} P[g_{P1}(x,\Theta) \le 0 \,|\, (v_0, m_v)]\, f_l(v_0)\, f(m_v)\mathrm{d}v\mathrm{d}m \tag{9.7}$$

where, P_{fP1}=Probability of failure for the performance levels P1 in impact level low (L), $g_{P1}(\mathbf{x},\boldsymbol{\Theta})$=limit state for the performance levels P1, $f_l(v_0)$=PDF of the distribution of the velocity of vehicle for low category, $f(m_v)$=PDF of the distribution of the mass of the vehicle, l_v = upper limit of the velocity of the vehicle for the low category of velocity given in Table 2.2, l_m = upper limit of the mass of the vehicle for the light category of mass given in Table 2.2.

Using the above information, the probability of the failure of RC column for performance level P2 in moderate impact level is estimated by

$$P_{fP2} = \int_{l_m}^{m_m} \int_{l_v}^{i_v} P[g_{P2}(x,\Theta) \le 0 \,|\, (v_0, m_v)] \, f_i(v_0) \, f(m_v) \mathrm{d}v \mathrm{d}m \tag{9.8}$$

where, P_{fP2} =Probability of failure for the performance levels P2 in impact level medium (M), $g_{P2}(\mathbf{x},\mathbf{\Theta})$ =limit state for the performance levels P1, $f_i(v_0)$ =PDF of the distribution of the velocity of vehicle for intermediate category, $f(m_v)$ =PDF of the distribution of the mass of the vehicle, l_v = upper limit of the velocity of the vehicle for the low category of velocity given in Table 2.2, i_v = upper limit of the velocity of the vehicle for the intermediate category of velocity given in Table 2.2, , l_m = upper limit of the mass of the vehicle for the light category of mass given in Table 2.2, m_m = upper limit of the mass of the vehicle for the medium category of mass given in Table 2.2.

Using the above information, the probability of the failure of RC column for performance level P3 in severe impact level is estimated by

$$P_{fP3} = \int_{m_m}^{h_m} \int_{i_v}^{h_v} P[g_{P3}(x,\Theta) \le 0 \,|\, (v_0, m_v)] \, f_h(v_0) \, f(m_v) \mathrm{d}v \mathrm{d}m \tag{9.9}$$

where, P_{fP3} =Probability of failure for the performance levels P3 in impact level severe (S), $g_{P3}(\mathbf{x},\mathbf{\Theta})$ =limit state for the performance levels P3, $f_h(v_0)$ =PDF of the distribution of the velocity of vehicle for high category, $f(m_v)$ =PDF of the distribution of the mass of the vehicle, i_v = upper limit of the velocity of the vehicle for the intermediate category of velocity given in Table 2.2, h_v = upper limit of the velocity of the vehicle for the high category of velocity given in Table 2.2, m_m = upper limit of the mass of the vehicle for

the medium category of mass given in Table 2.2, h_m = upper limit of the mass of the vehicle for the heavy category of mass given in Table 2.2,

Equation 9.7 relates the performance level P1 to the impact level low (L), thus estimating the reliability of the RC column subject to vehicle collision being fully operational and sustaining minor damage during low impact events. Similarly, Equation 9.8 relates the performance level P2 to the impact level moderate (M), thus estimating the reliability of the RC column subject to vehicle collision being operational with sustaining structural damage during medium impact events. Continuing as above, Equation 9.9 relates the performance level P3 to the impact level severe (S), thus estimating the reliability of the RC column subject to vehicle collision being in state of collapse prevention during severe impact events.

9.4 Conclusion

In the section, hazard curves are developed for the mass of the vehicle and the velocity of the vehicle that collide with the RC column. Code calibration to estimate the load and resistance factor for the three performance level is performed and load and resistance factors are proposed for the desired reliability index. The developed hazard curve in this section with the performance-based dynamic shear resistance and demand models are used to develop framework to evaluate the total probability or the reliability of the RC column subject to the vehicle collision. The performance level is tied to the impact levels to estimate the reliability of the RC column for the desired performance objectives. The equations to estimate the reliability for critical cases like the RC column

subject to vehicle collision being fully operational and sustaining minor damage during low impact events, the RC column subject to vehicle collision being operational with sustaining structural damage during medium impact events, and the RC column subject to vehicle collision being in state of total collapse during severe impact events is established. The section thus presents the code calibration to estimate the load and resistance factors as well as equations to achieve desired performance objectives of the RC column subject to vehicle collision.

10 CONCLUSION AND FUTURE WORK

The current work focuses on shifting the existing paradigm in the analysis and design of RC columns subject to vehicle impact in a number of ways. The proposed procedure shifts the existing methodology based on static or quasi-static analysis to the dynamic analysis which is a more realistic representation of the vehicle impact with structures.

The present research lays out a framework to quantify the different observed damages into applicable damage levels. The damage levels are then related to the appropriate performance levels. The performance levels are tied to the different impact scenarios of vehicle impacts to ensure that the desired performance of the structure is met when the RC column is impacted. Then a procedure to estimate the different dynamic shear resistance corresponding to performance levels is established. A method to estimate the dynamic shear force demand on the RC column during vehicle impact is also laid out. The dynamic shear force demand can be categorized into different demand levels depending on the intensity of the impact. Actual structural configurations and loading scenarios are used to evaluate the response which is more accurate in representing the complex impact scenario.

Performance-based resistance models are developed which can be used to achieve the desired behavior of the RC column under different impact scenarios. The probabilistic resistance model captures the dynamic behavior of the RC column and accounts for the associated uncertainties.

A demand model is developed which can be used to achieve the desired behavior of the RC column under different impact scenarios. The probabilistic demand model captures the dynamic interaction between the RC column the vehicle during collision and accounts for the associated uncertainties. A framework to assess the fragility of RC column subjected to vehicle impact based on performance-based models is developed.

Hazard curves are developed for the mass of the vehicle and the velocity of the vehicle that collide with the RC column. Code calibration to estimate the load and resistance factor for the three performance level is performed and load and resistance factors are proposed for the desired reliability index. The developed hazard curve together with the performance-based dynamic shear resistance and demand models are used to develop framework to evaluate the total probability or the reliability of the RC column subject to the vehicle collision. The performance level is tied to the impact levels to estimate the reliability of the RC column for the desired performance objectives. The framework to achieve desired performance objectives of the RC column subject to vehicle collision is developed.

The proposed procedure has its merits for application in the design and analysis of RC columns to minimize damage and meet a set of performance objectives during different vehicle impact scenarios.

Experimental data are required to further verify and assess the suitability of the developed models. More representative data is required to further refine the hazard models developed in this research. The performance-based proposed procedure can be used for other hazards such as high velocity impacts due to blasts or missiles impact.

The current work can be extended to estimate the capacity of and demand on for other members such as prestressed columns, steel columns, and beams. The state of knowledge can be applied to study similar cases of collision such as ship collision to a barge, projectile collision into concrete walls and develop adequate models.

REFERENCES

AASHTO (2007). *AASHTO LRFD Bridge Design Specifications*, American Association of State Highway and Transportation Officials, Washington, D.C.

ACI Committee 318 (2005). *Building Code Requirements for Structural Concrete (ACI 318-05) and Commentary (318R-05)*, American Concrete Institute, Farmington Hills, MI.

Akaike, H. (1974). "A new look at the statistical model identification," *IEEE Transaction on Automatic Control*, 19(6), 716-723.

Altair Computing (2003). *HyperMesh Ver. 6.0 Basic Tutorial*, Altair Engineering Inc., 1820 E. Big Beaver, Troy, MI 48083.

Atahan, A.O., Bonin, G., and Karacasu, M. (2007). "Development of a 30,000 kg heavy goods vehicle for LS-DYNA applications." *Int. J. Heavy Vehicle Systems*, 14(1), 1-19.

Box, G. E. P., and Tiao, G. C. (1992). *Bayesian Inference in Statistical Analysis*, Wiley, New York.

Briaud, J-L. (2007). *Introduction to Soil Erosion*, Texas A&M University, College Station, TX.

Buth, C.E., (2009). *Guidelines for Designing Bridge Piers and Abutments for Vehicle Collisions- Semi Annual Report*, Texas Transportaion Institute, College Station, TX.

Buth, C. E., Williams, W. F., Brackin, M. S., Lord, D., Geedipally, S. R., Abu-Odeh, A. Y., (2010). *Analysis of Large Truck Collisions with Bridge Piers: Phase 1. Report of Guidelines for Designing Bridge Piers and Abutments for Vehicle Collisions*, Texas Transportaion Institute, College Station, TX.

Ellingwood, B., Galambos, T., V., McGregor, J., G., Cornell, C., A. (1980). *Development of a Probability-Based Load Criterion for American National Standard A58*, Special Publication SP 577, National Bureau of Standards, Department of Commerce, Washington, D.C.

El-Tawil, S., Severino E., and Fonseca, P. (2005). "Vehicle Collision with Bridge Piers," *Journal of Bridge Engineering*, 10(3), 345-353.

EUR 23738 EN (2009). "COSIMB, Composite Column and Wall Systems for Impact and Blast Resistance," 189, 2009.

Gardoni, P., Der Kiureghian, A., and Mosalam, K. M. (2002). "Probabilistic capacity models and fragility estimates for reinforced concrete columns based on experimental observations," *Journal of Engineering Mechanics*, 128(10), 1024–1038.

Goldsmith, W. (1960). *Impact: Theory and physical behavior of colliding solids*, London, UK.

Hartik, I. E., Shaaban, A. M., Gesund, H., Valli, G. Y. S., Wang, S. T. (1990). "United States bridge failures 1951–1988," *Journal of Performance of Construction Facilities*, 4(4), 272–77.

Kloeden, C.N., McLean, A.J., Baldock, M.R.J., and Cockington, A.J.T. (1999). *Severe and Fatal Car Crashes Due to Roadside Hazards*, NHMRC Road Accident Research Unit, University of Adelaide, Australia.

Kowalsky, M.J. & Priestley, M.J.N. (2000). "An improved analytical model for shear strength of circular RC columns in seismic regions," *ACI Structural Journal*, 97(3), 388-396.

Livermore Software Technology Corporation (2003). *LSDYNA Keyword User's Manual, Version 970*, Livermore, CA.

Louw, J. M., Maritz G., Loedoeff, M.J. (1992). "The Behavior of RC Columns Under Impact Loading," *Die Siviele Ingenieur*, Suid-Afrika.

Malvar, L.J. (1998). "Review of static and dynamic properties of steel reinforcing bars," *ACI Materials Journal*, 95(5), 609-616.

Mander, J. B., Priestley, M. J., N., Park, R. (1988). "Theoretical stress-strain model for confined concrete," *Journal of Structural Engineering*, 114(8), 1804-1826.

Mendis, P.A., Pendyala, R., and Setunge, S. (2000). "Stress-strain model to predict the full range moment curvature behavior of high strength concrete sections," *Magazine of Concrete Research*, 52(4), 227-234.

Moehle, J. P., Elwood, K., and Sezen, H. (2000). "Shear failure and axial load collapse of existing reinforced concrete columns," *Proc., 2nd U.S.–Japan Workshop on Performance-Based Design Methodology for Reinforced Concrete Building Structures,* Sapporo, Japan, 241– 255.

Moehle, J. P., Lynn, A. C., Elwood, K., and Sezen, H. (1999). ‘‘Gravity load collapse of reinforced concrete frames during earthquakes,’’ *Proc., 1st U.S.–Japan Workshop on Performance-Based Design Methodology for Reinforced Concrete Building Structures,* Maui, Hawaii, 175–189.

Murray, Y.D., Abu-Odeh, A., and Bligh, R. (2007). *Evaluation of LS-DYNA Concrete Material Model 159, Report No.FHWA-HRT-05-063,* Federal Highway Administration, US Department of Transportation**.**

Myers, R. H., & Montgomery, D. C. (1995). *Response Surface Methodology. Process and Product Optimization Using Designed Experiments*, Wiley, New York.

NCAC (2010). “Finite Element Model Archive.” <http://www.ncac.gwu.edu/vml/models.html> (Oct. 10, 2009).

Nielson, B.G., & DesRoches, R. (2006). “Influence of modeling assumptions on the seismic response of multi-span simply supported steel girder bridges in moderate seismic zones,” *Engineering Structures,* 28, 1083–1092.

PEER (2010). “Structural Performance Database,”<http://www.ce.washington.edu/~peera1/>(Oct. 10, 2009).

Schwarz, G. (1978). “Estimating the dimension of a model,” *Annals of Statistics*, 6(2), 461-464.

Sharma H., Hurlebaus S., Gardoni, P. (2008). “Development of a bridge bumper to protect bridge girders from overheight vehicle impacts,” *Computer Aided Civil Infrastructure and Engineering*, 23(6), 415-426.

Sharma H., Hurlebaus S., Gardoni, P. (2009). "A Probabilistic Model for the Estimation of Shear Capacity of Bridge Piers Subjected to Dynamic Loading," *Proceedings of ASCE Structures Congress*, Austin ,TX, 537-546.

Staples, A. M. (2007). *Pier Protection*, LRFD Bridge Design Workshop, Minnesota Department of Transportation, MN.

Steffan, H., Hoschkopf, H., Geigl, B., and Moser, A. (1998). "Development of New Crash-Cushion Concept for Compatibility Purposes of Rigid Obstacles Near the Road," *Proc. 16th Int. Techn. Conf. on ESV*, Paper nr. 98-S3-O-11, Winsor Canada, 742-751.

Suter, R. (2005). "Reinforcement of Bridge Piers with FRP Sheets to Resist Vehicle Impact," *IABSE Symposium*, Lisbon, Portugal, 1-6.

Tsang, H. H., and Lam, N. T. K. (2008). "Collapse of reinforced concrete column by vehicle impact," *Computer –Aided Civil and Infrastructure Engineering*, 23, 427-436.

TxDOT (2010). "Bridge Standards." <http://www.dot.state.tx.us/insdtdot/orgchart/cmd/cserve/standard/bridge-e.htm> (Sep. 10, 2009).

Wardhana, K., & Hadipriono, F. C. (2003). "Analysis of recent bridge failures in the United States," *Journal of Performance of Construction Facilities*, 17(3), 144-150.

Ydenius, A., and Kullgren, A. (2001). "Injury Risk Functions in Frontal Impacts Using Recorded Crash Pulses," *International IRCOBI Conference on the Biomechanics of Impact*, Isle of Man, UK, 27-38.

APPENDIX-I

The FE simulation is discussed in detail in this Appendix section. The modeling aspects, input for the material models, contact algorithm, initial conditions are explained with suitable input files. The process to obtain the various quantities of interest in this dissertation is also laid out in detail. This section goes step by step into the complex FE modeling and simulation process and focuses to make the process understandable and easy to replicate.

I.1 Modeling of RC Column

The geometric modeling of the RC column is done using Hypermesh (Altair Computing, 2003). A three dimensional solid model is used for modeling RC column. The RC column is modeled by a fully integrated quadratic eight node element with nodal rotations. The required input from the user is as follows:

PID: Part identification number (Any number can be provided).

SECID: Section identification number (Any number can be provided).

MID: Material identification number (Any number can be provided).

ELFORM: Constant stress solid element (1).

Keep all other cards to their default value.

Sample input for RC column with solid elements.

*PART

$# title

```
$HMNAME PROPS      1conc_beam
$#    pid    secid      mid    eosid     hgid      grav    adpopt      tmid
        1        1        1        0      100         0         0         0
*SECTION_SOLID
$HMNAME PROPS      1conc_beam
$#  secid    elform      aet
        1        1        0
```

The reinforcement bars are modeled explicitly using a one dimensional element. The required input from the user for beam elements is as follows:

PID: Part identification number (Any number can be provided).

SECID: Section identification number (Any number can be provided).

MID: Material identification number (Any number can be provided).

ELFORM: Hughes-Liu with cross section integration (1).

SHRF: Default (1).

QR/IRID: 2X2 Gauss quadrature (2).

CST: Tubular (1).

SCOOR: 2

TS1-TS2: Beam outer diameter.

TT1-TT2: Beam inner diameter (0).

Keep all other cards to their default value.

Sample input for reinforcements with beam elements.

```
*PART
```

```
$# title
$HMNAME PROPS       2beam_transv
$#     pid     secid       mid     eosid      hgid      grav    adpopt      tmid
       2         2         2         0       100         0         0         0
*SECTION_BEAM
$#   secid    elform      shrf   qr/irid       cst     scoor       nsm
       2         1  1.000000         2         1  2.000000     0.000
$#     ts1       ts2       tt1       tt2     nsloc     ntloc
  25.4000   25.4000     0.000     0.000  1.000000  1.000000
```

The geometric modeling of the RC column is shown in Fig. I.1. The figure shows the concrete modeled as solid elements and reinforcements modeled as beam elements.

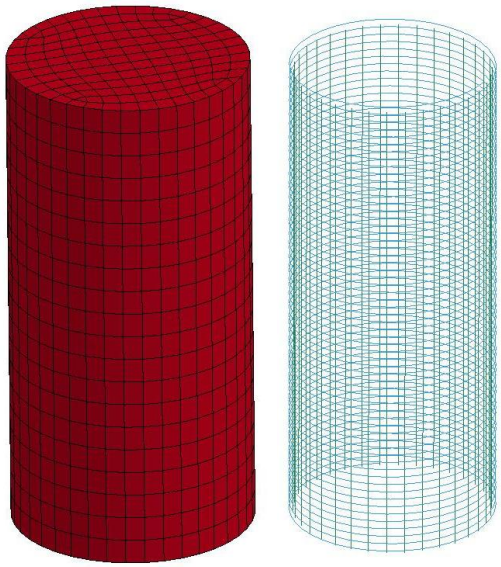

(a) (b)

Fig. I.1. Modeling of RC column (a) concrete modeled as solid elements, (b) reinforcements modeled as beam elements.

I.2 Material Properties of RC Column

The material model for concrete used in FE modeling is material type 159 (MAT-CSCM_CONCRETE). This is a smooth or continuous surface cap model and is available for solid elements in LS-DYNA. The material properties form experiment conducted can be used as input or default material properties for normal strength concrete can be used from the library of the materials. In the present modeling, the default material properties are used. The required input from the user is as follows:

MID: Material identification number (Any number can be provided).

RO: Mass density of the concrete.

NPLOT: Default option 1 is used to obtain maximum of brittle and ductile damages.

INCRE: Maximum strain increment for subincrementation (left blank).

IRATE: Rate effect model turned on (1).

ERODE: Set value of 1.1 for concrete.

RECOV: Set value of 1 for modulus to remain at the brittle damage level.

IRETRC: Cap retraction option set to 0.

PRED: Pre existing damage set to 0.

FPC: Unconfined compressive strength.

DAGG: Maximum aggregate size set to 19 mm.

UNITS: Option 2. Used units of MPa, mm, sec, Mg/mm^3, N.

Sample input for concrete with unconfined compressive strength of 30 MPa.

```
*MAT_CSCM_CONCRETE
$#     mid        ro     nplot     incre     irate     erode     recov   itretrc
         1 2.5000E-9         1     0.000         1  1.100000    1.0000         0
$#    pred
     0.000
$#     fpc      dagg     units
  30.00000      19.0         2
```

The material model used for modeling longitudinal and transverse steel is material type 24 (MAT_PIECEWISE_LINEAR_PLASTICITY). In this material type, an elasto-plastic material with a stress versus strain curve can be defined. A failure based on plastic strain is defined. The required input from the user is as follows:

MID: Material identification number (Any number can be provided).

RO: Mass density of the steel.

E: Young's modulus.

PR: Poisson's ratio.

SIGY: Yield stress.

ETAN: Tangent modulus (left blank).

FAIL: Plastic strain (0.2) considered for failure.

TDEL: Minimum time step size for automatic element deletion (left blank).

C: Strain rate parameter (left blank).

P: Strain rate parameter (left blank).

LCSS: Left blank.

LCSR: Load curve id defining strain rate scaling effect on yield stress (defined by DEFINE CURVE).

VP: Scale yield stress (0).

EPS1-EPS8: Left blank.

ES1-ES8: Left blank.

Sample input for steel with yield stress of 517 MPa.

```
*MAT_PIECEWISE_LINEAR_PLASTICITY
$#     mid        ro         e        pr      sigy      etan      fail      tdel
         3 7.8500E-9 210000.00  0.300000  517.0000     0.000  0.200000     0.000
$#       c         p      lcss      lcsr        vp
     0.000     0.000         0         3     0.000
```

```
$#    eps1      eps2      eps3      eps4      eps5      eps6      eps7      eps8
    0.000     0.000     0.000     0.000     0.000     0.000     0.000     0.000
$#     es1       es2       es3       es4       es5       es6       es7       es8
    0.000     0.000     0.000     0.000     0.000     0.000     0.000     0.000
*DEFINE_CURVE
$     LCID      SIDR      SCLA      SCLO      OFFA      OFFO
$#    lcid      sidr       sfa       sfo      offa      offo    dattyp
         3         0     0.000     0.000     0.000     0.000         0
$                A1                O1
$#               a1                o1
             0.000          1.0000000
         0.0000100          1.0100000
         1.0000000          1.2100000
         5.0050000          1.7100000
       100.0000000          2.0000000
    100000.0000000          2.0000000
```

I.3 Contact Definitions and Initial Conditions

The bond between the concrete and transverse reinforcement and longitudinal reinforcement is defined by Lagrangian coupling method. In this method, the need to match the nodes between concrete and reinforcements is not necessary hence this is effective and efficient method. The concrete element is treated as master element and

reinforcements are treated as slave elements. The required input from the user is as follows:

COUPID: Coupling identification number (Any number can be provided).

SLAVE: ID of the reinforcement.

MASTER: ID of the concrete.

Keep all other cards to their default value.

Sample input for concrete and reinforcement is as follows:

```
*CONSTRAINED_LAGRANGE_IN_SOLID_TITLE
$#  coupid                                          title
     150
$#  slave    master     sstyp     mstyp     nquad     ctype     direc     mcoup
       2         1         1         1         0         2         1         0
$#  start       end      pfac      fric    frcmin      norm   normtyp      damp
    0.0001.0000E+10  0.100000     0.000  0.500000         0         0     0.000
$#     cq      hmin      hmax     ileak     pleak   lcidpor     nvent  blockage
    0.000     0.000     0.000         0  0.010000         0         0         0
$#  iboxid   ipenchk   intforc   ialesof    lagmul    pfacmm      thkf
       0         0         0         0     0.000         0     0.000
```

The contact between the vehicle and RC column is defined by CONTACT_AUTOMATIC_SINGLE_SURFACE_ID. This contact type is efficient and less costly in evaluating response of the structure during crash. The required input from the user is as follows:

CID: Contact identification number (Any number can be provided).

SSID: Slave segment number. It is left blank so that all part ID's are included.

MSID: Master segment id (leave blank).

FS: Static coefficient of friction (0.3).

FD: Dynamic coefficient of friction (0.3).

SOFT: Used due to large variation in the elastic moduli of the materials (1).

Keep all other cards to their default value.

Sample input for contact between RC column and vehicle is as follows:

```
*CONTACT_AUTOMATIC_SINGLE_SURFACE_ID
$#     cid                                          title
       10
$#    ssid     msid     sstyp     mstyp    sboxid    mboxid      spr      mpr
         0        0         0         0         0         0        0        0
$#      fs       fd       dc       vc      vdc    penchk       bt       dt
  0.300000  0.300000    0.000    0.000    0.000         0    0.0001.0000E+20
$#     sfs      sfm      sst      mst     sfst     sfmt      fsf      vsf
  1.000000  1.000000    0.000    0.000  1.000000  1.000000  1.000000  1.000000
$#    soft    sofscl    lcidab    maxpar    sbopt    depth    bsort    frcfrq
         1  0.100000         0  1.025000  2.000000        2        0        1
$#  penmax    thkopt    shlthk     snlog     isym    i2d3d    sldthk    sldstf
    0.000         0         0         0         0         0    0.000     0.000
$#    igap    ignore    dprfac    dtstif   unused    unused    flangl
```

1 1 0.000 0.000 0 0 0.000

Gravity and initial load at the top of the column are applied by dynamic relaxation (CONTROL_DYNAMIC_RELAXATION).

Keep all other cards to their default value.

Sample input for dynamic relaxation is as follows:

*CONTROL_DYNAMIC_RELAXATION

$# nrcyck drtol drfctr drterm tssfdr irelal edttl idrflg

250 0.001000 0.9950001.0000E+28 0.000 0 0.040000 1

The total time required to run the simulation is controlled by the user (CONTROL_TERMINATION). A maximum time of 0.1 s is used to run the simulations.

ENDTIM: Maximum time required to run the simulation.

Keep all other cards to their default value.

Sample input for dynamic relaxation is as follows:

*CONTROL_TERMINATION

$$ ENDTIM ENDCYC DTMIN ENDENG ENDMAS

$# endtim endcyc dtmin endeng endmas

0.100000

I.4 Modeling and Material Properties of Vehicle

The vehicles used for loading are a 8,000 kg (8 Mg) Ford truck (NCAC, 2010), a 30,000 kg (30 Mg) IVECO truck (Atahan et al., 2007), a 38,000 kg (38 Mg) tractor trailer

(NCAC, 2010), and a 50,000 kg (50 Mg) IVECO truck (Atahan et al., 2007) as shown in Fig. I.2.

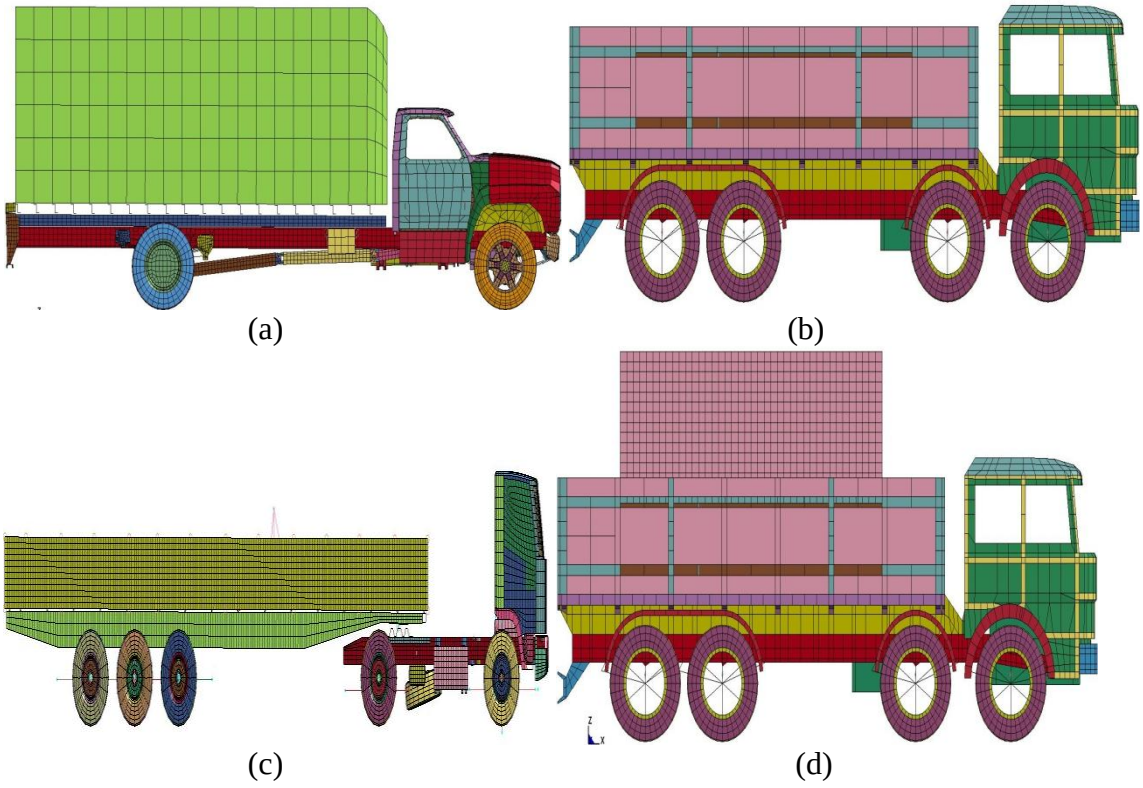

Fig. I.2. FE model of the vehicles (a) 8 Mg Ford truck, (b) 30 Mg IVECO truck, (c) 38 Mg tractor trailer, (d) 50 Mg IVECO truck.

The vehicle models are given different initial velocities to model different traffic scenarios. The initial velocity of the vehicle is varied using initial velocity generation card (INITIAL_VELOCITY_GENERATION). In this method all the parts of the

vehicle are assigned same initial velocity instantaneously. The required input from the user is as follows:

PID: Part id to be assigned the initial velocity (select all parts of the vehicle).

VX, VY, VZ: Assign the initial velocity in the appropriate direction.

Keep all other cards to their default value.

Sample input for giving initial velocity of 47.4 m/s to the vehicle is as follows:

```
*INITIAL_VELOCITY_GENERATION
$HMNAME LOADCOLS       1InitialVelGen_1
$HMCOLOR LOADCOLS      1       1
$#nsid/pid     styp    omega       vx       vy       vz    ivatn     icid
       1        1    0.000 47376.100    0.000    0.000        0        0
$#     xc       yc       zc       nx       ny       nz    phase    iridid
   0.000    0.000    0.000    0.000 1.000000    0.000        0        0
```

I.4 Analysis

The RC column and vehicle models need to be combined together in order to simulate the collision between them. In order to do that, a transformation card is defined (DEFINE_TRANSFORMATION and INCLUDE_TRANSFORMATION). The required input from the user is as follows:

TRANSID: Transformation identification number (Any number can be provided).

SCALE: Scaling the vehicle model (Use 1 for no scaling).

TRANSL: Placing the vehicle model with respect to the RC column.

FILENAME: Name of the file of vehicle model.

IDNOFF: Offset to the node id.

IDEOFF: Offset to the element id.

IDPOFF: Offset to the part id.

IDMOFF: Offset to the material id.

IDSOFF: Offset to the set id.

IDFOFF: Offset to the function or table id.

IDDOFF: Offset to the define id.

IDROFF: Offset to the section and hourglass id.

FCTMAS: Mass transformation factor (1).

FCTTIM: Time transformation factor (1).

FCTLEN: Length transformation factor (1).

FCTTEM: Temperature transformation factor (1).

Sample input combining the RC column and 50 M vehicle is given as follows:

```
*DEFINE_TRANSFORMATION
$#  tranid
         1
$# option        a1        a2        a3        a4        a5        a6        a7
SCALE       1.000000  1.000000  1.000000
TRANSL       700.000     0.000     0.000
*INCLUDE_TRANSFORM
$# filename
```

```
trk_mod.k
$#  idnoff    ideoff    idpoff    idmoff    idsoff    idfoff    iddoff
   400000    400000       500       500       500       500       500
$#  idroff
      500
$#  fctmas    fcttim    fctlen    fcttem   incout1
  1.000000  1.000000  1.000000  1.000000         1
$#  tranid
         1
```

The combined file is given to LS-DYNA solver for analysis. A job file is used since the process requires more than 20 minutes. The simulation is carried on an IBM-AIX machine. The job file is given as follows:

```
# ---------------- Begining of ls-dyna sample job1 -------------
#@ shell           = /bin/ksh
#@ job_name        = smp_ls-dyna
#@ output          = $(job_name).o$(schedd_host).$(jobid)
#@ error           = $(job_name).e$(schedd_host).$(jobid)
#@ job_type        = parallel
#@ wall_clock_limit = 5:00:00
#@ resources       = ConsumableCpus(4) ConsumableMemory(2000mb)
#@ notification    = error
#@ queue
```

```
export OBJECT_MODE=64
export OMP_DYNAMIC=FALSE
export OMP_NUM_THREADS=4
export AIXTHREAD_SCOPE=S
export LSTC_INTERNAL_CLIENT=fork
module load ls-dyna-971-R4.2
ls-dyna_d i=c5.k memory=200m ncpu=4
# ---------- End of ls-dyna sample job1 ----------
```

The time required for a single case to run is approximately 5 hours on 4 cpus.

I.6 Result

The output files are viewed in LS-PREPOST viewing software. The time history simulation, force time history and all other requested output is obtained by this software. The d3plot files show the progress of the crash process at each 1 millisecond instance. The ASCII files contain all the requested outputs. The total energy, energy ratio, hourglass energy is checked to verify the numerical validity of the simulation.

The shear force at the base of the column is monitored. The simulation is monitored. The shear force at the instant when the stress in the longitudinal reinforcement exceeds the yield stress is recorded as dynamic shear resistance corresponding to the performance level P1. The shear force at the instant when the spalling of cover starts to occur and the reinforcements are exposed is recorded as dynamic shear resistance corresponding to the performance level P2. The shear force at

the instant when the core of the RC column starts to erode/break or the reinforcement begins to buckle is recorded as dynamic shear resistance corresponding to the performance level P3. The maximum force imparted by the vehicle is recorded as the maximum force applied to the RC column. As per the length and point of application of the vehicular load and the boundary conditions, the maximum applied force is transformed to the dynamic shear demand. In this way the quantities of interest are calculated from the FE simulation.

I.7 Conclusion

In this section, the details involved in the FE simulation are presented. The modeling of the RC column, material properties, contact algorithm, initial conditions is discussed in details. The input parameters are explained with appropriate examples. The vehicles used in the FE simulation are shown and the way to vary the velocity to these vehicles is explained. The combination of the RC column and the vehicle to run crash scenario is also explained. The process to check the numerical stability and validity of the FE model is discussed. The process to obtain the various dynamic shear resistances corresponding to different performance levels is laid out. The process to obtain the dynamic shear demand from the FE simulation is also mentioned. This appendix presents a detailed account of the FE simulation used in this dissertation. By following the procedure mentioned in this appendix, the results presented in this dissertation can be recreated and/or future work can be carried out.

APPENDIX-II

The shear resistance of RC column has components of inertial resistance, damping resistance and shear strength of the RC column also called shear capacity. In this appendix, the contribution of the shear capacity will be evaluated. The strength of the concrete and steel increases due to the effect of strain rate. This in turn increases the shear capacity of the RC column. The shear capacity thus depends on the strain rate and in turn with the velocity at which the RC column is moving. This shear contribution is called dynamic shear capacity.

II.1 Static Shear Capacity

The static shear capacity will be evaluated by performing a moment curvature analysis of the RC column. The maximum obtained moment is used to calculate the shear capacity. The idealization of the vehicle collision with RC column is shown in Fig. II.1.

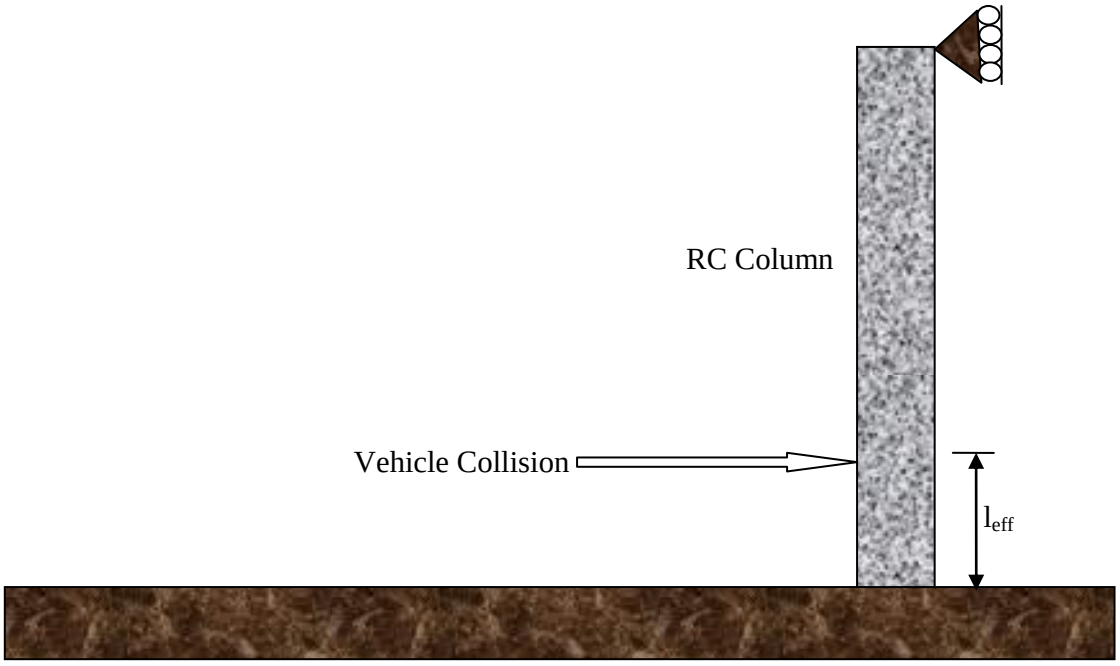

Fig. II.1. Idealization of vehicle collision with RC column.

In order to perform the moment curvature analysis, the material properties of concrete and steel are obtained. The material property of concrete is obtained as per Mander et al., 1988. The Popovics equation is modified in order to obtain the stress strain behavior in the unconfined concrete. The stress in the unconfined concrete is given by

$$\frac{f_c}{f_c'} = \frac{n\left(\frac{\varepsilon_c}{\varepsilon_{co}}\right)}{(n-1)+\left(\frac{\varepsilon_c}{\varepsilon_{co}}\right)^n+\left(\frac{\varepsilon_c}{\varepsilon_{spall}}\right)^{10}} \qquad \text{(II.1)}$$

where, f_c = stress in steel corresponding to the strain ε_c, $f_c^{'}$ = unconfined concrete strength, ε_{co} = strain (.002) corresponding to maximum unconfined concrete strength, ε_{spall} = spalling strain of confined concrete, $n = \frac{E_c}{E_c - E_{\sec}}$, E_c = modulus of elasticity of concrete, $E_{\sec}$ = Secant modulus given by $\frac{f_c^{'}}{\varepsilon_{co}}$.

The stress in the confined concrete is given by

$$\frac{f_c}{f_{cc}^{'}} = \frac{n_c\left(\frac{\varepsilon_c}{\varepsilon_{cco}}\right)}{(n_c - 1) + \left(\frac{\varepsilon_c}{\varepsilon_{cco}}\right)^n + \left(\frac{\varepsilon_c}{\varepsilon_{hoopfr}}\right)^{30}} \qquad \text{(II.2)}$$

where, f_c = stress in steel corresponding to the strain ε_c, $f_{cc}^{'}$ = confined concrete strength ($kf_c^{'}$), ε_{cco} = strain corresponding to maximum confined concrete strength ($\varepsilon_{co}\left[1+5\left(k-1\right)\right]$), ε_{hoopfr} = fracture strain of transverse reinforcement ($5\varepsilon_{cco}$), $n_c = \frac{E_c}{E_c - E_{c\sec}}$, E_c = modulus of elasticity of concrete, $E_{c\sec}$ = Secant modulus given by $\frac{f_{cc}^{'}}{\varepsilon_{cco}}$. The confining strength ratio k is given by

$$k = \frac{f_{cc}^{'}}{f_c^{'}} = -1.254 + 2.254\sqrt{1 + 7.94\frac{f_l^{'}}{f_c^{'}}} - 2\frac{f_l^{'}}{f_c^{'}} \qquad \text{(II.3)}$$

The stress-strain behavior of reinforcing steel including the strain hardening branch is given by the following equation

$$f_s = \frac{E_s \varepsilon_s}{\left\{1+\left|\frac{E_s \varepsilon_s}{f_y}\right|^{1/20}\right\}} + \left(f_{su} - f_y\right)\left[1 - \frac{\left|\varepsilon_{su} - \varepsilon_s\right|^P}{\left\{\left|\varepsilon_{su} - \varepsilon_{sh}\right|^{20P} - \left|\varepsilon_{su} - \varepsilon_s\right|^{20P}\right\}^{1/20}}\right] \qquad \text{(II.4)}$$

where, $P = \frac{E_{sh}\left(\varepsilon_{su} - \varepsilon_{sh}\right)}{\left(f_{su} - f_y\right)}$, f_s = stress in reinforcing steel at strain ε_s, E_s = modulus of elasticity of steel, E_{sh} = strain hardening modulus of steel, f_y = yield strength of steel, f_{su} = ultimate strength of steel, ε_{su} = ultimate strain, ε_{sh} = strain hardening strain.

The moment curvature analysis is performed by following the algorithm in Mander et al, 1988. In this process the curvature is fixed and the centroidal strain is adjusted to obtain the target axial load. The step are given as follows

1) To the value of the last known solution, the curvature increment is added to give the new curvature

$$\phi_k = \phi_{k-1} + \Delta\phi \qquad \text{(II.5)}$$

2) From the out of balance force remaining from the last solution, $\Delta P = P_{k-1} - N$, the required change in section centroidal strain necessary to obtain force equilibrium is determined by the following

$$\Delta\varepsilon_{ok} = \frac{\Delta P - \left(\frac{\delta P}{\delta\phi}\right)_{k-1} \Delta\phi_k}{\left(\frac{\delta P}{\delta\phi}\right)_{k-1}} \qquad \text{(II.6)}$$

The total reference axis strain is obtained from the following

$$\varepsilon_{ok} = \varepsilon_{ok-1} + \Delta\varepsilon_{ok} \qquad \text{(II.7)}$$

The revised strain profile is given by

$$\varepsilon(y)_k = \varepsilon_{ok} + \phi_k y \tag{II.8}$$

The total force in the section is given by

$$P_k = \langle f_s \rangle_k^T \langle A_s \rangle + \langle f_c \rangle_k^T \langle A_c \rangle + \langle f_{cc} \rangle_k^T \langle A_{cc} \rangle \tag{II.9}$$

The out of balance force is given by

$$\Delta P = P_{k-1} - N \tag{II.10}$$

If $|\Delta P| < tolerance$, then the moment is calculated as given in the next step, otherwise the algorithm reverts back to step 2.

3) The moment is calculated as

$$M_k = \langle f_s \rangle_k^T \langle A_s \rangle \langle y_s \rangle^T + \langle f_c \rangle_k^T \langle A_c \rangle \langle y_c \rangle^T + \langle f_{cc} \rangle_k^T \langle A_{cc} \rangle \langle y_{cc} \rangle^T \tag{II.9}$$

The following stopping criterion are checked to stop the moment-curvature analysis

a) Spalling of core concrete: The moment-curvature analysis is stopped when the strain in the core concrete exceeds the hoop fracture strain of the transverse reinforcement.

b) Fracture of longitudinal reinforcing bars: The moment-curvature analysis is terminated when the strains in the longitudinal reinforcement exceeds the fracture strain of the longitudinal reinforcing bars.

4) The shear capacity of the RC column is calculated from the maximum moment capacity of the column given by

$$V_{static} = \frac{2M_{\max}}{l_{eff}} \tag{II.10}$$

where, V_{static} = static shear capacity of the RC column, $M_{\max}$ = maximum value of the moment capacity obtained from the moment curvature analysis, l_{eff} = distance between base of the column to the point of vehicle collision as shown in Fig. II.1.

II.2 Dynamic Shear Capacity

The dynamic shear capacity is defined as the shear capacity of the RC column when the RC column is moving with velocity v_s. The shear capacity increases due to the increase in strength of the material due to the strain rate effect. In order to calculate the dynamic shear capacity, first the force deformation analysis of the RC column is performed for length equal to $l_{eff}/2$ as this portion of the column acts as a cantilever (the moment at the distance is approximately zero). The displacement is then divided by velocity v_s to obtain the time to reach the displacement. The maximum strain in concrete and steel is then divided by the time to obtain the corresponding maximum strain rates at maximum displacement. The strain rate is then varied linearly from zero to the maximum strain rate as the curvature (displacement) increases. The corresponding strain rate at each instant is used to obtain the increase in the strength of concrete and steel. This in turn gives the increase in moment-curvature relationship. The increased moment is again used to calculate the dynamic shear capacity of the column.

The material model of the concrete and steel are multiplied by the corresponding Dynamic Increase Factor (DIF) to get the increase in strength. The DIF for concrete as per Mander et al., 1988 is given by

$$DIF_c = \frac{1+\left[\frac{\varepsilon_c}{0.035\left(f_c^{'}\right)^2}\right]^{1/6}}{1+\left[\frac{0.00001}{0.035\left(f_c^{'}\right)^2}\right]^{1/6}} \qquad \text{(II.11)}$$

The DIF for mild steel is given as per Mander et al., 1988 by

$$DIF_s = 0.953\left[1+\left|\frac{\dot{\varepsilon}}{700}\right|^{1/6}\right] \qquad \text{(II.12(a))}$$

and for high strength steel is given by

$$DIF_s = 0.953\left[1+\left|\frac{\dot{\varepsilon}}{50X10^6}\right|^{1/6}\right] \qquad \text{(II.12(b))}$$

The force deformation plot is obtained from the moment curvature analysis. The force deformation analysis is done in two stages viz. non-linear elastic behavior and post-yield non linear behavior.

1) Non Linear elastic behavior

In this stage of analysis the elastic deformation is given by

$$\Delta_e = \frac{L^2}{6M_m^2}\sum_{k=1}^{m}\left(M_k - M_{k-1}\right)\left[\phi_k\left(2M_k + M_{k-1}\right) + \phi_{k-1}\left(M_k + 2M_{k-1}\right)\right] \qquad \text{(II.13)}$$

where, Δ_e = elastic deformation, M_m = moment at the current point, M_k and ϕ_k are the moment and the curvature at the kth point, L = length of the cantilever portion.

The total deformation is given by

$$\Delta = \Delta_e + \Delta_{stub} \qquad \text{(II.14)}$$

where, $\Delta_{stub} = \frac{ML_{stub}}{2EI_{stub}}\left(L + \frac{L_{stub}}{4}\right)$, $EI_{stub} = \frac{\alpha L_{stub}^4}{12}E_c$, α varying form 0.1 for RC column with less axial load to 1 for columns with heavy axial load.

2) Post Yield non linear behavior

The displacement in this stage of the analysis consists of two parts, the elastic and the plastic component of displacement.

The elastic deformation is given by

$$\Delta_e = \frac{ML^2}{3EI_{eff}} \tag{II.15}$$

where, $EI_{eff} = \frac{M_y L^2}{3\Delta_y}$, M_y = yield moment, Δ_y = yield curvature.

The plastic deformation is given by

$$\Delta_p = \theta_p\left(L - 0.25L_{pc}\right) \tag{II.16}$$

where, $\theta_p = \left(\phi_m - \phi_e\right)\left[\frac{L_{pc}}{3} + 4400\varepsilon_y d_b\right]$, $L_{pc} = L\left(1 - \frac{M_y}{M_{\max}}\right)$, $\phi_e = \phi_y \frac{M_m}{M_y}$.

For squat columns with low aspect ratio, the deformation caused by shear is significant; therefore, the contribution due to shear deformation is added to obtain the total displacement. The shear deformation is given by

$$\Delta_s = V\left[\frac{d_c}{E_s A_{sh}\left(\frac{L}{s}\right)} + \left(\frac{\left(2\tan\alpha + 0.78\cot\alpha\right)^2}{E_c bh}\right)\right] \tag{II.17}$$

where, $\tan\alpha = \frac{d_c}{L}$, A_{sh} = area of shear reinforcement across a cross section.

The total deformation in the post yield region is given by

$$\Delta = \Delta_e + \Delta_p + \Delta_{stub} + \Delta_s \qquad \text{(II.18)}$$

For each case of the vehicle collision, the total deformation is divided with the velocity at which the RC column is moving in order to obtain the time taken to reach the total deformation as given by $t_c = \frac{\Delta}{v_s}$. The time obtained is divided by the maximum strain in the concrete and steel to get the maximum strain rate in concrete and steel given by $\dot{\varepsilon}_{c/s} = \frac{\varepsilon_{c/s}}{t_c}$. Now the moment curvature analysis is again performed by linearly increasing the strain rate for concrete and steel from zero to the maximum strain rate obtained at the maximum deformation. The strength of the material is modified as per Equations II.11 and II.12 to account for the increase in strength. The new maximum moment is called the dynamic moment capacity from which the Dynamic Shear Capacity (DSC) is calculated as follows

$$V_{dynamic} = \frac{2M_{dynamic}}{l_{eff}} \qquad \text{(II.19)}$$

The ratio of the dynamic shear capacity and the static shear capacity obtained as above from the moment curvature analysis is called Dynamic Shear Ratio (DSR) given by

$$DSR = \frac{V_{dynamic}}{V_{static}} \qquad \text{(II.20)}$$

Fig. 7.1 shows the variation of the DSR with the velocity v_s at which the RC column is moving during a vehicle collision.

II.3 Case Study

This section presents the estimation of static shear capacity, dynamic shear capacity and DSR for two RC columns used in this dissertation. A step by step procedure is followed with numerical values in order to calculate the value of DSR. Table II.1 describes the configuration of the two RC columns C3 and C4.

Table II.1. Configuration of RC Columns.

No.	Diameter [m]	Length [m]	Longitudinal Reinforcement	Transverse Reinforcement	Axial load N [kN]
C3	1.00	6.00	32- ϕ 25 mm bars	ϕ 12.7 mm-0.06 m pitch	2961
C4	0.58	3.78	8- ϕ 25 mm bars	ϕ 9.6 mm-0.08 m pitch	2354

Table II.2 and Table II.3 lists the material properties of the RC column C3 and C4.

Table II.2. Material Properties of RC Columns C3.

Material	Density ρ [kg/m^3]	Modulus of Elasticity E [GPa]	Poisson's ratio υ	Unconfined Compressive Strength [MPa]	Unconfined Tensile Strength [MPa]	Yield Stress [MPa]
Concrete	2500	25.7	0.2	30.0	3.0	-
Steel	7850	210.0	0.3	-	-	415

Table II.3. Material Properties of RC Columns C4.

Material	Density ρ [kg/m^3]	Modulus of Elasticity E [GPa]	Poisson's ratio υ	Unconfined Compressive Strength [MPa]	Unconfined Tensile Strength [MPa]	Yield Stress [MPa]
Concrete	2500	34.9	0.2	55.0	5.0	-
Steel	7850	210.0	0.3	-	-	250

Following the procedure outlined in the Sub-section II.1, the moment curvature analysis is performed for C3 and C4. As per Equation II.9, the maximum moment $M_{\max}$ sustained by C3 is 3072.4 kNm and $M_{\max}$ for C4 is 540.4 kNm. The static shear capacity V_{static} as given by Equation II.10 for C3 is 4096.5 kN and V_{static} for C4 is 720.5 kN. The l_{eff} for both of the RC columns is taken as 1.5 m assuming that both of the columns are subject to collision with the same type of vehicle.

In order to evaluate the dynamic shear capacity $V_{dynamic}$ for the two RC columns under different loading conditions the procedure described in Sub-section II.2 is followed. First, the force-deformation analysis is performed on C3 and C4. The effective length of the cantilever portion is taken as half of l_{eff} which is 0.75 m as at this position the moment in the column is approximately zero. So, the effective length L of the cantilever portion of the RC columns is taken 0.75 m. The maximum displacement Δ is calculated from the force-deformation analysis for C3 and C4. Then the different cases loadings are examined where the column is subject to different velocities v_s. The

different time taken to reach the total deformation is calculated by $t_c = \frac{\Delta}{v_s}$. Using the total time t_c and the maximum strain in the outer fiber, the maximum strain rate $\dot{\varepsilon}_{c/s}$ for concrete and steel is calculated. The value of maximum strain rate $\dot{\varepsilon}_{c/s}$ is again used in the moment-curvature analysis as described in Sub-section II.2 to calculate the maximum dynamic moment $M_{dynamic}$ for C3 and C4 under different velocities. From the dynamic moment $M_{dynamic}$ the value of dynamic shear capacity $V_{dynamic}$ is calculated using Equation II.19. Table II.4 and Table II.5 present the results of the above mentioned case study.

Table II.4. Intermediate Values in Calculating Dynamic Moment.

Column	Displacement Δ [m]	Velocity v_s [m/s]	Time t_c [s*10^{-3}]	Strain rate $\dot{\varepsilon}_{c/s}$ [1/s]	Static Moment M_{static} [kNm]	Dynamic Moment $M_{dynamic}$ [kNm]
C3	0.026	15.0	1.73	14.4	3072	4686
		25.0	1.04	23.9		4845
		35.0	0.74	33.6		4959
		45.0	0.58	42.9		5045
		55.0	0.47	52.9		5122
C4	.019	15.0	1.27	13.7	540	787
		25.0	0.76	22.9		812
		35.0	0.54	32.2		829
		45.0	0.42	41.4		843
		55.0	0.35	49.7		853

Table II.4 shows the value of the maximum displacement of C3 and C4 obtained by force-deformation analysis. Five values of velocities v_s are used as shown in Table II**.4** to evaluate the increase in the capacity of the RC columns. From the velocities, the value of time t_c taken to undergo the respective displacements is calculated. Using the time t_c the maximum strain rate $\dot{\varepsilon}_{c/s}$ is calculated from the maximum strain value $\varepsilon_{c/s}$ of 0.0249 for C3 and 0.0174 for C4. The maximum strain rate $\dot{\varepsilon}_{c/s}$ is used to calculate the dynamic moment from the moment-curvature analysis, the values of maximum dynamic moment $M_{dynamic}$ is presented in Table II.4.

Table II.5 presents the value of static shear capacity, dynamic shear capacity and DSR calculated from the procedure outlined in Sub-section II.2.

Table II.5. Dynamic Quantities of Interest for RC Column.

Column	Velocity v_s [m/s]	Static Shear Capacity V_{static} [kN]	Dynamic Shear Capacity $V_{dynamic}$ [kN]	Dynamic Shear Ratio DSR
C3	15.0	4096	6249	1.53
	25.0		6460	1.58
	35.0		6612	1.61
	45.0		6727	1.64
	55.0		6830	1.67
C4	15.0	720	1050	1.46
	25.0		1083	1.5
	35.0		1106	1.54
	45.0		1125	1.56
	55.0		1138	1.58

Fig. II.2 shows the variation of DSR with the velocity v_s of the RC columns. The DSR increases with a non-linear trend with the increase in the velocity v_s of the RC columns. The DSR is also influenced by the static capacity of the RC column. The DSR value is more for C3 than C4, which can be attributed to the larger static shear capacity of C3 than C4.

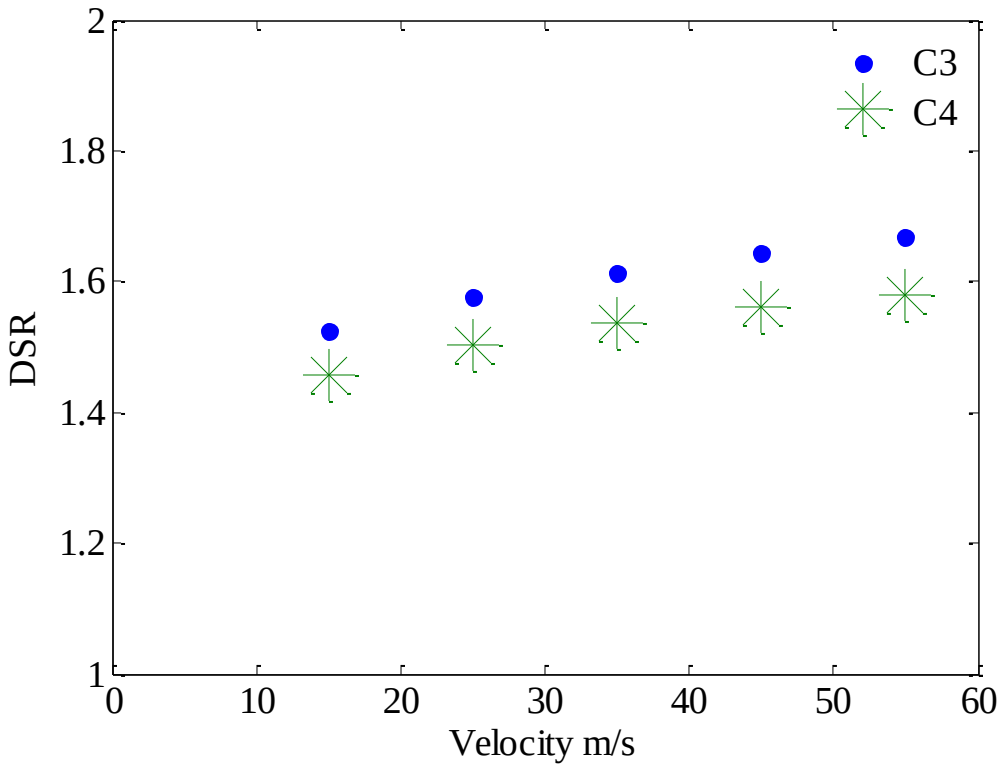

Fig. II.2. Increase in DSR of RC column with velocity.

II.4 Conclusion

In this section, the details for calculating static shear capacity form moment curvature analysis are presented. This section also details the process of calculating dynamic shear capacity by accounting for the increase in strength due to strain rate. The DSR is defined which represents the increase in strength of shear capacity of RC column with the movement of the RC column with velocity v_s. The contribution of the shear capacity is uncoupled from the total shear resistance and is analyzed to see the effect of velocity and in turn the strain rate on the shear capacity of RC column. Case study for two RC columns is presented in this section. A step by step procedure is shown with numerical values to calculate DSR. The variation of DSR for two example RC columns is shown. The DSR varies from 1 to 2 for the range of velocities analyzed in this dissertation. So for a very severe impact scenario, the contribution of the shear capacity can double from the static shear contribution.

VITA

Name Hrishikesh Sharma

Address Zachry Department of Civil Engineering

Texas A&M University

College Station

Texas 77843-3136

Email: shrishi@neo.tamu.edu

shrishikeshsharma@gmail.com

Education B.E. (Structural) 2003 Visvesvaraya National Institute of Technology, Nagpur, India

M.S (Structural) 2007 Texas A&M University, College Station, Texas, USA